

1 This document includes:
2

- 3 i. Point-by-point responses to Referee #1 and Referee #2.
- 4 ii. The revised manuscript (including changes, as requested by Referee #1 and #2, which are
5 highlighted in yellow. Grey highlights are for general edits.
- 6 iii. Manuscript supplement.
7
8

9 **Manuscript format description:**

10 Black text shows the original referee comment, blue text shows the authors response, and red text
11 shows quoted manuscript text. Changes to the manuscript text are shown as *italicized and underlined*.
12 We used bracketed comment numbers for referee comments (e.g., [R1.1]) and author's responses
13 (e.g., [A1.1]). Line numbers refer to the discussion/review manuscript.
14
15
16
17

18 **Response to referee comments and suggestions on amt-2018-390 by Könemann et al.**
19

20 **Anonymous Referee #1**

21 Received: 25 November 2018
22

23 General comment:

24 The paper describes an instrument that should be much superior to the WIBS or UVAPS in charac-
25 terizing fluorescent aerosol. The 16-channel fluorescence spectra should provide far more infor-
26 mation for characterizing aerosol than existing WIBS instruments, while still measuring very large
27 numbers of spectra per day. This instrument appears to be able to significantly expand our under-
28 standing of bioaerosols and other fluorescent particles in the atmosphere. The paper is clearly written.
29 It should be published. I suggest the authors think about the following.
30

31 **Author response:** We want to thank Referee #1 for his/her positive and constructive assessment.
32

33 Specific/technical comment:

34 [R1.1] The title and abstract say, “a new instrument for . . .” Then line 144 is: “Introduced here is a
35 new instrument for the detection and characterization of individual particles; the Spectral Intensity

36 Bioaerosol Sensor (SIBS, Droplet Measurement Technologies).” Then later the text says, “The SIBS
37 was originally designed and marketed to record time-resolved fluorescence lifetime.” If it has already
38 been marketed, the use of “new” seems possibly inaccurate. How long has it been marketed? I suggest
39 dropping “new” from the title and the text. There is no need for it. Also, a book chapter by Huffman
40 (one of the authors of the present paper) and Santarpia, “Online Techniques for Quantification and
41 Characterization of Biological Aerosols,” in Microbiology of Aerosols eds., Anne-Marie Delort and
42 P Amato (2017) mentions both types of SIBS (the breakdown spectroscopy SIBS and the spectral
43 intensity SIBS). That chapter was published over a year ago and was presumably written many
44 months before that.

45
46 [A1.1] We agree with Referee#1 and took out the word “new” from the title and abstract. It is
47 true that the SIBS was briefly introduced within the book chapter “Online Techniques for
48 Quantification and Characterization of Biological Aerosols” (Huffman and Santarpia, 2017).
49 This reference is based on the same unit as discussed in amt-2018-390 and referenced by a
50 conference poster, because no other citation was available at that time. Information stated in
51 this book chapter was based on unpublished and non-peer-reviewed data, available because we
52 had already been working together with Alex Huffman in 2015 with respect to the earliest
53 version of the SIBS. Since then, the instrument underwent many modifications (hardware and
54 software) and revisions for which the SIBS unit from 2015 and the unit in its current state are
55 not comparable anymore.

56
57 [R1.2] A new and noteworthy part of this paper (maybe the most new and noteworthy part) is that
58 the instrument is commercially available. Instruments that could do the key parts of what is done here
59 (two fluorescence spectra each with a different excitation wavelength is measured for each particle)
60 have been around for some years, e.g., Huang, Pan et al., and Pan et al. But routine measurements
61 were far from feasible by others. I suggest stating in the abstract and introduction that the instrument
62 is built by DMT and commercially available. I suspect more people will read it if they know they
63 could buy one. Many instruments described in papers, especially new instruments, can only be used
64 by the researchers that built and know how to use them.

65
66 [A1.2] As suggested by Referee#1, we added a reference to DMT within the abstract and con-
67 clusions for clarification. The linkage between the SIBS and DMT is already given, within the
68 introduction, in:

69

70 (P5, L155-156): “Introduced here is a new instrument for the detection and characterization of
71 individual particles; the Spectral Intensity Bioaerosol Sensor (SIBS, Droplet Measurement
72 Technologies).”

73
74 [R1.3] RE: “originally designed and marketed to record time-resolved fluorescence lifetimes”. Are
75 spectra required for measuring fluorescence lifetimes? Was the SIBS designed and marketed to meas-
76 ure spectra at two excitation wavelengths? I think what is meant is: It was designed and marketed to
77 measure time- and spectrally-resolved fluorescence lifetimes.

78
79 [A1.3] Correct. The SIBS was originally designed to measure time- and spectrally-resolved
80 fluorescence lifetimes at two excitation wavelengths. As suggested by Referee #1, the follow-
81 ing sentence was changed from:

82
83 (P15, L495-496): “The SIBS was originally designed and marketed to record time-resolved
84 fluorescence lifetime.”

85
86 To (P15, L495-496): “The SIBS was originally designed and marketed to record time- and
87 spectrally-resolved fluorescence lifetimes at two excitation wavelengths.”

88
89 [R1.4] Make Fig. 2 higher resolution so it can be seen in detail on a large monitor.

90
91 [A1.4] Within the current manuscript version, figures were used in lower resolution to keep
92 file sizes as low as possible. The final version will include high resolution images and figures.

93
94 [R1.5] RE: SIBS (Spark Induced Breakdown Spectroscopy) already has a meaning in the measure-
95 ment of aerosol particles, either single particles or many at a time. It is confusing to see SIBS used
96 for the name of an instrument that has nothing to do with spark induced breakdown. SIBS (original
97 meaning) provides information similar to LIBS, i.e., elemental composition of single-particles or
98 multiple-particles. I imagine SIBS (or LIBS) may eventually be combined with an instrument such
99 as the SIBS described in this paper, to provide both breakdown spectra and fluorescence spectra for
100 each particle. Since the SIBS of Konemann et al., is already marketed, and been around for a while,
101 it is likely too late for this comment to be relevant, but I hope not.

102

103 [A1.5] It is indeed unfortunate that two similar acronyms exist for two different instruments.
104 We added the following sentence to hopefully avoid potential misconceptions, including refer-
105 ences as suggested by Referee#1:

106
107 (P12, L370-373): *“To avoid potential misunderstanding, it is important to note that the SIBS*
108 *described in this study is not related to spark-induced breakdown spectroscopy instrumenta-*
109 *tion, which uses the same acronym (e.g., Bauer & Sonnenfroh, 2009; Hunter et al., 2000;*
110 *Khalaji et al., 2012; Schmidt & Bauer, 2010).”*

111
112 It is true that the combination of both breakdown- und fluorescence spectra on single particle
113 scale would provide a completely new level for particle characterization. However, this topic
114 is beyond the scope of this manuscript.

115

116 **References**

- 117 Bauer, A. J. R. and Sonnenfroh, D. M.: Spark-induced breakdown spectroscopy-based classification of bioaerosols, in
118 Safety, Security & Rescue Robotics (SSRR), 2009 IEEE International Workshop on, pp. 1–4, IEEE., 2009.
- 119 Huffman, J. A. and Santarpia, J.: Online Techniques for Quantification and Characterization of Biological Aerosols,
120 Microbiol. Aerosols, 83–114, 2017.
- 121 Hunter, A. J. R., Morency, J. R., Senior, C. L., Davis, S. J. and Fraser, M. E.: Continuous emissions monitoring using
122 spark-induced breakdown spectroscopy, J. Air Waste Manage. Assoc., 50(1), 111–117, 2000.
- 123 Khalaji, M., Roshanzadeh, B., Mansoori, A., Taefi, N. and Tavassoli, S. H.: Continuous dust monitoring and analysis by
124 spark induced breakdown spectroscopy, Opt. Lasers Eng., 50(2), 110–113, 2012.
- 125 Schmidt, M. S. and Bauer, A. J. R.: Preliminary correlations of feature strength in spark-induced breakdown spectroscopy
126 of bioaerosols with concentrations measured in laboratory analyses, Appl. Opt., 49(13), C101–C109, 2010.

127 **Response to referee comments and suggestions on amt-2018-390 by Könemann et al.**

128

129 **Referee #2 Dr. Ian Crawford**

130 Received: 4 December 2018

131

132 General comment:

133 This paper examines the technical capabilities of the new SIBS UV-LIF bioaerosol spectrometer and
134 describes several technical corrections and calibrations that are necessary to deliver high quality and
135 accurate data products. As a long term WIBS user it is encouraging to see the next generation of high
136 spectral resolution UV-LIF spectrometers that are coming to market being examined in detail early
137 on in their lifecycle; while there is still undoubtedly still utility in broadband spectrally integrated
138 instruments such as the WIBS for broad bioaerosol detection, it has been clear for some time now
139 that deeper specificity/classification requires greater spectral resolution so these technical develop-
140 ments are timely. The authors present a fair assessment of SIBS capability to resolve key biofluoro-
141 phores and make a number of suggestions and cautions that apply to the SIBS and also UV-LIF
142 spectrometers generally. Overall the paper is well written and the technical validation experiments
143 are well thought out. The results and methodologies reported here will serve as a useful framework
144 for assessing the performance of other multichannel high spectral resolution UV-LIF spectrometers
145 which are entering circulation. I recommend publication after the following comments have been
146 addressed.

147

148 **Author response: We want to thank Dr. Crawford (Referee #2) for his positive assessment and con-**
149 **structive suggestions.**

150

151 Specific/technical comment:

152 [R2.1] L98: Can you please check the size range reported for the WIBS-NEO. It is my understanding
153 that the instrument sizes over the range of 0.5-30 μm .

154

155 [A2.1] Thanks a lot for pointing that out. The size range we stated for the WIBS-NEO origi-
156 nated from information we had in the beginning of 2017. Since then, DMT seem to have up-
157 dated related information. The size range, within the manuscript, is now changed from ~0.3 –
158 100 μm to ~0.5 – 30 μm for the WIBS-NEO, according to: [http://www.dropletmeasure-](http://www.dropletmeasurement.com/wideband-integrated-bioaerosol-sensor-wibs-neo)
159 [ment.com/wideband-integrated-bioaerosol-sensor-wibs-neo](http://www.dropletmeasurement.com/wideband-integrated-bioaerosol-sensor-wibs-neo)

160

161 [R2.2] L125: I think that a short sentence summarising some of the validation work would round this
162 out while showing some of the limitations of the instrument/approach. A statement on how the Craw-
163 ford et al. (2015) method was validated by Gosselin et al. (2016) by showing a good correlation
164 between fungal molecular tracers and assumed fungal clusters but poor agreement between bacterial
165 tracers and assumed bacterial clusters would contextualise this. It may also be worth commenting
166 that the relatively high lower size limit of 0.8 μm used in this study due to instrument limitations may
167 have impacted the latter which may potentially be alleviated by an improved lower detection limit.

168

169 [A2.2] As suggested, the following sentences have been added to round out the topic of cur-
170 rently used clustering approaches regarding online LIF:

171

172 (P4-5, L130-139): *“For example, it was shown for a rural forest study in Colorado that a*
173 *cluster derived using WIBS-3 data, assigned to fungal spores (Crawford et al., 2015), corre-*
174 *lated well with the mass concentration of molecular fungal tracers (e.g., arabitol and mannitol)*
175 *measured with offline chemical techniques (Gosselin et al., 2016). In contrast, the clusters in*
176 *the same study that were assigned to bacteria correlated only poorly with endotoxins, used as*
177 *bacterial molecular tracers (Gosselin et al., 2016). This provides evidence of a limitation to*
178 *using LIF instrumentation with low spectral resolution to separate or identify some PBAP*
179 *types. Additionally, the bacterial cluster allocation might have also been hampered in that case*
180 *by the minimum detectable particle size of the WIBS ($\sim 0.8 \mu\text{m}$), resulting in a lower detection*
181 *efficiency for bacteria.”*

182

183 [R2.3] L209: Can you comment further on the choice of 1σ thresholding use here. I appreciate that
184 the conventional wisdom used to determine the threshold for WIBS instruments may not carry over
185 here due to the differences in the optical setup but 3σ and 9σ thresholds are used later in the paper
186 when reporting ambient concentrations.

187

188 [A2.3] As pointed out by Dr. Crawford, it is currently unknown if thresholding strategies con-
189 ventionally used for several WIBS models perform similar when applied to the optical setup of
190 the SIBS. For the current manuscript, we decided to use a rather simple 1σ approach, because
191 for the assessment of the spectral accuracy, measuring sets of homogenous particle types
192 (PSLs, biofluorophores), the thresholding plays only a minor role. In contrast, conventional
193 thresholding strategies were applied to a set of ambient data as a first attempt to qualitatively
194 match SIBS results with data derived from established online LIF instruments like the WIBS
195 and UV-APS. In this context, we added the following sentence:

196
197
198
199
200
201
202
203
204
205
206
207
208
209
210
211
212
213
214
215
216
217
218
219
220
221
222
223
224
225
226
227
228
229

(P7, L223-227): “Optimization of the thresholding strategy is still an on-going work, for example to investigate whether the often applied 3σ threshold used for the WIBS (e.g., Gabey et al., 2010) also works well with respect to the optical setup of the SIBS. For the assessment of the accuracy of measured fluorescence emissions from reference compounds, a threshold of 1σ was used here.”

[R2.4] L218: This looks like it may be due to coincidence errors arising from multiple particles being present in the sample volume causing odd scattering behaviour. This is a known problem when sampling high concentrations with forward scattering cloud probes, resulting in spectral broadening (e.g., Cooper, 1988).

[A2.4] Thanks a lot for this hint. The stated reference might indeed be an explanation for the effects we have observed for asymmetry factor measurements with the SIBS. The following sentence was added:

(P8, L235-237): “However, one explanation could be optical coincidences caused by high particle concentrations, resulting in multiple particles being simultaneously present within the scattering volume, as reported by Cooper (1988) using forward-scattering signatures of cloud probes.”

[R2.5] L435: This is a very interesting point that is raised here about the range irradiance imbalance between xenon lamps. This confirms some of my suspicious about the utility of presenting ABC analysis in general terms without appropriate caveats or a calibration standard and I think this is worth further comment. The Hernandez et al. (2016) work showed some of the results of the issues mentioned here when they compared two WIBS-4As where there were some significantly different classifications between the two units for the same test particle. They speculated that the difference between units was due to detector gain but your results suggest that xenon intensity may significantly contribute towards the observed differences. As a follow on comment this also shows the need for a common calibration reference standard to be adopted by the UV-LIF community (e.g., Robinson et al., 2017). This potentially raises a significant challenge for UV-LIF spectrometers with increased spectral resolution as I don't know if there is likely to be a single fluorophore that will adequately cover the whole spectral range?

230 [A2.5] This observation is indeed a critical point when it comes to the interpretation of fluo-
231 rescence data derived from online LIF instruments using similar optical setups. Observed dif-
232 ferences, between similar instruments as stated in, e.g., Hernandez et al. (2016), are most likely
233 based on the complex interaction of multiple technical components, batch-to-batch variability
234 etc. However, if prospective experiments verify a general imbalance between xenon sources /
235 optical filtering for the WIBS and SIBS, this issue might turn out to be a major contributor to
236 this topic. We agree with Dr. Crawford that it is absolutely necessary to adopt a calibration
237 standard within the online bioaerosol community. However, to the best of our knowledge, there
238 is currently no compound available that fulfills the requirements (e.g., stability, repeatability,
239 broad spectral range etc.) for being a standard calibrant for multi-channel, multi-excitation LIF-
240 instruments.

241
242 Within “5. Summary and conclusions”, this existing text passage briefly discuss the data inter-
243 pretation issue:

244
245 (P24, L799-805): “These observations are valid not only for the SIBS, but also for the WIBS-
246 4A and WIBS-NEO and lead to important implications for interpretation of particle data. In
247 particular, a particle that exhibits measurable fluorescence in WIBS channel FL1, but only weak
248 fluorescence in channel FL3 could be assigned as an “A-type” particle in one instrument but an
249 “AC-type” particle in an instrument with slightly stronger xenon 2 irradiance. These differences
250 in classification can be extremely important to interpretation of ambient data (Perring et al.,
251 2015; Savage et al., 2017).”

252
253 Additionally, we added the following sentence regarding instrument intercomparisons / cali-
254 brant standards:

255
256 (P24, L794-799): “Additionally, alternating irradiance properties might significantly contrib-
257 ute to observed differences in performance of similar instrument types (e.g., Hernandez et al.,
258 2016), expressly underlining the need for a fluorescence calibrant applicable across LIF-in-
259 struments (e.g., Robinson et al., 2017). Nevertheless, to the best of our knowledge, there is
260 currently no standard reference available that fulfills the requirements to serve as a calibrant
261 for multi-channel, multi-excitation LIF-instruments.”

262
263 [R2.6] L517: In my experience of calibrating forward scattering cloud probes it is often common to
264 find a dip in sizing performance in the lower region of an instruments detection range due to Mie-

265 Lorenz resonances in the applied Mie curve exceeding the bin thresholds or the bin thresholds being
266 relatively narrow. Mis-sizing can also be further exacerbated by the particles position in the sample
267 area as recently demonstrated by Faber et al. (2018), however this is less likely to be an issue with
268 SIBS/WIBS type instruments as the sample flow jet should be well constrained to the central sam-
269 pling region. Given that the fit to the calibration has a slope of approximately 1 and a negligible
270 intercept the assumed Mie curve appears to be adequate, however, should there routinely be a dip in
271 the particle size distribution around this size this may explain why.

272

273 [A2.6] We considered this possibility, and almost added a comment to the discussion manu-
274 script to this effect. Looking into the Mie curves in more detail, however, we did not find a
275 solid evidence that may serve as an explanation for the effect observed in a size range between
276 0.6 – 0.8 μm . Because the idea was not strongly supported and to avoid inadvertently leading
277 readers astray, we decided to leave the issue with unknown cause.

278

279 [R2.7] Fig. 7: Can you add to the caption what the red line represents. I assume it is the rebinned
280 reference spectra as in Fig. 5.

281

282 [A2.7] True, red dashed lines show re-binned reference spectra as stated in Fig. 5 for **c** and **d**.
283 The caption was modified for all corresponding figures (manuscript and supplement) as re-
284 requested.

285

286 [R2.8] Fig. S10: This would be easier to interpret if the two plots were scaled over the same x-axis
287 range.

288

289 [A2.8] Within the supplement manuscript, Fig. S10 was modified as requested.

290

291 **References**

- 292 Cooper, W. A.: Effects of coincidence on measurements with a forward scattering spectrometer probe, *J. Atmos. Ocean.*
293 *Technol.*, 5(6), 823–832, 1988.
- 294 Crawford, I., Ruske, S., Topping, D. O. and Gallagher, M. W.: Evaluation of hierarchical agglomerative cluster analysis
295 methods for discrimination of primary biological aerosol, *Atmos. Meas. Tech.*, 8(11), 4979–4991, 2015.
- 296 Gabey, a. M., Gallagher, M. W., Whitehead, J., Dorsey, J. R., Kaye, P. H. and Stanley, W. R.: Measurements and
297 comparison of primary biological aerosol above and below a tropical forest canopy using a dual channel
298 fluorescence spectrometer, *Atmos. Chem. Phys.*, 10(10), 4453–4466, doi:10.5194/acp-10-4453-2010, 2010.
- 299 Gosselin, M. I., Rathnayake, C. M., Crawford, I., Pöhlker, C., Fröhlich-Nowoisky, J., Schmer, B., Després, V. R.,
300 Engling, G., Gallagher, M., Stone, E., Pöschl, U., and Huffman, J. A.: Fluorescent bioaerosol particle, molecular
301 tracer, and fungal spore concentrations during dry and rainy periods in a semi-arid forest, *Atmos. Chem. Phys.*,

302 16(23), 15165–15184, 2016.

303 Hernandez, M., Perring, A. E., McCabe, K., Kok, G., Granger, G. and Baumgardner, D.: Chamber catalogues of optical
304 and fluorescent signatures distinguish bioaerosol classes, *Atmos. Meas. Tech.*, 9(7), 3283–3292, 2016.

305 Perring, A. E., Schwarz, J. P., Baumgardner, D., Hernandez, M. T., Spracklen, D. V., Heald, C. L., Gao, R. S., Kok, G.,
306 McMeeking, G. R., McQuaid, J. B. and Fahey, D. W.: Airborne observations of regional variation in fluorescent
307 aerosol across the United States, *J. Geophys. Res. Atmos.*, 120(3), 1153–1170, doi:10.1002/2014JD022495,
308 2015.

309 Savage, N. J., Krentz, C. E., Könemann, T., Han, T. T., Mainelis, G., Pöhlker, C. and Huffman, J. A.: Systematic
310 characterization and fluorescence threshold strategies for the wideband integrated bioaerosol sensor (WIBS)
311 using size-resolved biological and interfering particles, *Atmos. Meas. Tech.*, 10(11), 4279–4302,
312 doi:10.5194/amt-10-4279-2017, 2017.

313

30 Abstract

31 Primary biological aerosol particles (PBAP) in the atmosphere are highly relevant for the Earth sys-
32 tem, climate, and public health. The analysis of PBAP, however, remains challenging due to their
33 high diversity and large spatiotemporal variability. For real-time PBAP analysis, light-induced fluo-
34 rescence (LIF) instruments have been developed and widely used in laboratory and ambient studies.
35 The interpretation of fluorescence data from these instruments, however, is often limited by a lack of
36 spectroscopic information. This study introduces a **new** instrument – the Spectral Intensity Bioaer-
37 osol Sensor (SIBS, *Droplet Measurement Technologies (DMT, Longmont, CO, USA)*) – that resolves
38 fluorescence spectra for single particles and, thus, promises to expand the scope of fluorescent PBAP
39 quantification and classification.

40
41 The SIBS shares key design components with the latest versions of the Wideband Integrated Bioaer-
42 osol Sensor (WIBS) and the findings presented here are also relevant for the widely deployed WIBS-
43 4A and WIBS-NEO as well as other LIF instruments. The key features of the SIBS and findings of
44 this study can be summarized as follows:

- 45 - Particle sizing yields reproducible linear responses for particles in the range of 300 nm to 20 μm .
46 The lower sizing limit is significantly smaller than for earlier commercial LIF instruments (e.g.,
47 WIBS-4A and the Ultraviolet Aerodynamic Particle Sizer (UV-APS)), expanding the analytical
48 scope into the accumulation mode size range.
- 49 - Fluorescence spectra are recorded for two excitation wavelengths ($\lambda_{\text{ex}} = 285$ and 370 nm) and a
50 wide range of emission wavelengths ($\lambda_{\text{mean}} = 302 - 721$ nm) with a resolution of 16 detection
51 channels, which is higher than for most other commercially available LIF bioaerosol sensors.
- 52 - Fluorescence spectra obtained for 16 reference compounds confirm that the SIBS provides suffi-
53 cient spectral resolution to distinguish major modes of molecular fluorescence. For example, the
54 SIBS resolves the spectral difference between bacteriochlorophyll and chlorophyll *a/b*.
- 55 - A spectral correction of the instrument-specific detector response is essential to use the full fluo-
56 rescence emission range.
- 57 - Asymmetry factor (AF) data were assessed and were found to provide only limited analytical
58 information.
- 59 - In test measurements with ambient air, the SIBS worked reliably and yielded characteristically
60 different spectra for single particles in the coarse mode with an overall fluorescent particle frac-
61 tion of $\sim 4\%$ (3σ threshold), which is consistent with earlier studies in comparable environments.

62 1. Introduction

63 Aerosol particles are omnipresent in the atmosphere, where they are involved in many environmental
64 and biogeochemical processes (e.g., Baron & Willeke, 2001; Després et al., 2012; Fuzzi et al., 2006;
65 Hinds, 1999; Pöschl, 2005; Pöschl & Shiraiwa, 2015). Primary biological aerosol particles (PBAP),
66 also termed bioaerosols, represent a diverse group of airborne particles, consisting of whole or frag-
67 mented organisms including, e.g., bacteria, viruses, archaea, algae, and reproductive units (pollen
68 and fungal spores), as well as decaying biomass (e.g., Deepak & Vali, 1991; Després et al., 2012;
69 Fröhlich-Nowoisky et al., 2016; Jaenicke, 2005; Madelin, 1994; Pöschl, 2005) and can span sizes
70 from few nanometers up to $\sim 100 \mu\text{m}$ (Hinds, 1999; Schmauss and Wigand, 1929). The increasing
71 awareness of the importance of PBAP regarding aerosol-cloud interactions, health aspects, and
72 spread of organisms on local, continental or even intercontinental scales has led to a growing interest
73 by scientific researchers and the public (e.g., Després et al., 2012; Fröhlich-Nowoisky et al., 2016;
74 [Yao, 2018](#)).

75 Due to inherent limitations (e.g., poor time resolution and costly laboratory analyses) of tradi-
76 tional off-line techniques (e.g., light microscopy and cultivation-based methods) for PBAP quantifi-
77 cation, several types of real-time techniques have been developed within the last several decades to
78 provide higher time resolution and lower user costs (e.g., Caruana, 2011; Després et al., 2012;
79 Fennelly et al., 2017; Ho, 2002; [Huffman and Santarpia, 2017](#); Jonsson and Tjärnhage, 2014; Sodeau
80 and O'Connor, 2016). One promising category of real-time instruments – meaning that particles are
81 sampled and analyzed both instantly and autonomously – involves application of light- induced flu-
82 orescence (LIF). The main principle of this technique is the detection of intrinsic fluorescence from
83 fluorophores ubiquitous in biological cells, such as those airborne within PBAP. These fluorophores
84 include a long list of biological molecules such as aromatic amino acids (e.g., tryptophan and tyro-
85 sine), co-enzymes (e.g., reduced pyridine nucleotides (NAD(P)H)), flavin compounds (e.g., ribofla-
86 vin), as well as biopolymers (e.g., cellulose and chitin) and chlorophyll (e.g., Hill et al., 2009; Li et
87 al., 1991; Pan et al., 2010; Pöhlker et al., 2012, 2013). Detailed information of biological fluorophores
88 can be found elsewhere (Pöhlker et al., 2012 and references therein).

89 Today, commercial on-line LIF instruments such as the Ultraviolet Aerodynamic Particle Sizer
90 (UV-APS, TSI Inc. Shoreview, MN, USA) and the Wideband Integrated Bioaerosol Sensor (WIBS,
91 developed [at by](#) the University of Hertfordshire, U.K. and currently licensed and manufactured by
92 Droplet Measurement Technologies (DMT, Longmont, CO, USA)) are commonly applied for re-
93 search purposes. Detailed descriptions of the UV-APS (e.g., Agranovski et al., 2003; Brosseau et al.,
94 2000; Hairston et al., 1997) and the WIBS series (e.g., Foot et al., 2008; Kaye et al., 2000, 2005;
95 Stanley et al., 2011) are given elsewhere. Concisely, the UV-APS uses an $\lambda_{\text{ex}} = 355 \text{ nm}$ laser excita-
96 tion source and spans an emission range between $\lambda_{\text{em}} = 420\text{-}575 \text{ nm}$. In contrast, the WIBS applies

97 two pulsed xenon flash lamps emitting at $\lambda_{\text{ex}}=280$ and 370 nm, whereas fluorescence emission is
98 detected in three detection channels, $\lambda_{\text{em}}=310-400$ nm (at $\lambda_{\text{ex}}=280$ nm) and $\lambda_{\text{em}}=420-650$ nm (at
99 $\lambda_{\text{ex}}=280$ and 370 nm). Both instruments provide spectrally unresolved fluorescence information. The
100 latest WIBS model is currently the WIBS-NEO, whose design is based on a WIBS-4A but with an
101 extended particle size detection range between **~300 ~500 nm and 400 30 μm** (nominal). Both UV-
102 APS and WIBS models have been examined in a variety of laboratory validations (e.g., Agranovski
103 et al., 2003, 2004; Brosseau et al., 2000; Healy et al., 2012; Hernandez et al., 2016; Kanaani et al.,
104 2007; O'Connor et al., 2013; Saari et al., 2013, 2014; Savage et al., 2017; Toprak & Schnaiter, 2013)
105 and have been deployed to investigate both indoor and outdoor atmospheric aerosol via longer-term
106 measurements (e.g., Bhangar et al., 2014; [Calvo et al., 2018](#); Crawford et al., 2015b; Fernández-
107 Rodríguez et al., 2018; Foot et al., 2008; Gabey et al., 2010, 2013; Gosselin et al., 2016; Healy et al.,
108 2014; Huffman et al., 2010, 2012, 2013; [Ma et al., 2019](#); Perring et al., 2015; Schumacher et al.,
109 2013; Twohy et al., 2016; Ziemba et al., 2016).

110 Although LIF instruments do not offer the same *qualitative* ability to *qualitatively* identify sam-
111 pled particles as, e.g., off-line microscopy, mass spectrometry, or culture-based methods, they pro-
112 vide size-resolved information as well as fast sampling and fine-scale temporal information for single
113 particles not accessible with off-line techniques. Nevertheless, these instruments present significant
114 challenges. For example, quantification of PBAP by LIF instruments is hindered by the fact that some
115 biological materials reveal weak fluorescence characteristics that does not rise above detection
116 thresholds (Huffman et al., 2012). In addition to this complication, the detection threshold is not a
117 universally defined parameter and varies for each channel between different units of the same type
118 of instruments (e.g., Hernandez et al., 2016; Savage et al., 2017). Furthermore, unambiguous spec-
119 troscopic characterization of bioparticles is fundamentally challenging, because fluorescence spectra
120 of even individual molecules in condensed matter are relatively broad due to radiative decay path-
121 ways of excited electrons. Further, bioparticles are chemically complex, each comprised of a mixture
122 of *at least* dozens of types of fluorophores that can each emit a unique emission spectrum that smears
123 together into an even broader fluorescence spectrum from each particle (Hill et al., 2009, 2015; Pan,
124 2015). Another difficulty is that many non-biological particles, such as certain mineral dusts and
125 polycyclic aromatic hydrocarbons (PAHs), may fluoresce, making it more difficult to distinguish
126 patterns arising from biological particles (e.g., Pöhlker et al., 2012 and references therein; Savage et
127 al., 2017). Lastly, most currently available commercial LIF instrumentation are limited to recording
128 data in 1-3 spectrally integrated emission channels, which limits the interpretation of fluorescence
129 information. Recent efforts to apply more complex clustering algorithms to the spectrally unresolved
130 WIBS-type data are proving helpful at adding additional discrimination ([e.g., Crawford et al., 2015a;](#)
131 [Robinson et al., 2013; Ruske et al., 2017; Savage & Huffman, 2018](#));. For example, it was shown for

132 *a rural forest study in Colorado that a cluster derived using WIBS-3 data, assigned to fungal spores*
133 *(Crawford et al., 2015a), correlated well with the mass concentration of molecular fungal tracers*
134 *(e.g., arabitol and mannitol) measured with offline chemical techniques (Gosselin et al., 2016). In*
135 *contrast, the clusters in the same study that were assigned to bacteria correlated only poorly with*
136 *endotoxins, used as bacterial molecular tracers (Gosselin et al., 2016). This provides evidence of a*
137 *limitation to using LIF instrumentation with low spectral resolution to separate or identify some*
138 *PBAP types. Additionally, the bacterial cluster allocation might have also been hampered in that*
139 *case by the minimum detectable particle size of the WIBS (~0.8 μm), resulting in a lower detection*
140 *efficiency for bacteria. ~~but aerosol characterization using instrumentation with such low spectra res-~~*
141 *olution is likely to be fundamentally limited (e.g., Robinson et al., 2013; Ruske et al., 2017; Savage*
142 *& Huffman, 2018).*

143 The evolution of LIF techniques over the last several decades has significantly expanded our
144 knowledge on spatiotemporal patterns of PBAP abundance in the atmosphere. Nevertheless to further
145 improve the applicability of LIF instrumentation to widespread PBAP detection, it is necessary both
146 to design LIF instrumentation with adequate instrumental properties (e.g., high spectral resolution)
147 and to standardize their operation by characterizing instruments thoroughly with known standards
148 (Robinson et al., 2017). Working toward this goal, a number of LIF instruments *have been developed*
149 *to analyze ~~that offer analysis of~~ single bioparticles by collecting ~~providing~~ resolved fluorescence*
150 *spectra ~~have been developed~~ (e.g., Hill et al., 1999; Pan et al., 2010, 2003; Pinnick et al., 2004; Ruske*
151 *et al., 2017), however relatively little has been done to offer these commercially. Examples for com-*
152 *mercially available instruments providing resolved fluorescence spectra are the PA-300 ($\lambda_{\text{ex}}= 337$*
153 *nm; $\lambda_{\text{em}}= 390 - 600$ nm, 32 fluorescence detection channels) (Crouzy et al., 2016; Kiselev et al.,*
154 *2011, 2013) and the follow-up model Rapid-E ($\lambda_{\text{ex}}= 337$ nm; $\lambda_{\text{em}}= 350 - 800$ nm, 32 fluorescence*
155 *detection channels) (<http://www.plair.ch/>), both manufactured by Plair SA, Geneva, Switzerland. ~~Be-~~*
156 *side of resolved fluorescence detection-In addition to collecting resolved fluorescence spectra, both*
157 *instruments also provide measurements of the decay of fluorescence signals, also referred to as flu-*
158 *orescence lifetime.*

159 Introduced here is *an new* instrument for the detection and characterization of individual particles;
160 the Spectral Intensity Bioaerosol Sensor (SIBS, Droplet Measurement Technologies). Technical
161 properties of the instrument are described in detail and its performance is validated with sizing and
162 fluorescence particle standards, as well as with *particles in* ambient air. Due to the dual excitation
163 and spectrally resolved fluorescence in combination with a broad size detection range, the SIBS has
164 the potential to increase the selectivity of fluorescent biological and non-biological particle detection
165 and discrimination. Because the SIBS uses a comparable optical system as the WIBS-4A and WIBS-
166 NEO, technical details presented here are broadly important to a growing community of scientists

167 investigating both indoor and outdoor aerosol. Insights and data presented will thus contribute to
168 ongoing discussions within the community of LIF users and will also stimulate discussions about
169 needs for future instrument improvements.

170

171 **2. Materials and methods**

172 **2.1 Chemicals and materials**

173 Supplemental table S1 summarizes 19 polystyrene latex spheres (PSLs, 5 doped with fluorescent
174 dye) and 6 polystyrene divinylbenzene (PS-DVB) particles, which were purchased from Thermo
175 Fisher (Waltham, MA, USA), Bangs Laboratories Inc. (Fishers, IN, USA), Duke Scientific Corp.
176 (Palo Alto, CA, USA), and Polysciences Inc. (Warrington, PA, USA). A detailed study regarding
177 steady-state fluorescence properties of PSLs and PS-DVB particles used within this study can be
178 found in Könemann et al. (2018). Additionally, we analyzed particles comprised separately of seven
179 pure biofluorophores (tyrosine, tryptophan, NAD, riboflavin, chlorophyll *a* and *b*, and bacteriochloro-
180 phyll) (Table S2) as well as one microorganism (*Saccharomyces cerevisiae*; baker's yeast, bought
181 at a local supermarket). Table S2 also includes reference particles used for asymmetry measurements,
182 namely iron oxide (Fe₃O₄), carbon nanotubes, and ammonium sulfate. Ultrapure water (MilliQ, 18
183 MΩ) and ≥ 99.8 % ethanol (CAS Nr. 64-17-5, Carl Roth GmbH und Co. KG, Karlsruhe, Germany)
184 were used as solvents.

185

186 **2.2 Aerosolization of reference particles**

187 PSLs were aerosolized from aqueous suspensions with a portable aerosol generator (AG-100; DMT).
188 For both fluorescent and non-fluorescent PSLs, one drop of the suspension (or alternatively three
189 drops for 3 and 4 μm PSLs) was diluted into 10 ml ultrapure water in plastic medical nebulizers
190 (Allied Healthcare, St. Louis, MO, USA). The majority of water vapor from the aerosolization pro-
191 cess condenses inside the mixing chamber (~570 cm³) of the aerosol generator. By using a tempera-
192 ture and relative humidity (RH) sensor (MSR 145 data logger, MSR Electronics GmbH, Seuzach,
193 Switzerland) monitoring the flow directly after the aerosol generator we measured RH values of
194 ~33% (sample flow: 1.4 l/min, dilution: 5 l/min), ~39% (sample flow: 1.4 l/min, dilution: 4 l/min),
195 and ~54% (sample flow: 2.3 l/min, dilution: 2 l/min). Because of the low RH measured, we did not
196 use additional drying (e.g., diffusion dryer) to decrease humidity in the sample flow. Hence, the outlet
197 of the aerosol generator was directly connected to the SIBS inlet with ~30 cm of conductive tubing
198 ($\frac{1}{4}$ inch). PSLs were measured for 1 min. Non-fluorescent 4.52 μm PSLs were measured for 2 min,
199 because of the low number concentrations due to poor aerosolization efficiency and gravitational
200 settling of larger particle sizes.

201 *S. cerevisiae* was analyzed using a method similar to the one stated above, with the exceptions
202 that the suspension was prepared with a spatula tip of material mixed into ultrapure water and that a
203 diffusion dryer (20 cm, 200 g silica) was added to remove excess water vapor. *S. cerevisiae* was
204 measured for 5 min. Chlorophyll *a*, *b*, and bacteriochlorophyll samples were diluted in 10 ml ethanol.
205 Between each measurement, the setup was cleaned by aerosolizing ultrapure water for 5 min.

206 PS-DVB particles and biofluorophores (Table S1 and S2) were aerosolized in a dry state. For this
207 purpose, air at a flowrate of ~0.6 l/min was sent through a HEPA filter into a 10 ml glass vial. A
208 small amount of each solid powder sample (~1 g) was placed inside the vial and entrained into the
209 particle-free airstream. Additionally, the sample was physically agitated by tapping the vial. The
210 outlet was connected with ~20 cm conductive tubing into the inlet of the SIBS. The tubing and glass
211 vial were cleaned after each measurement to prevent particle contaminations from previous meas-
212 urements. Each powder was sampled until cumulative number concentrations > 5000 particles were
213 reached.

214 In contrast to the monodisperse and spherical PSL standards, the biofluorophore aerosolization
215 process provided a polydisperse and morphologically heterogeneous particle distribution with sig-
216 nificant particle fractions at sizes < 1 μm . Therefore, we only used particles in a size range between
217 1 and 2 μm with sufficient fluorescence intensity values for subsequent data analysis. The only ex-
218 ceptions are the chlorophyll types, where a size range between 0.5 and 2 μm (chlorophyll *a* and *b*)
219 and 0.5 and 1 μm (bacteriochlorophyll) were used due to a less efficient particle aerosolization.

220 The fluorescent background of the SIBS was measured daily by firing the xenon lamps into the
221 optical chamber in the absence of particles (forced trigger mode). In this case, the diaphragm pump
222 was turned off and the inlet blocked to prevent particles reaching the optical chamber. One forced
223 trigger mode was performed per day with 100 xenon shots per min over a duration of 5 min. The
224 *average* background signal (+ 1 σ standard deviation (SD)) was subtracted from derived fluorescence
225 emission of each sample. Additionally, the background signal was reviewed periodically between
226 each biofluorophore measurement to verify that, e.g., optical components ~~are~~ *were* not coated with
227 residues from previous measurements. ~~A~~ No significant changes in background signal ~~were~~ *was not*
228 observed between individual measurements. *Optimization of the thresholding strategy is still an on-*
229 *going work, for example to investigate whether the often applied 3 σ threshold used for the WIBS*
230 *(e.g., Gabey et al., 2010) also works well with respect to the optical setup of the SIBS. For the as-*
231 *essment of the accuracy of measured fluorescence emissions from reference compounds, a threshold*
232 *of 1 σ was used here.*

233 For particle asymmetry measurements, iron (II, III) oxide (Fe₃O₄), carbon nanotubes, and ammo-
234 nium sulfate were aerosolized in dry state, and 2 μm non-fluorescent PSLs and ultrapure water were
235 aerosolized with the aerosol generator method outlined above with SIBS integration times of 3 min

236 in all cases. Due to the broad distribution of asymmetry factor (AF) values for particles below 1 μm ,
237 only the size fraction $\geq 1 \mu\text{m}$ was used for subsequent analyses. Furthermore, we observed that AF
238 bins between 0 and 1, and AF bin 100 tend to produce increased signal responses, especially for high
239 particle concentrations, for which they were discarded within the analyses. The origin of this effect
240 is unknown, *but most likely related to detector noise. However, one explanation could be optical*
241 *coincidences caused by high particle concentrations, resulting in multiple particles being simultane-*
242 *ously present within the scattering volume, as reported by Cooper (1988) using forward-scattering*
243 *signatures of cloud probes.*

244 For collection of particles for microscopy measurements, the sample flow was bypassed and led
245 through a custom-made particle impactor, which was connected to a mass flow controller (D-6321-
246 DR, Bronkhorst High-Tech B.V., Ruurlo, Netherlands) and a membrane pump (N816.1.2KN.18,
247 KNF, Freiburg, Germany). Particles were collected out of the sample flow onto glass cover slips (15
248 mm diameter) at a flow rate of 2 l/min over a duration of 1 min.

249

250 **2.3 Reference fluorescence spectra**

251 A Dual-FL fluorescence spectrometer (Horiba Instruments Incorporated, Kyoto, Japan) was used as
252 an offline reference instrument to validate the SIBS spectra. Aqualog V3.6 (Horiba) software was
253 used for data acquisition. The spectrometer was manufacturer-calibrated with NIST Fluorescence
254 Standard Reference Materials (SRMs 2940, 2941, 2942, and 2943). Aforementioned standard fluor-
255 ophores were analyzed using the SIBS excitation wavelengths at $\lambda_{\text{ex}} = 285$ and 370 nm. The Dual-
256 FL¹ spectrometer uses a xenon arc lamp as excitation source and a CCD (charge-coupled device) as
257 emission detector, capable of detecting fluorescence emission between 250 and 800 nm. Unless oth-
258 erwise stated, a low detector gain setting (2.25 e⁻ per count) and an emission resolution of 0.58 nm
259 was used for all measurements with the Dual-FL. Subsequently, we use the term “reference spectra”
260 for all measurements performed with the Dual-FL. In total, 100 individual spectra were recorded for
261 each sample and averaged spectra were analyzed in Igor Pro (Wavemetrics, Lake Oswego, Oregon
262 USA). Background measurements (solvent² in the absence of particles) were taken under the same
263 conditions as for sample measurements and subtracted from the emission signal. For direct compar-
264 ison to spectra recorded by the SIBS, reference spectra were re-binned by taking the sum of the
265 fluorescence intensity within the spectral bin width of each SIBS detection channel (Table 1).

266 For PSL measurements, 1.5 μl of each PSL stock solution was diluted in 3.5 ml ultrapure water
267 in a 10 x 10 x 40 mm UV quartz cuvette (Hellma Analytics, Müllheim, Germany) and constantly
268 stirred with a magnetic stirrer to avoid particle sedimentation during measurements. Chlorophyll *a*

¹ Technical information taken from Dual-FL operation manual, rev. A, 30 NOV 2012; Horiba.

² *Note that $\geq 99.8\%$ ethanol was used as solvent for chlorophyll *a*, *b*, and bacteriochlorophyll instead of ultrapure water.*

269 and *b* and bacteriochlorophyll were handled equally, however concentrations were individually ad-
270 justed to prevent the detector from being saturated and to avoid self-quenching or inner filter effects
271 (Sinski and Exner, 2007). Concentrations were used as follows: chlorophyll *a*: 300 nmol/l, chloro-
272 phyll *b*: 1 μ mol/l, and bacteriochlorophyll: 3 μ mol/l. PSLs, chlorophyll *b*, and bacteriochlorophyll
273 measurements were performed with an integration time of 2 s. For chlorophyll *a* an integration time
274 of 1 s was used.

275 All other biofluorophores, *S. cerevisiae*, and PS-DVB particles were measured in dry state using
276 a front surface accessory (Horiba). The sample was placed into the surface holder and covered with
277 a synthetic fused silica window. To limit detector saturation from more highly fluorescent particle
278 types, the surface holder was placed at a 70° angle to the fluorescence detector for NAD and ribofla-
279 vin, 75° for tyrosine, 80° for *S. cerevisiae*, and 85° for tryptophan and PS-DVB particles and subse-
280 quently excited at λ_{ex} =285 and 370 nm. Emission resolution and detector gain settings were used as
281 for measurements of samples in solution, except for an integration time of 1 s for all dry samples.
282 Background measurements were performed as described above and subtracted from each sample.
283 Excitation-emission matrices (EEMs) were measured with the same samples as for single wavelength
284 measurements. EEMs were recorded at excitation wavelengths between $\lambda_{\text{ex}} = 240$ and 800 nm (1 nm
285 increments) and an emission range between $\lambda_{\text{em}} = 247$ and 829 nm (0.58 nm increments). Exposure
286 times of 1 s were used, except for 2 μ m green, 3 μ m non-fluorescent PSLs (2 s), and NAD (0.5 s).
287 EEMs were analyzed using Igor Pro.

288

289 **2.4 Calibration lamps and spectral correction**

290 The relative responsivity of a fluorescence detector can vary substantially across its emission range
291 and, therefore, must be spectrally corrected as a function of emission wavelength (e.g., DeRose,
292 2007; Lakowicz, 2004). For spectral correction it was important to choose: (i) light sources covering
293 the full spectral emission range of the SIBS, with temporal stability on the timescale of many months
294 and (ii) a calibrated and independent spectrometer to serve as spectral reference.

295 A deuterium-halogen lamp (DH-Mini; Ocean Optics, Largo, FL, USA) and a halogen projector
296 lamp (EHJ 24 V, 250 W; Ushio Inc., Tokyo, Japan) were used as calibration light sources. Both
297 lamps were connected to a 50 cm optical fiber (FT030, Thorlabs, Newton, NJ, USA) and vertically
298 fixed inside the optical chamber of the Dual-FL spectrometer. An aluminum mirror was attached to
299 the end fitting of the optical fiber, reflecting light in a 90° angle into the detector opening. The pro-
300 jector halogen lamp was allowed to warm up for 30 s before each measurement. For all power levels
301 (100, 150, 200, and 250 W), an integration time of 3 s was used. The DH-Mini was operational for
302 30 min before each measurement. Settings were used as for the projector halogen lamp, however,
303 due to the low emission a high detector gain setting (9 e⁻ per count) was used with an integration time

304 of 25 s. As described in Sect. 2.3, 100 single measurements were taken and averaged (Fig. S1). For
305 the SIBS, both light sources were measured in the same way as for the reference spectra. Measure-
306 ments were performed with a detector amplification at 610 V (see Sect. 4.2). Background measure-
307 ments were taken as described in Sect. 2.2. Projector halogen lamp spectra (at all power levels) were
308 recorded for 3 min, the DH-Mini, due to its low emission intensity, for a duration of 5 min.

309 For the halogen projector lamp, averaged intensity values in each spectral bin were acquired at
310 each power level (150, 200, and 250 W). Spectra measured at 100 W were discarded due to the low
311 and unstable emission at wavelengths shorter than ~ 500 nm (Fig. S1). Reference spectra and spectra
312 recorded by the SIBS were normalized onto the SIBS detection channel 9 ($\lambda_{\text{mean}} = 528.0$ nm), which
313 is, theoretically, the detection channel with the highest responsivity (see Sect. 4.3). The individual
314 spectral correction factors were calculated by dividing the reference spectra by the spectra derived
315 from the SIBS. The final correction factors are a combination ~~of~~ of both light sources where the
316 detection channels 1-5 ($\lambda_{\text{mean}} = 302.2 - 415.6$ nm) include the correction factors for the DH-Mini and
317 the detection channels 6-16 ($\lambda_{\text{mean}} = 443.8 - 721.1$ nm) the correction factors for the halogen projector
318 lamp. At the intersection between channel 5 and 6, both corrections (DH-Mini, halogen) are in good
319 agreement ($\Delta_{\text{correction}} = 0.6$ in channel 6). For all particle measurements described in the following
320 sections, the background signal and raw sample spectra recorded by the SIBS were multiplied by
321 those correction factors.

322

323 2.5 Microscopy of selected reference particles

324 Bright field microscopy was conducted using an Eclipse Ti2 (Nikon, Tokyo, Japan) with a 60x im-
325 mersion oil objective lens and an additional optical zoom factor of 1.5, resulting in a 90x magnifica-
326 tion. Glass cover slips, used as collection substrates in the particle impactor (Sect. 2.2), were put onto
327 a specimen holder and fixed with tape. Images were recorded using a DS Qi2 monochrome micro-
328 scope camera with 16.25 megapixels and z-stacks of related images were created using the software
329 NIS-Elements AR (both Nikon).

330

331 2.6 Ambient measurement setup and data analysis

332 The SIBS was operated between the 5th of April to the 7th of May 2018 from a fourth floor roof
333 laboratory on the roof (fourth floor inside a roof laboratory) of at the Max Planck Institute for Chem-
334 istry in Mainz, Germany (49°59'28.2"N, 8°13'44.5"E) similar to measurements as described in
335 Huffman et al. (2010) using a UV-APS. The period between the 12th and 18th of April 2018 is de-
336 scribed here to highlight the capability of the SIBS to monitor ambient aerosol. Beside of the SIBS,

337 four additional instruments (data not shown within this study) were connected with ~20 cm conduc-
338 tive tubing ($\frac{1}{4}$ inch) to a sample airflow splitter (Grimm Aerosol Technik GmbH & Co. KG, Ain-
339 ring, Germany). The splitter was connected to 1.5 m conductive tubing ($\frac{5}{8}$ inch), bent out of the
340 window, and connected to 2.4 m stainless steel tubing ($\frac{5}{8}$ inch, Dockweiler AG, Neustadt-Glewe,
341 Germany) vertically installed. Between a TSP head (total suspended particles, custom-made) and the
342 stainless steel tubing, a diffusion dryer (1 m, 1 kg silica) was installed. Silica was exchanged every
343 third to fourth day and periodic forced trigger measurements were performed *daily*. The total flow
344 was ~8.4 l/min.

345 For measurements presented here, *only* particles were *only* included if they showed fluorescence
346 emission in at least two consecutive spectral channels. This filter was applied to limit noise intro-
347 duced from measurement artifacts from a variety of sources and will need to be investigated in more
348 detail. The conservative analysis approach here suggests that the values reported are likely to be a
349 lower limit for fluorescent particle number and fraction. The observations are in line with previous
350 measurements, however, giving general support that the SIBS measurements are reasonable. Note
351 that the maximum repetition rate of the xenon lamps is 125 Hz, corresponding to maximum concen-
352 trations of 20 particles per cm^{-3} (see Sect. 3.3). Because ~50% of the total coarse particle number
353 were excited by xenon 1 and xenon 2, the fluorescent particle concentrations and fluorescent fractions
354 are corrected accordingly.

355

356 **3. Design and components of the SIBS**

357 The SIBS is based on the general optical design of the WIBS-4A (e.g., Foot et al., 2008; Healy et al.,
358 2012; Hernandez et al., 2016; Kaye et al., 2005; Perring et al., 2015; Robinson et al., 2017; Savage
359 et al., 2017; Stanley et al., 2011) with improvements based on a lower particle sizing limit, resolved
360 fluorescence detection, and a broader emission range. The instrument provides information about
361 size, particle asymmetry, and fluorescence properties for individual particles in real-time. The exci-
362 tation wavelengths are optimized for the detection of the biological fluorophores tryptophan,
363 NAD(P)H, and riboflavin. However, other fluorophores in PBAP will certainly fluoresce at these
364 excitation wavelengths as many of them cluster in two spectral fluorescence “hotspots” as summa-
365 rized in Pöhlker et al. (2012 and references therein) and as shown for WIBS-4A measurements by
366 Savage et al. (2017). Figure 1 shows an overview of excitation wavelengths and emission ranges of
367 the UV-APS, WIBS-4A, WIBS-NEO, and SIBS for bioaerosol detection in relation to the spectral
368 location of selected biofluorophores, such as tyrosine, tryptophan, NAD(P)H, riboflavin, and chloro-
369 phyll *b*. At $\lambda_{\text{ex}} = 285$ nm, the SIBS excites fluorophores in the “protein hotspot”, at $\lambda_{\text{ex}} = 370$ nm
370 fluorophores in the “flavin/coenzyme hotspot” (Pöhlker et al., 2012). In contrast to the UV-APS, the
371 SIBS is able to detect fluorescence signals from chlorophyll due to the extended upper spectral range

372 of detection (up to $\lambda_{em} = 721$ nm). Both the WIBS-4A and WIBS-NEO cover the spectral emission
373 range for chlorophyll *b*, however, cannot provide resolved spectral information to separate it from
374 other fluorophores. Table 2 summarizes and compares parameters and technical components of the
375 SIBS, WIBS-4A, and WIBS-NEO. The individual components are described in detail in the subse-
376 quent sections.

377 *To avoid potential misunderstanding, it is important to note that the SIBS described in this study*
378 *is not related to spark-induced breakdown spectroscopy instrumentation, which uses the same acro-*
379 *nym (e.g., Bauer & Sonnenfroh, 2009; Hunter et al., 2000; Khalaji et al., 2012; Schmidt & Bauer,*
380 *2010). The DMT SIBS discussed here was recently used as part of a study investigating aerosols in*
381 *several ambient outdoor environments (Nasir et al., 2018), but the study here is the first to discuss*
382 *important technical details of the instrument design and operation.*

383

384 **3.1 Aerosol inlet and flow diagram**

385 The design for the aerosol inlet of the SIBS is identical to the inlet of the WIBS-4A and WIBS-NEO.
386 A detailed flow diagram is shown in Figure S2. Aerosol is drawn in via an internal pump as laminar
387 air flow through a tapered delivery nozzle (Fig. S2a) where sheath (~2.2 l/min) and sample flow (~0.3
388 l/min) are separated.

389

390 **3.2 Size and shape analysis**

391 After passing the delivery nozzle, entrained particles traverses a 55 mW continuous-wave diode laser
392 at $\lambda = 785$ nm (#2 in Fig. 2 and position #1 in Fig. S3). Unlike in the WIBS-4A and WIBS-NEO (635
393 nm diode laser), the triggering laser in the SIBS is in the near-infrared (IR) region (> 700 nm) and,
394 therefore, outside the detectable emission range of the 16-channel photomultiplier tube (PMT) to
395 avoid scattered light from the particle trigger laser being detected (see Fig. 1). The side and forward
396 scattered light is collected and used for subsequent measurements. Side scattered light is collected
397 by two concave mirrors, which are directed at 90° from the laser beam axis, and reflect the collected
398 light onto a dichroic beam splitter (#7 in Fig. 2). A PMT (H10720-20, Hamamatsu Photonics K.K.,
399 Japan) converts incoming light signals into electrical pulses, which are used for particle triggering
400 and sizing (#6 in Fig. 2). For the determination of the optical particle size, the SIBS uses a calculated
401 calibration curve according to the Lorenz-Mie Theory, assuming spherical and monodisperse PSLs
402 with a refractive index of 1.59 (Brandrup et al., 1989; Lorenz, 1890; Mie, 1908). Compared to aero-
403 dynamic sizing, which depends on particle morphology and density (e.g., Reid et al., 2003; Reponen
404 et al., 2001), the calculated optical diameter can vary significantly if the assumption of sphericity is

405 not fulfilled. In contrast, optical sizing is not as affected by differences in material density. The in-
406 strument operator must thus be aware of uncertainties in measured particle size due to, e.g., particle
407 morphology, spatial orientation of a particle when traversing the trigger laser or changing refractive
408 indices. In contrast to the WIBS-4A, the SIBS and WIBS-NEO detect **a the full** range of particle sizes
409 **between (SIBS: ~0.3 and 100 μm (nominal); WIBS-NEO: ~0.5 and 30 μm (nominal)), achievable** by
410 using one PMT gain setting instead of switching between a “Low Gain” and “High Gain” setting.
411 Physical and technical details of this Gain-switching method are patent pending and are not publicly
412 available.

413 The forward-scattered light is measured by a quadrant PMT (#5 in Fig. 2) to detect the scatter
414 asymmetry for each particle (Kaye et al., 1991, 1996). A OG-515 long pass filter (Schott AG, Mainz,
415 Germany) prevents incoming light from the xenon flash lamps in a spectral range below 515 ± 6 nm
416 from reaching the Quadrant PMT. To calculate the AF, the root-mean-square variations for each
417 quadrant of the PMT of the forward-scattered light intensities are used (Gabey et al., 2010). The AF
418 broadly relates whether a particle is more spherical or fibril. Theoretically, for a perfectly spherical
419 particle, the AF would be 0, whereas an elongated particle would correspond to an AF of 100 (Kaye
420 et al., 1991). However, due to electrical and optical noise of the Quadrant PMT, the AF value of a
421 sphere is usually between ca. 2 and 6 (according to WIBS-4A service manual (DOC-0345 Rev A)).
422 Because the AF value depends on physical properties of optical components, the baseline for spher-
423 ical particles may shift even within identical instruments (Savage et al., 2017). For example, the study
424 by Toprak & Schnaiter (2013) reported an average AF value for spherical particles of 8 using a
425 WIBS-4A. In contrast, AF values shown by Foot et al. (2008) were, on average, below ~5 for
426 spherical particles measured with a WIBS-2s prototype.

427

428 3.3 Fluorescence excitation

429 Two xenon flash lamps (L9455-41, Hamamatsu) (#3 and #4 in Fig. 2) are used to induce fluores-
430 cence. They emit light pulses, which exhibit a broad excitation wavelength range of 185 to 2000 nm.
431 The light is optically filtered to obtain a **relatively monochromatic defined** excitation wavelength.
432 Further information about spectral properties of the xenon flash lamps can be found elsewhere (Spec-
433 ification sheet TLSZ1006E04, Hamamatsu, May 2015). Figure 3 displays relevant optical properties
434 of the lamps and filters used within the SIBS, WIBS-4A, and WIBS-NEO. For the SIBS, a Bright-
435 Line® FF01-285/14-25 (Semrock Inc., Rochester, NY, USA) single-band bandpass filter is used with
436 $\lambda_{\text{mean}} = 285$ nm and an effective excitation band³ of 14 nm width is used for xenon 1. For xenon 2,

³ The effective excitation band is defined as “guaranteed minimum bandwidth” (GMBW), describing the spectral region a bandpass filter transmits light relative from the mean wavelength. For example, a GMBW of 14 nm means that light is transmitted in a 7 nm spectral range above and below the mean wavelength.

437 the single-band bandpass filter BrightLine® FF01-370/36-25 (Semrock) is used with $\lambda_{\text{mean}} = 370$ nm
438 and with an effective excitation band of 36 nm width. The only difference between all three instru-
439 ments is that the WIBS-4A and WIBS-NEO use a different single-band bandpass filter for xenon 1
440 (Semrock, BrightLine® FF01-280/20-25; $\lambda_{\text{mean}} = 280$ nm; effective excitation band of 20 nm). The
441 excitation light beam for all three instruments is focused on the sample flow within the optical cavity,
442 resulting in a rectangular beam shape of ~5 mm by 2 mm. Xenon 1 is triggered when particles pass
443 position 2 in Figure S3 and approximately 10 μs later xenon 2 is triggered as the particles move
444 further to position 3 in Figure S3. After firing, the flash lamps need ~5 ms to recharge. During the
445 recharge period, particles are counted and sized but no fluorescence information is recorded. The
446 maximum repetition rate of the xenon lamps yields a measurable particle number concentration of
447 $\sim 2 \times 10^4 \text{ l}^{-1}$ (corresponding to 20 cm^{-3}).

448 Irradiance values from light sources becomes a crucial factor when interpreting derived fluores-
449 cence data of LIF instruments because the fluorescence intensity is directly proportional to the inten-
450 sity of incident radiant power, described by the relationship:

451

$$452 \quad F = \phi I_0 (1 - e^{-\epsilon bc}) \quad (1)$$

453

454 ϕ : quantum efficiency, I_0 : intensity of incident light, ϵ : molar absorptivity, b : path length (cell), c :
455 molar concentration (Guilbault, 1990).

456 To measure the irradiance of each xenon lamp after optical filtering, we used a thermal power
457 head (S425C, Thorlabs), which was placed at a distance of 11.3 cm (focus length from xenon arc
458 bow to sample flow intersection) from the xenon lamp measuring over a duration of 1 min at 10
459 xenon shots per s. By measuring new xenon lamps, we observed an average irradiance of 14.8
460 mW/cm^2 for xenon 1 and 9.6 mW/cm^2 for xenon 2, corresponding to ~154 % higher irradiance (spec-
461 trally integrated) from xenon 1. A second set of lamps, used intermittently for three years including
462 several months of continuous ambient measurements and a lab study with high particle concentra-
463 tions, exhibited average irradiance values of 10.8 mW/cm^2 (1σ SD 1.8 mW/cm^2) for xenon 1 and 4.9
464 mW/cm^2 (1σ SD 1.9 mW/cm^2) for xenon 2, corresponding to ~220 % higher irradiance from xenon
465 1. Comparing the nominal, transmission-corrected irradiance data from the two xenon lamps pro-
466 vided by the lamp supplier (Fig. 3a and 3b, red dashed lines), an irradiance imbalance between xenon
467 1 and xenon 2 can be assumed for all three LIF instruments discussed here (SIBS, WIBS-4A, and
468 WIBS-NEO).

469 Results shown here are comparable to multiple WIBS studies (e.g., Hernandez et al., 2016;
470 Perring et al., 2015; Savage et al., 2017), where fluorescence emission intensities at $\lambda_{\text{ex}} = 280$ nm
471 (xenon 1) also show a tendency to be higher than those at $\lambda_{\text{ex}} = 370$ nm (xenon 2).

472 3.4 Spectrally resolved fluorescence detection

473 Fluorescence emission from excited particles is collected by two parabolic mirrors in the optical
474 cavity and delivered onto a custom-made dichroic beam splitter (Semrock, #7 in Fig. 2). The beam
475 splitter allows transmission of incoming light between ~300 and 710 nm, with an average transmis-
476 sion efficiency of 96%. At wavelengths shorter than 300 nm, the transmission decreases rapidly to <
477 20% at 275 nm. At the upper detection end of the SIBS ($\lambda_{\text{mean}} = 721$ nm), the transmission efficiency
478 decreases to ~89%. The scattering light from the diode laser is reflected at a 90° angle onto the PMT
479 used for particle detection and sizing. At the excitation wavelength of 785 nm, the reflection effi-
480 ciency is stated at ~95% (Fig. S4).

481 After passing the dichroic beamsplitter, the photons are led into a grating polychromator (A
482 10766, Hamamatsu) (#8 in Fig. 2). A custom-made transmission grating (Hamamatsu) is used to
483 diffract incoming light within a nominal spectral range between 290.8 – 732.0 nm. In case of the
484 SIBS, a grating with 300 g/mm groove density and 400 nm blaze wavelength is used, resulting in a
485 nominal spectral width of 441.2 nm and a resolution of 28.03 nm/mm. After passing the transmission
486 grating, the diffracted light hits a 16-channel linear array multi-anode PMT (H12310-40, Hamama-
487 tsu) (#9 in Fig. 2) with defined mean wavelengths for each channel as shown in Table 1.

488 For each single particle detected, two spectra are recorded, at $\lambda_{\text{ex}} = 285$ and 370 nm. The detect-
489 able band range of the PMT overlaps the excitation wavelength of xenon 2. Therefore, a notch optical
490 filter (Semrock) is placed between the optical chamber and the grating polychromator to prevent the
491 detector from being saturated. Incoming light at wavelengths shorter than 300 nm and from 362 to
492 377 nm is blocked from reaching the PMT resulting in a reduced spectral bin width for detection
493 channels 1, 3 and 4. The first three detection channels are omitted because their mean wavelengths
494 are below $\lambda_{\text{ex}} = 370$ nm (see also Fig. 1). Accordingly, the emission spectra for xenon 2 excitation
495 begin at channel 4 ($\lambda_{\text{mean}} = 387.3$ nm).

496 Technical data (xenon flash lamps, filters, dichroic beam splitter, PMT responsivity, and trans-
497 mission grating) described in the previous sections (3.3 and 3.4) were provided by Hamamatsu and
498 Semrock. Note that transmission/reflection efficiencies of the dichroic beam splitter, cathode radiant
499 sensitivity of the PMT, and diffraction efficiency data are modeled. Thus, individual components
500 may differ slightly from modeled values, even within the same production batch. Neither company
501 assumes data accuracy or provides warranty, either expressed or implied.

502 *The SIBS was originally designed and marketed to record time- and spectrally-resolved fluores-*
503 *cence lifetimes at two excitation wavelengths.* The fluorescence lifetime of most biofluorophores,
504 serving as targets for bioaerosol detection, are usually below 10 ns (e.g., Chorvat & Chorvatova,
505 2009; Herbrich, et al., 2012; O'Connor et al., 2014; Richards-Kortum & Sevick-Muraca, 1996).
506 However, by choosing xenon lamps as excitation source, recording relevant fluorescence lifetimes

507 in this ns range is hampered by the relatively long decay time of the xenon lamp excitation pulse
508 (~1.5 μ s). In principle, fluorescence lifetime measurements would be possible if the xenon lamps
509 were replaced by appropriate laser excitation sources in the SIBS optical design.

510

511 **3.5 Software components and data output**

512 The SIBS uses an internal computer (#10 in Fig. 2) with embedded LabView-based data acquisition
513 software allowing the user to control functions in real time and change multiple measurement param-
514 eters. As an example, the “Single Particle” tab out of the SIBS interface is shown in Figure S5. Here,
515 the user can define, e.g., the sizing limits of the SIBS (upper and lower threshold) and the minimum
516 size of a particle being excited by the xenon flash lamps. Furthermore, forced trigger measurements
517 can be performed while on this particular tab. Subsequently, the term “forced trigger measurement”
518 will be replaced by “background signal measurement”. A local Wi-Fi network is installed so that the
519 SIBS can be monitored and controlled remotely. A removable hard drive is used for data storage.
520 Data is stored in a HDF5 format to minimize storage space and optimize data write speed. Resulting
521 raw data are processed in Igor Pro. As an example: by using a minimum sizing threshold of 500 nm,
522 the SIBS data output per day, operating in a relatively clean environment (~40 particles per cm^{-3}),
523 can span several hundreds of MB. In contrast, the data output can increase up to ~3 GB daily in
524 polluted areas (~680 particles per cm^{-3}). By lowering the minimum sizing threshold to 300 nm, the
525 data volume can exceed 10 GB per day when sampling in a moderately polluted environment (~180
526 particles per cm^{-3}).

527

528 **4. Results and data validation**

529 **4.1 Validation of SIBS sizing**

530 To validate the optical sizing of the SIBS, twenty particle size standards were analyzed, covering a
531 broad size range from 0.3 to 20 μ m in particle diameter. Overall, the particle size measurements from
532 the SIBS (optical diameter) show good agreement with the corresponding measurements of physical
533 diameter reported by PSL and PS-DVB manufacturers (Fig. 4). For the SIBS and WIBS-NEO, the
534 manufacturer states a nominal minimum size detection threshold of 300 nm. Figure 4 shows that a
535 linear response between optical particle size and physical particle size extends *down* to at least 300
536 nm. Smaller particles were not investigated. The upper size detection threshold is reported by the
537 manufacturer to be nominally 100 μ m. However, the upper limit was not investigated here due to the
538 difficulty in aerosolizing particles larger than this. In most field applications, the upper particle size
539 cut is often far below this value due to unavoidable sedimentation losses of large particles in the inlet

540 system (e.g., Moran-Zuloaga et al., 2018.; Von der Weiden et al., 2009). Note that the size distribu-
541 tions of physical diameter for PS-DVB standards are broader compared to the PSL standards, as
542 reported by the manufacturer (Table S1). This also translates to broader distributions of optical di-
543 ameter measured by the SIBS *for PS-DVB* than for *the* PSL particles. The 0.356 μm PSL sample was
544 an outlier with respect to the overall trend, showing an optical diameter of 0.54 μm . We suspect that
545 this deviation between physical and optical size can be explained by a poor quality of this particular
546 PSL sample lot rather than an instrumental issue, and so it was not included in the calculation of the
547 trend line (Fig. 4). Furthermore, the SIBS was shown to *slightly* undersize the PSLs between 0.6 and
548 0.8 μm , however, the overall trend exhibits a coefficient of determination of $r^2 > 0.99$ ⁸.

549 As mentioned in Sect. 3.2, an important point regarding the SIBS and WIBS-NEO is that the size
550 calibration within the unit cannot be changed by the user, meaning that the PMT output voltages are
551 transformed directly to outputted physical diameter within the internal computer using a proprietary
552 calculation. It is still important, however, for the user to perform sizing calibration checks frequently
553 to verify and potentially post-correct particle sizing of all particle sizing instruments, including the
554 SIBS and WIBS-NEO.

555

556 4.2 Amplification of fluorescence detector

557 As with all optical detection techniques, adequate understanding of detection thresholds is an essen-
558 tial aspect of instrument characterization and use (e.g., Jeys et al., 2007; Savage et al., 2017). Appli-
559 cation of appropriate voltage gain settings must be applied to the physical detection process so as not
560 to lose information about particles that cannot be recovered by post-processing of data. Yet particles
561 in the natural atmosphere exhibit an extremely broad range of fluorescence intensities (many orders
562 of magnitude), arising from the breadth of quantum yields for fluorophores occurring in aerosols and
563 from the steep increase of fluorescence emission intensity with particle size (2nd to 3rd power) (e.g.,
564 Hill et al., 2015; Könemann et al., 2018; Sivaprakasam et al., 2011; Swanson & Huffman, 2018).
565 This range of fluorescence properties is generally broader than the dynamic range of any single in-
566 strument, and so a UV-LIF instrument can be operated, e.g., to either: (i) apply a higher detector gain
567 to allow high sensitivity toward detecting weakly fluorescing particles, often from rather small par-
568 ticles ($< 1 \mu\text{m}$), at the risk of losing fluorescence information for large or strongly fluorescent parti-
569 cles due to detector saturation or (ii) apply a lower detector gain to preferentially detect a wide range
570 of more highly fluorescent particles, but at the risk of not detecting weakly fluorescent or small par-
571 ticles.

572 Amplification voltage of the 16-channel PMT used in the SIBS can be adjusted between 500 and
573 1200 V. Each of the 16 detection channels can also be individually adjusted using digital gain settings
574 within the SIBS acquisition software. This channel-specific gain does not affect the amplification

575 process (e.g., the dynode cascade), but rather modifies the output signal of single detection channels
576 digitally. The digital gain is applied only after the signal collection process, and so cannot compensate
577 for a signal that is below the noise threshold or that saturates the detector. The digital gain was thus
578 left at the maximum gain level (255 arbitrary units (a.u.)) for all channels during particle measure-
579 ments discussed here.

580 To explore the influence of amplification voltage on particle detectability, 0.53 μm purple PSLs
581 were chosen to arbitrarily represent the lower limit of detectable fluorescence intensity. Using larger
582 (0.96 μm) particles comprised of the same purple fluorophore, Könemann et al. (2018) showed that
583 the particles were only narrowly detectable above the fluorescence threshold in each of the three
584 channels of a WIBS-4A (same unit as used in Savage et al., 2017) and so the smaller, 0.53 μm PSLs
585 were chosen here as a first proxy for the most weakly fluorescing particles we would expect to detect.
586 To improve the signal to noise ratio (SNR) for the lower fluorescence detection limit, the PMT am-
587 plification voltage was varied in seven steps between 500 and 1000 V (corresponding to a gain from
588 10^3 to 10^6 , specification sheet TPMO1060E02, Hamamatsu, June 2016) for purple PSLs and back-
589 ground signals (Fig. 5a). Whereas PSL spectra at a PMT amplification of 500 V were indistinguish-
590 able from the background signal ($+1\sigma$ SD), spectra show a discernable peak at $\lambda_{\text{mean}} = 415.6$ nm
591 above 600 V. Subsequently, the SIBS was operated with a PMT amplification voltage of 610 V
592 corresponding to the lowest SNR threshold accepted (Fig. 5a, b). The detection of small biological
593 particles was tested by measuring the emission spectrum of *S. cerevisiae* as an example of a PBAP
594 (see also Pöhlker et al., 2012). On average, the size of intact *S. cerevisiae* particles range between ~ 2
595 – 10 μm (e.g., Pelling et al., 2004; Shaw et al., 1997). To test the ability of the SIBS to detect low
596 intensity emissions, we separately analyzed *S. cerevisiae* particles between 0.5 and 1 μm , which most
597 likely includes cell fragments caused by the aerosolization process (Fig. 5c). The tryptophan-like
598 emission, peaking in detection channel 2 ($\lambda_{\text{mean}} = 330.6$ nm) for $\lambda_{\text{ex}} = 285$ nm, reveals intensity values
599 below 100 a.u., which are comparable to fluorescence intensity values derived from 0.53 μm purple
600 PSLs (detection channel 5, $\lambda_{\text{mean}} = 415.6$ nm, Fig. 5d). These two tests for *S. cerevisiae* and 0.53 μm
601 purple PSLs confirmed the instruments ability to detect emission spectra from particles at least as
602 strongly fluorescent as these two test cases, leaving a wide range to detect larger and more intensely
603 fluorescing particles. By using a 3σ SD threshold, the fluorescence peak at $\lambda_{\text{mean}} = 415.6$ nm of 0.53
604 μm purple PSLs is still detectable but cannot be distinguished from the background signal at a 6σ SD
605 threshold anymore. Therefore, fluorescence intensity values at the lower detection limit should be
606 treated with care. Corrected spectra of both *S. cerevisiae* and 0.53 μm purple PSLs can be found in
607 the supplement (Fig. S6). By operating the SIBS at relatively low detector amplification, very weak
608 fluorescence, especially from small particles (< 1 μm) might not exceed the detection threshold dur-

609 ing field applications and would be missed. Further investigation will be necessary to choose ampli-
610 fication voltages appropriate for individual applications where smaller or otherwise weakly fluores-
611 cent particles might be particularly important. For all subsequent measurements discussed here, a
612 PMT amplification voltage of 610 V was used.

613 Saturation only occurred for 15 and 20 μm non-fluorescent PS-DVB particles. As highlighted in
614 Figure S7, the polystyrene/detergent signal (Könemann et al., 2018) at $\lambda_{\text{ex}} = 285 \text{ nm}$ for 10 μm PS-
615 DVB particles can be spectrally resolved (Fig. S7b), whereas the spectrum for 15 μm PS-DVB par-
616 ticles (Fig. S7e) is altered due to single particles ($\sim 10\%$ out of 400 particles) saturating the detector
617 (at 62383 a.u.). By comparing the defined lower detection end (Fig. 5) to the upper end (Fig. S7), a
618 quantitative difference of approximately three orders of magnitude can be estimated, indicating a
619 wide detectable range at the chosen amplification voltage setting.

620

621 **4.3 Wavelength-dependent spectral correction of detector**

622 The 16 cathodes of the PMT should be considered as independent detectors with wavelength depend-
623 ent, individual responsivity and amplification characteristics. In combination with physical properties
624 of technical components (e.g., excitation sources, optical filters, gratings), an instrumental-specific
625 spectral bias might result in incorrect or misleading spectral patterns if not corrected (e.g., DeRose,
626 2007; DeRose et al., 2007; Holbrook et al., 2006). To compensate for such potential instrumental
627 biases, we used a spectral correction approach as described in Sect. 2.4. The spectral correction fac-
628 tors are comparable to the theoretical responsivity of the PMT with the highest correction for chan-
629 nels 1-4 ($\lambda_{\text{mean}} = 302.2 - 387.3 \text{ nm}$) and 14-16 ($\lambda_{\text{mean}} = 666.5 - 721.1 \text{ nm}$) (Fig. 6). Channel 8 (λ_{mean}
630 $= 500.0 \text{ nm}$) shows the highest responsivity and channels 6 and 7 ($\lambda_{\text{mean}} = 443.8$ and 471.9 nm) exhibit
631 a noticeable lower responsivity than their adjacent channels (see also Sect. 4.4.1). The spectral cor-
632 rection shows several peaks (e.g., detector channels 3, 5, and 8) and dips (e.g., detector channels 4,
633 6, and 7) (Fig. 6), however, this pattern is due to gain variations for different channels and is not
634 noise.

635 It is important to note that the detector settings and spectral correction uniquely refer to the SIBS
636 unit as it was used for the current study. Due to technical and physical variability as stated above, it
637 is likely that the spectral correction required for other SIBS units would be somewhat different. Fur-
638 thermore, the wavelength-dependent detector correction may change over time due to material fa-
639 tigue or contaminations in the optical chamber affecting background signal measurements. Periodic
640 surveillance and adjustments are therefore required, especially after measurements where the instru-
641 ment was exposed to high particle concentrations or was operated during extreme weather or envi-
642 ronmental conditions (e.g., temperature, humidity, vibration). For particle sizing verification, we rec-
643 ommend the use of 0.5, 1, and 3 μm non-fluorescent PSLs. Regarding a fluorescence response check,

644 we recommend 2 μm green and 2 μm red PSLs for the validation of the spectral responsivity maxi-
645 mum and the upper (near-IR) detection range. To our knowledge, no fluorescent dyed PSLs are avail-
646 able to verify the response within the lower spectral detection range (UV) of the SIBS. However, the
647 polystyrene signal of 3 μm non-fluorescent PSLs (Fig S7g, h, i, see also Könemann et al., 2018)
648 represents a compromise between signal strength at $\lambda_{\text{ex}} = 285 \text{ nm}$ and aerosolization efficiency (com-
649 pared to PSLs with larger sizes) for a spectral responsivity validation.

650

651 **4.4 Fluorescence spectra of standards**

652 **4.4.1 PSL standards**

653 The SIBS spectra for the four different PSL standards, covering an emission range from UV to near-
654 IR, generally agree well with the corresponding reference spectra (Fig. 7). Each of the two excitation
655 wavelengths probe separate fluorescent modes, which appear at approximately the same emission
656 wavelength for a given PSL type (e.g., $\lambda_{\text{em}} = \sim 580 \text{ nm}$ for red PSLs, Fig. 7j), as discussed by
657 Könemann et al. (2018). Moreover, even the rather weak polystyrene and detergent fluorescence,
658 systematically associated with PSL suspensions (Könemann et al., 2018), is resolved by the SIBS at
659 $\lambda_{\text{ex}} = 285 \text{ nm}$ and $\lambda_{\text{em}} = \sim 300 \text{ nm}$ (Fig. 7b, e, h, k). It is further noteworthy that emissions **intensity** at
660 $\lambda_{\text{ex}} = 285 \text{ nm}$ **are is** generally higher than derived emissions **intensity** at $\lambda_{\text{ex}} = 370 \text{ nm}$ (Fig. 7c, f, i, l),
661 supporting the finding that a particle receives higher irradiance values from xenon 1 than from xenon
662 2 (see also Sect. 3.3).

663 As mentioned in Sect. 4.3, detection channels 6 and 7 require relatively large correction factors.
664 For 2.07 μm purple PSLs (Fig. 7b, c), the SIBS spectra closely match the references spectra after
665 correction. For the 2.1 μm blue PSLs (Fig. 7e, f), however, the corrected spectrum matches the ref-
666 erence spectrum well, except at detection channel 6 ($\lambda_{\text{mean}} = 443.8 \text{ nm}$), where the SIBS spectrum is
667 lower than the reference spectrum by approximately 50%. This effect was also observed for 1 μm
668 blue PSLs (Thermo Fisher, B0100), doped with the same fluorophore (data not **shown included in**
669 **this study**). The reason for this **discrepancy malfunction** is unknown. Nevertheless, because this effect
670 only occurs noticeably for highly fluorescent blue PSLs and NAD (see also Sect. 4.4.2), one expla-
671 nation could be that the instrument-dependent dynode cascade (the electronic amplification stages)
672 for this particular detection channel is suppressed, resulting in a lower amplification efficiency. In
673 this case, relatively low signals could be amplified correctly, whereas medium or high intensity emis-
674 sion could only be amplified up to a certain level. The amplification threshold for detection channel
675 6 is, however, unknown and needs further verification.

676

677

678 4.4.2 Biofluorophore standards

679 Figure 8 and 9 highlight fluorescence spectra of different biofluorophores measured by the SIBS,
680 which correspond to related reference spectra (compare also Pöhlker et al., 2012), showing that amino
681 acids (fluorescence emission only at $\lambda_{\text{ex}} = 285$ nm), co-enzymes and flavin compounds (fluorescence
682 emission at $\lambda_{\text{ex}} = 285$ and 370 nm), and chlorophylls (fluorescence emission only at $\lambda_{\text{ex}} = 370$ nm)
683 can be spectrally distinguished.

684 The uncorrected spectrum of tryptophan (Fig. S9) highlights the necessity of a spectral correction
685 to compensate for the low detector responsivity within the UV and near-IR bins. If the fluorescence
686 signal of tryptophan remains uncorrected, the spectra is shifted slightly to longer wavelengths (red-
687 shifted) due to the low responsivity of channel 2 in comparison to channel 3, resulting in misleading
688 spectral information. For NAD (Fig. 8h, i), fluorescence intensity values of channel 6 are lowered
689 due the suppressed amplification efficiency in this particular channel as described for blue PSLs
690 (Sect. 4.4.1).

691 All biofluorophores (except chlorophyll types) were aerosolized as dry powders (see Sect. 2.2)
692 to avoid fluorescence solvatochromism effects, ~~means solvent dependent spectral shifts relative to~~
693 ~~the dry fluorophore state, which serves as a reference case here~~ (e.g., Johnson et al., 1985). Solva-
694 tochromism of fluorophores in aqueous solution – the only atmospherically relevant case – typically
695 shifts fluorescence emissions to longer wavelengths due to the stabilized excited state caused by polar
696 solvents (Lakowicz, 2004). This spectral red-shift can be seen in Figure S10, where the peak maxi-
697 mum for NAD shows a difference of ~15 nm between a dry and water-solv~~ated~~ state, whereas
698 riboflavin reveals an even higher shift of ~37 nm. Here, solvatochromism serves as an example for
699 fluorescence spectra that vary substantially as a function of the fluorophore's microenvironments
700 (e.g., solvent polarity, pH, temperature).

701 Each of the three types of chlorophyll exhibit the weakest emission of all biofluorophores meas-
702 ured within this study, however the SIBS was able to detect the fluorescence signal at $\lambda_{\text{ex}} = 370$ nm
703 for all three (Fig. 9). The spectral difference between chlorophyll *a* and *b* is only minor at $\lambda_{\text{ex}} = 370$
704 nm ($\Delta\lambda = 8.3$ nm) for which the spectral resolution of the SIBS is not capable of distinguishing be-
705 tween ~~both~~ types (Fig. 9a, b, c, d and Fig. S11) (e.g., French et al., 1956; Welschmeyer, 1994). Nev-
706 ertheless, the SIBS shows the ability to distinguish between chlorophyll *a* and *b*, and bacteriochloro-
707 phyll due to the red-shift in the bacteriochlorophyll spectrum ($\Delta\lambda = 28.5$ nm at $\lambda_{\text{ex}} = 370$ nm, between
708 chlorophyll *a* and bacteriochlorophyll). This may provide a further discrimination level regarding
709 algae, plant residues, and cyanobacteria. Bacteriochlorophyll also shows a second and even stronger
710 emission peak at $\lambda_{\text{ex}} = 370$ nm ($\lambda_{\text{em}} = \sim 800$ nm) that could help further distinguish it from chlorophyll
711 *a* and *b*, but the SIBS spectrometer cannot currently detect this far into the IR (e.g., Rijgersberg et
712 al., 1980; Van Grondelle et al., 1983).

713 Overall, fluorescence emissions recorded by the SIBS are in good agreement with measured ref-
714 erence spectra. However, care must be taken as to the interpretation of fluorescence emissions cov-
715 ering broad spectral ranges, which span regimes with large differences between individual correction
716 factors (e.g., channel 15 ($\lambda_{\text{mean}} = 693.9$ nm, Fig.7l) and channel 2 ($\lambda_{\text{mean}} = 330.6$ nm, Fig.8k). For the
717 SIBS, namely the first two UV detection channels and the last two near-IR channels *should have to*
718 be treated with care. Further investigations *are* is required for a careful assessment of how the spectral
719 correction can be applied properly *with respect to onto* fluorescent and non-fluorescent atmospheric
720 particles.

721

722 4.5 Particle asymmetry measurements

723 The AF of spherical particles such as PSLs (Fig. 10a, b) and ultrapure water droplets is approximately
724 10 (Table 3), which is slightly higher than reported values for spherical particles by, e.g., Savage et
725 al. (2017) (AF= ~5) or Toprak & Schnaiter (2013) (AF= ~8) using a WIBS. It is noteworthy that the
726 AF of water droplets increases slightly with increasing droplet size and, therefore, contributes to the
727 mean value (Fig. S13). This effect is most likely based on a decreasing surface tension with increas-
728 ing droplet size for which the droplet morphology is changed to a more oval shape within the sample
729 flow. A similar effect regarding a potential droplet deformation using an Airborne Particle Classifier
730 (APC) was observed by Kaye et al., (1991). Even if the morphology of ammonium sulfate (crystal-
731 line, Fig. 10d) and Fe₃O₄ (irregular clusters, Fig. 10f) is diverse, the *if* difference *s* in AF *s* is only
732 minor (~13 and 14, Table 3), indicating that most naturally occurring aerosols (e.g., sea salt, soot,
733 various bacterial and fungal clusters) will occur in a AF regime between ~10 and 20. Only rod-shaped
734 carbon nanotubes (110-170 nm diameter, 5-9 μm length) show increased AFs with a mean value at
735 ~22 (Table 3) at which also, e.g., bacteria would occur (Fig. 10h). No particles observed exhibited
736 average AF values >25, as would have been expected for, e.g., carbon nanotubes. Because the range
737 of AF values for homogenous particles is relatively broad and the differences between morphologi-
738 cally diverse particle types is only minor (Table 3), the question can be raised to what extent particles
739 could be distinguished based on the AF under ambient conditions. *Similar broad AF ranges were*
740 *found in Healy et al., (2012), measuring sodium chloride, chalk, and several pollen and fungal spores*
741 *types.* As also discussed by Savage et al. (2017), the AF values reported by SIBS and WIBS units
742 should be treated with extreme care.

743 The validation of asymmetry measurements is challenging due to unavoidable particle and aero-
744 solization effects (e.g., particle agglomeration and spatial orientation within the sample flow) and the
745 lack of standardized procedures for AF calibrations. Measurements performed in this study do, there-
746 fore, only serve as a rough AF assignment. Moreover, even if both the SIBS and WIBS use the same
747 technical components for defining AFs, a direct intercomparison cannot be applied due to technical

748 variability (e.g., PMT related signal-to-noise ratio or the alignment of optical components). Addi-
749 tionally, it is currently unknown in how far the 785 nm diode laser of the SIBS affect asymmetry
750 measurements compared to the WIBS using a 635 nm diode laser.

751

752 4.6 Initial ambient measurements

753 Several weeks of initial ambient SIBS measurements *have been were* conducted on the roof of the
754 Max Planck Institute for Chemistry in Mainz, Germany. At *a nearby building site the same location*,
755 Huffman et al. (2010) conducted one of the first ambient UV-APS studies *in the year 2006*. Moreo-
756 ver, Toprak & Schnaiter (2013) conducted a WIBS-4A study at a comparable site in central Germany
757 *from 2010 to 2011*. The aim of this brief ambient section is to validate that the SIBS-derived key
758 aerosol and fluorescence data are *reasonable and relatively* consistent with the aforementioned stud-
759 ies. We found a good agreement between the coarse mode ($\geq 1 \mu\text{m}$) number concentrations ($N_{T,c}$) of
760 the SIBS ($N_{T,c}$ ranging from *0.25 0.19* to *1.59 1.24* cm^{-3} , with a mean of *0.76 0.59* cm^{-3}) *and previous*
761 *data from* the UV-APS (mean $N_{T,c}$: 1.05 cm^{-3} (Huffman et al., 2010)) *and the WIBS-4A* (mean $N_{T,c}$:
762 0.58 cm^{-3} (Toprak and Schnaiter, 2013)) (Fig.11a). Furthermore, good agreement was found between
763 coarse mode fluorescent number concentrations ($N_{F,c}$) of the SIBS *with a 3 σ SD threshold* (mean $N_{F,c}$
764 (3σ): *0.025 0.019* cm^{-3}), the UV-APS (mean $N_{F,c}$: 0.027 cm^{-3} (Huffman et al., 2010)), and the WIBS-
765 4A *with a 3 σ SD threshold* (mean $N_{F,c}$ (3σ): 0.031 cm^{-3} (Toprak and Schnaiter, 2013)) (Fig.11a). Sim-
766 ilarly, the fraction of fluorescent particles in the coarse mode ($N_{F,c}/N_{T,c}$) compares well between SIBS
767 *with a 3 σ SD threshold* (mean $N_{F,c}(3\sigma)/N_{T,c}$: 4.2 %), the UV-APS (mean $N_{F,c}/N_{T,c}$: 3.9 % (Huffman et
768 al., 2010)), and the WIBS-4A *with a 3 σ SD threshold* (mean $N_{F,c}(3\sigma)/N_{T,c}$: 7.3 % (Toprak and
769 Schnaiter, 2013)) (Fig.11b). Expectedly, a 1σ SD threshold gives much higher *SIBS* fluorescent frac-
770 tions of 39.2 %, whereas a 6σ SD threshold corresponds with much lower fluorescent fractions of
771 1% (Fig.11b). Note that no perfect match between our results and the studies by Huffman et al.
772 (2010), and Toprak & Schnaiter (2013) can be expected, since the measurements took place with
773 different sampling setups and during different seasons. Furthermore, the spectrally resolved SIBS
774 data makes the definition of fluorescent fraction more complex than for UV-APS and WIBS data
775 (see Sect. 2.6). However, the overall good agreement confirms that the SIBS produces reasonable
776 results in an ambient setting. Further, the single particle fluorescence spectra are reasonable with
777 respect to typical biofluorophore emissions (Pöhlker et al., 2012). Exemplary spectra ($\lambda_{\text{ex}} = 285$ and
778 370 nm) of ambient single particles can be found in the supplement (Fig.S14). An in-depth analysis
779 of extended SIBS ambient datasets is subject of ongoing work.

780

781

782 5. Summary and conclusions

783 Real-time analysis of atmospheric bioaerosols using commercial LIF instruments has largely been
784 restricted to data recorded in only 1-3 spectrally integrated emission channels, limiting the interpret-
785 ation of fluorescence information. Instruments that can record resolved fluorescence spectra over a
786 broad range of emission wavelengths may thus be required to further improve the applicability of
787 LIF instrumentation to ambient PBAP detection. Introduced here is the SIBS (DMT, Longmont, CO,
788 USA), as a new aerosol fluorescence detector, which is an instrument that provides resolved fluores-
789 cence spectra ($\lambda_{\text{mean}} = 302 - 721$ nm) from each of two excitation wavelengths ($\lambda_{\text{ex}} = 285$ and 370 nm)
790 for single particles. The current study introduces the SIBS by presenting and experimentally validat-
791 ing its key functionalities. This work critically assesses the strengths and limitations of the SIBS with
792 respect to the growing interest in real-time bioaerosol quantification and classification. It should be
793 noted that the study is an independent evaluation that was not conducted, ~~or~~ endorsed, ~~or co-authored~~
794 by the manufacturer ~~or representatives~~. Overall, this work confirms a precise particle sizing between
795 300 nm and 20 μm and the particle discrimination ability based on spectrally resolved fluorescence
796 information of several standard compounds.

797 The SIBS was operated at a low PMT detector amplification setting (610 V) to retain capacity to
798 detect large or brightly fluorescent particles. It was confirmed, however, that even weak fluorescence
799 signals from 0.53 μm purple PSLs and from small *S. cerevisiae* fragments (0.5 - 1 μm) can be clearly
800 distinguished from the background signal. Saturation events were only observed for the polysty-
801 rene/detergent signal from relatively large 15 and 20 μm PS-DVB particles. Nevertheless, the fluo-
802 rescence intensity detection threshold is highly instrument-dependent due to the complex interaction
803 of single technical components across individual instruments. For example, xenon 1 exhibited ~154
804 % higher irradiance than xenon 2 (both new lamps) due to differences in the properties of xenon
805 emission and the optical filters used. For used xenon lamps (> 4000 hours of use), an even higher
806 difference of ~220 % was observed. Thus, a defined fluorescence detection threshold will most likely
807 change over time due to, e.g., material fatigue. *Additionally, alternating irradiance properties might*
808 *significantly contribute to observed differences in performance of similar instrument types (e.g.,*
809 *Hernandez et al., 2016), expressly underlining the need for a fluorescence calibrant applicable*
810 *across LIF-instruments (e.g., Robinson et al., 2017). Nevertheless, to the best of our knowledge, there*
811 *is currently no standard reference available that fulfills the requirements to serve as a calibrant for*
812 *multi-channel, multi-excitation LIF-instruments.* ~~These o~~bservations *in this study* are valid not only
813 for the SIBS, but also for the WIBS-4A and WIBS-NEO and lead to important implications for in-
814 terpretation of particle data. In particular, a particle that exhibits measurable fluorescence in WIBS
815 channel FL1, but only weak fluorescence in channel FL3 could be assigned as an “A-type” particle

816 in one instrument but an “AC-type” particle in an instrument with slightly stronger xenon 2 irradi-
817 ance. These differences in classification can be extremely important to interpretation of ambient data
818 (e.g., Perring et al., 2015; Savage et al., 2017).

819 The PMT used in the SIBS shows a wavelength-dependent sensitivity distribution along all 16
820 detection channels. To compensate for this characteristic and to be able to use the broadest possible
821 fluorescence emission range, the measured emission spectra were corrected with respect to reference
822 spectra acquired from deuterium and halogen lamps. A spectral correction over a broad emission
823 range also introduces drawbacks, however, that LIF-instrument users should keep in mind while in-
824 terpreting derived fluorescence information. In particular, the first two (UV) and the last two (near-
825 IR) detection channels should be treated with care, because they have require larger correction factors
826 compared to adjacent channels. Ultimately, the correction factor and amplification voltages applied
827 to the detector will be experiment-specific and will need to be investigated with respect to individual
828 experimental aims. To this extent, possible differences between instruments and important calibra-
829 tions complicate the concept of the instrument being commercially available. Individual users may
830 desire to be able to purchase the SIBS as a “plug-and-play” detector, but using without a critical
831 understanding of these complexities would not be appropriate at this time and could lead to inad-
832 vertent misinterpretation of the data.

833 Fluorescence spectra of fluorescent PSLs, amino acids, co-enzymes, and flavins measured by the
834 SIBS agree well with corresponding spectra recorded with an offline reference spectrometer. Thus,
835 the SIBS was shown to be capable of clearly distinguishing between different particle types based on
836 resolved fluorescence information. Furthermore, the extended fluorescence emission range ($\lambda_{em} = >$
837 700 nm) enables the SIBS also to distinguish chlorophyll *a* and *b* from bacteriochlorophyll, poten-
838 tially opening new possibilities for the detection of, e.g., algae, plant residues, and cyanobacteria.

839 Particle asymmetry measurements revealed that spherical PSLs have an AF of 9.9 (\pm 3.6),
840 whereas other materials (ammonium sulfate, Fe₃O₄, and carbon nanotubes) show AF values of 13.1
841 (\pm 8.1), 14.4 (\pm 7.4), and 21.6 (\pm 12.7), respectively. Because differences of measured AF value
842 between morphologically diverse particle types are small and within the ranges of uncertainty for the
843 measurement of a given set of particles, it is questionable how well particles can be distinguished
844 based on the AF as presently measured by the quadrant PMT as presently measured. Users of SIBS
845 and WIBS instruments should apply extreme care if using AF data. It is also likely that different
846 instrument units may have very different AF responses with respect to this measurement. At a mini-
847 mum, each individual unit needs to be rigorously calibrated to known particle types to determine if
848 AF values are sufficiently different (e.g., separated by several standard deviations) to justify scientific
849 conclusions based on the metric.

850 Exemplary ambient data, measured between the 12th and 18th of April 2018 on the roof of the
851 Max Planck Institute for Chemistry in Mainz (Germany), are consistent with LIF measurement data
852 using a UV-APS (Huffman et al., 2010) and a WIBS-4A (Toprak and Schnaiter, 2013). Total coarse
853 particle number concentrations revealed a mean value of 0.76 ~~0.59~~ cm⁻³ (1.05 cm⁻³ (Huffman et al.,
854 2010); 0.58 cm⁻³ (Toprak and Schnaiter, 2013)) of which ~4.2% are considered to be fluorescent
855 using a 3 σ SD threshold (3.9% (Huffman et al., 2010); 7.3% (Toprak and Schnaiter, 2013)), including
856 only particles that show fluorescence emission in at least two adjoining detection channels. Using
857 a 1 σ and 6 σ SD threshold results in fluorescent fractions of 39.2% and 1% respectively. However,
858 the applicability of different threshold strategies for the SIBS is currently under investigation and
859 needs further verifications.

860 The results suggest that the SIBS has the ability to increase the selectivity of detection of fluo-
861 rescent biological and non-biological particles by use of two excitation wavelengths and 16-channel
862 resolved fluorescence information in combination with a broad detectable emission range. The ap-
863 plicability of described methods onto ambient datasets is currently under investigation. Data shown
864 here and the detailed insights of technical components used in the SIBS will be broadly beneficial
865 for users of LIF instruments providing resolved fluorescence information, but also for users of vari-
866 ous generations of WIBS and other LIF instruments widely applied within the bioaerosol community.

867

868 **6. Data availability**

869 The data of the key results presented here can be provided upon request. For specific data requests,
870 please refer to the corresponding authors.

871

872 **Acknowledgements**

873 This work was supported by the Max Planck Society (MPG) and the Max Planck Graduate Center
874 with the Johannes Gutenberg-University Mainz (MPGC). Financial support for Nicole Savage was
875 provided by the Phillipson Graduate Fellowship from the University of Denver. We thank Maria
876 Praß, Mira Pöhlker, Jan-David Förster, Meinrat O. Andreae, Peter Hoor, Viviane Després, Benjamin
877 Swanson, Jorge Saturno, Bruna Holanda, Florian Ditas, Daniel Moran-Zuloaga, Björn Nillius, Jing
878 Ming, Gavin McMeeking, Gary Granger, Alexis Attwood, Greg Kok, Robert MacAllister, John
879 Walker, Matt Mahin, Matt Freer, Uwe Kuhn, Minghui Zhang, Petya Yordanova, Naama Lang-Yona,
880 and members of the Mainz Bioaerosol Laboratory (MBAL) for their support and stimulating discus-
881 sions.

882 7. References

- 883 Agranovski, V., Ristovski, Z., Hargreaves, M., Blackall, P. . and Morawska, L.: Real-time measurement of bacterial
884 aerosols with the UVAPS: performance evaluation, *J. Aerosol Sci.*, 34(3), 301–317, doi:10.1016/S0021-
885 8502(02)00181-7, 2003.
- 886 Agranovski, V., Ristovski, Z. D., Ayoko, G. A. and Morawska, L.: Performance Evaluation of the UVAPS in Measuring
887 Biological Aerosols: Fluorescence Spectra from NAD(P)H Coenzymes and Riboflavin, *Aerosol Sci. Technol.*,
888 38(4), 354–364, doi:10.1080/02786820490437505, 2004.
- 889 Baron, P. A. and Willeke, K.: *Aerosol fundamentals*, *Aerosol Meas. Princ. Tech. Appl.*, 2, 2001.
- 890 Bauer, A. J. R. and Sonnenfroh, D. M.: Spark-induced breakdown spectroscopy-based classification of bioaerosols, in
891 Safety, Security & Rescue Robotics (SSRR), 2009 IEEE International Workshop on, pp. 1–4, IEEE., 2009.
- 892 Bhangar, S., Huffman, J. A. and Nazaroff, W. W.: Size-resolved fluorescent biological aerosol particle concentrations
893 and occupant emissions in a university classroom, *Indoor Air*, 24(6), 604–617, 2014.
- 894 Brandrup, J., Immergut, E. H., Grulke, E. A., Abe, A. and Bloch, D. R.: *Polymer handbook*, Wiley New York etc., 1989.
- 895 Brosseau, L. M., Vesley, D., Rice, N., Goodell, K., Nellis, M. and Hairston, P.: Differences in detected fluorescence
896 among several bacterial species measured with a direct-reading particle sizer and fluorescence detector, *Aerosol*
897 *Sci. Technol.*, 32(6), 545–558, 2000.
- 898 Calvo, A. I., Baumgardner, D., Castro, A., Fernández-González, D., Vega-Maray, A. M., Valencia-Barrera, R. M.,
899 Oduber, F., Blanco-Alegre, C. and Fraile, R.: Daily behavior of urban Fluorescing Aerosol Particles in
900 northwest Spain, *Atmos. Environ.*, 184, 262–277, 2018.
- 901 Caruana, D. J.: Detection and analysis of airborne particles of biological origin: present and future, *Analyst*, 136(22),
902 4641–4652, 2011.
- 903 Chorvat, D. and Chorvatova, A.: Multi-wavelength fluorescence lifetime spectroscopy: a new approach to the study of
904 endogenous fluorescence in living cells and tissues, *Laser Phys. Lett.*, 6(3), 175–193,
905 doi:10.1002/lapl.200810132, 2009.
- 906 Cooper, W. A.: Effects of coincidence on measurements with a forward scattering spectrometer probe, *J. Atmos. Ocean.*
907 *Technol.*, 5(6), 823–832, 1988.
- 908 Crawford, I., Ruske, S., Topping, D. O. and Gallagher, M. W.: Evaluation of hierarchical agglomerative cluster analysis
909 methods for discrimination of primary biological aerosol, *Atmos. Meas. Tech.*, 8(11), 4979–4991, 2015a.
- 910 Crawford, I., Lloyd, G., Bower, K. N., Connolly, P. J., Flynn, M. J., Kaye, P. H., Choularton, T. W. and Gallagher, M.
911 W.: Observations of fluorescent aerosol–cloud interactions in the free troposphere at the Sphinx high Alpine
912 research station, Jungfraujoeh, *Atmos. Chem. Phys.*, 15(19), 26067–26088, 2015b.
- 913 Crouzy, B., Stella, M., Konzelmann, T., Calpini, B. and Clot, B.: All-optical automatic pollen identification: Towards
914 an operational system, *Atmos. Environ.*, 140, 202–212, doi:http://dx.doi.org/10.1016/j.atmosenv.2016.05.062,
915 2016.
- 916 Deepak, A. and Vali, G.: *The International Global Aerosol Program (IGAP) plan: Overview (Vol. 1)*, A. Deepak Pub.,
917 1991.
- 918 DeRose, P. C.: *Standard guide to fluorescence: Instrument calibration and validation*, US Department of Commerce,
919 Technology Administration, National Institute of Standards and Technology., 2007.
- 920 DeRose, P. C., Early, E. A. and Kramer, G. W.: Qualification of a fluorescence spectrometer for measuring true
921 fluorescence spectra, *Rev. Sci. Instrum.*, 78(3), 33107, 2007.
- 922 Després, V. R., Huffman, J. A., Burrows, S. M., Hoose, C., Safatov, A. S., Buryak, G., Fröhlich-Nowoisky, J., Elbert,

923 W., Andreae, M. O., Pöschl, U. and Jaenicke, R.: Primary biological aerosol particles in the atmosphere: A
924 review, *Tellus, Ser. B Chem. Phys. Meteorol.*, 64, doi:10.3402/tellusb.v64i0.15598, 2012.

925 Fennelly, M. J., Sewell, G., Prentice, M. B., O'Connor, D. J. and Sodeau, J. R.: The Use of Real-Time Fluorescence
926 Instrumentation to Monitor Ambient Primary Biological Aerosol Particles (PBAP), *Atmosphere (Basel)*., 9(1),
927 1, 2017.

928 Fernández-Rodríguez, S., Tormo-Molina, R., Lemonis, N., Clot, B., O'Connor, D. J. and Sodeau, J. R.: Comparison of
929 fungal spores concentrations measured with wideband integrated bioaerosol sensor and Hirst methodology,
930 *Atmos. Environ.*, 175, 1–14, 2018.

931 Foot, V. E., Kaye, P. H., Stanley, W. R., Barrington, S. J., Gallagher, M. and Gabey, A.: Low-cost real-time
932 multiparameter bio-aerosol sensors, *Proc. SPIE*, 7116, 71160I–71160I–12, doi:10.1117/12.800226, 2008.

933 French, C. S., Smith, J. H. C., Virgin, H. I. and Airth, R. L.: Fluorescence-Spectrum Curves of Chlorophylls,
934 Pheophytins, Phycoerythrins, Phycocyanins and Hypericin., *Plant Physiol.*, 31(5), 369, 1956.

935 Fröhlich-Nowoisky, J., Kampf, C. J., Weber, B., Huffman, J. A., Pöhlker, C., Andreae, M. O., Lang-Yona, N., Burrows,
936 S. M., Gunthe, S. S., Elbert, W., Su, H., Hoor, P., Thines, E., Hoffmann, T., Després, V. R. and Pöschl, U.:
937 Bioaerosols in the Earth System: Climate, Health, and Ecosystem Interactions, *Atmos. Res.*, 182, 346–376,
938 <https://doi.org/10.1016/j.atmosres.2016.07.018>, 2016.

939 Fuzzi, S., Andreae, M. O., Huebert, B. J., Kulmala, M., Bond, T. C., Boy, M., Doherty, S. J., Guenther, A., Kanakidou,
940 M., Kawamura, K., Kerminen, V.-M., Lohmann, U., Russell, L. M. and Pöschl, U.: Critical assessment of the
941 current state of scientific knowledge, terminology, and research needs concerning the role of organic aerosols
942 in the atmosphere, climate, and global change, *Atmos. Chem. Phys.*, 6(7), 2017–2038, doi:10.5194/acp-6-2017-
943 2006, 2006.

944 Gabey, A. M., Gallagher, M. W., Whitehead, J., Dorsey, J. R., Kaye, P. H. and Stanley, W. R.: Measurements and
945 comparison of primary biological aerosol above and below a tropical forest canopy using a dual channel
946 fluorescence spectrometer, *Atmos. Chem. Phys.*, 10(10), 4453–4466, doi:10.5194/acp-10-4453-2010, 2010.

947 Gabey, A. M., Vaitilingom, M., Freney, E., Boulon, J., Sellegri, K., Gallagher, M. W., Crawford, I. P., Robinson, N. H.,
948 Stanley, W. R. and Kaye, P. H.: Observations of fluorescent and biological aerosol at a high-altitude site in
949 central France, *Atmos. Chem. Phys.*, 13(15), 7415–7428, doi:10.5194/acp-13-7415-2013, 2013.

950 Gosselin, M. I., Rathnayake, C. M., Crawford, I., Pöhlker, C., Fröhlich-Nowoisky, J., Schmer, B., Després, V. R.,
951 Engling, G., Gallagher, M., Stone, E., Pöschl, U., and Huffman, J. A.: Fluorescent bioaerosol particle, molecular
952 tracer, and fungal spore concentrations during dry and rainy periods in a semi-arid forest, *Atmos. Chem. Phys.*,
953 16(23), 15165–15184, 2016.

954 Van Grondelle, R., Hunter, C. N., Bakker, J. G. C. and Kramer, H. J. M.: Size and structure of antenna complexes of
955 photosynthetic bacteria as studied by singlet-singlet quenching of the bacteriochlorophyll fluorescence yield,
956 *Biochim. Biophys. Acta (BBA)-Bioenergetics*, 723(1), 30–36, 1983.

957 Guilbault, G. G.: *Practical fluorescence (Vol. 3)*, CRC Press., 1990.

958 Hairston, P. P., Ho, J. and Quant, F. R.: Design of an instrument for real-time detection of bioaerosols using simultaneous
959 measurement of particle aerodynamic size and intrinsic fluorescence, *J. Aerosol Sci.*, 28(3), 471–482,
960 doi:10.1016/S0021-8502(96)00448-X, 1997.

961 Healy, D. A., O'Connor, D. J., Burke, A. M. and Sodeau, J. R.: A laboratory assessment of the Waveband Integrated
962 Bioaerosol Sensor (WIBS-4) using individual samples of pollen and fungal spore material, *Atmos. Environ.*,
963 60, 534–543, doi:10.1016/j.atmosenv.2012.06.052, 2012.

964 Healy, D. A., Huffman, J. A., O'Connor, D. J., Pöhlker, C., Pöschl, U. and Sodeau, J. R.: Ambient measurements of

965 biological aerosol particles near Killarney, Ireland: a comparison between real-time fluorescence and
966 microscopy techniques, *Atmos. Chem. Phys.*, 14(15), 8055–8069, doi:10.5194/acp-14-8055-2014, 2014.

967 Herbrich, S., Gehder, M., Krull, R. and Gericke, K.-H.: Label-free spatial analysis of free and enzyme-bound NAD (P)
968 H in the presence of high concentrations of melanin, *J. Fluoresc.*, 22(1), 349–355, 2012.

969 Hernandez, M., Perring, A. E., McCabe, K., Kok, G., Granger, G. and Baumgardner, D.: Chamber catalogues of optical
970 and fluorescent signatures distinguish bioaerosol classes, *Atmos. Meas. Tech.*, 9(7), 3283–3292, 2016.

971 Hill, S. C., Pinnick, R. G., Niles, S., Pan, Y., Holler, S., Chang, R. K., Bottiger, J., Chen, B. T., Orr, C. and Feather, G.:
972 Real-time measurement of fluorescence spectra from single airborne biological particles, *F. Anal. Chem.*
973 *Technol.*, 3(4-5), 221–239, 1999.

974 Hill, S. C., Mayo, M. W. and Chang, R. K.: Fluorescence of Bacteria, Pollens, and Naturally Occurring Airborne
975 Particles: Excitation / Emission Spectra, *Army Res. Lab. Appl. Phys.*, (February), 2009.

976 Hill, S. C., Williamson, C. C., Doughty, D. C., Pan, Y.-L., Santarpia, J. L. and Hill, H. H.: Size-dependent fluorescence
977 of bioaerosols: Mathematical model using fluorescing and absorbing molecules in bacteria, *J. Quant. Spectrosc.*
978 *Radiat. Transf.*, 157, 54–70, doi:10.1016/j.jqsrt.2015.01.011, 2015.

979 Hinds, W. C.: *Aerosol Technology: Properties, Behavior, and Measurement of airborne Particles* (2nd), 1999.

980 Ho, J.: Future of biological aerosol detection, *Anal. Chim. Acta*, 457(1), 125–148, doi:http://dx.doi.org/10.1016/S0003-
981 2670(01)01592-6, 2002.

982 Holbrook, R. D., DeRose, P. C., Leigh, S. D., Rukhin, A. L. and Heckert, N. A.: Excitation–emission matrix fluorescence
983 spectroscopy for natural organic matter characterization: a quantitative evaluation of calibration and spectral
984 correction procedures, *Appl. Spectrosc.*, 60(7), 791–799, 2006.

985 Huffman, J. A. and Santarpia, J.: Online Techniques for Quantification and Characterization of Biological Aerosols,
986 *Microbiol. Aerosols*, 83–114, 2017.

987 Huffman, J. A., Treutlein, B. and Pöschl, U.: Fluorescent biological aerosol particle concentrations and size distributions
988 measured with an Ultraviolet Aerodynamic Particle Sizer (UV-APS) in Central Europe, *Atmos. Chem. Phys.*,
989 10(7), 3215–3233, doi:10.5194/acp-10-3215-2010, 2010.

990 Huffman, J. A., Sinha, B., Garland, R. M., Snee-Pollmann, A., Gunthe, S. S., Artaxo, P., Martin, S. T., Andreae, M. O.
991 and Pöschl, U.: Size distributions and temporal variations of biological aerosol particles in the Amazon
992 rainforest characterized by microscopy and real-time UV-APS fluorescence techniques during AMAZE-08,
993 *Atmos. Chem. Phys.*, 12, 11997–12019, doi:10.5194/acp-12-11997-2012, 2012.

994 Huffman, J. A., Prenni, A. J., Demott, P. J., Pöhlker, C., Mason, R. H., Robinson, N. H., Fröhlich-Nowoisky, J., Tobo,
995 Y., Després, V. R., Garcia, E., Gochis, D. J., Harris, E., Müller-Germann, I., Ruzene, C., Schmer, B., Sinha, B.,
996 Day, D. A., Andreae, M. O., Jimenez, J. L., Gallagher, M., Kreidenweis, S. M., Bertram, A. K. and Pöschl, U.:
997 High concentrations of biological aerosol particles and ice nuclei during and after rain, *Atmos. Chem. Phys.*,
998 13, 6151–6164, doi:10.5194/acp-13-6151-2013, 2013.

999 Hunter, A. J. R., Morency, J. R., Senior, C. L., Davis, S. J. and Fraser, M. E.: Continuous emissions monitoring using
1000 spark-induced breakdown spectroscopy, *J. Air Waste Manage. Assoc.*, 50(1), 111–117, 2000.

1001 Jaenicke, R.: Abundance of cellular material and proteins in the atmosphere., *Science*, 308, 73,
1002 doi:10.1126/science.1106335, 2005.

1003 Jeys, T. H., Herzog, W. D., Hybl, J. D., Czerwinski, R. N. and Sanchez, A.: Advanced trigger development, *Lincoln*
1004 *Lab. J.*, 17(1), 29–62, 2007.

1005 Johnson, I. D., Thomas, E. W. and Cundall, R. B.: Fluorescence solvatochromism of nitrodiphenylhexatrienes, *J. Chem.*
1006 *Soc. Faraday Trans. 2 Mol. Chem. Phys.*, 81(9), 1303–1315, 1985.

1007 Jonsson, P. and Tjärnhage, T.: Trends in Biological Detection BT - Bioaerosol Detection Technologies, edited by P.
1008 Jonsson, G. Olofsson, and T. Tjärnhage, pp. 317–322, Springer New York, New York, NY., 2014.

1009 Kanaani, H., Hargreaves, M., Ristovski, Z. and Morawska, L.: Performance assessment of UVAPS: Influence of fungal
1010 spore age and air exposure, *J. Aerosol Sci.*, 38(1), 83–96, doi:10.1016/j.jaerosci.2006.10.003, 2007.

1011 Kaye, P. H., Stanley, W. R., Hirst, E., Foot, E. V, Baxter, K. L. and Barrington, S. J.: Single particle multichannel bio-
1012 aerosol fluorescence sensor, *Opt. Express*, 13(10), 3583–3593, doi:10.1364/OPEX.13.003583, 2005.

1013 Kaye, P. H., Eyles, N. A., Ludlow, I. K. and Clark, J. M.: An instrument for the classification of airborne particles on
1014 the basis of size, shape, and count frequency, *Atmos. Environ. Part A. Gen. Top.*, 25(3–4), 645–654, 1991.

1015 Kaye, P. H., Alexander-Buckley, K., Hirst, E., Saunders, S. and Clark, J. M.: A real-time monitoring system for airborne
1016 particle shape and size analysis, *J. Geophys. Res. Atmos.*, 101(D14), 19215–19221, 1996.

1017 Kaye, P. H., Barton, J. E., Hirst, E. and Clark, J. M.: Simultaneous light scattering and intrinsic fluorescence
1018 measurement for the classification of airborne particles., *Appl. Opt.*, 39(21), 3738–3745,
1019 doi:10.1364/AO.39.003738, 2000.

1020 Khalaji, M., Roshanzadeh, B., Mansoori, A., Taefi, N. and Tavassoli, S. H.: Continuous dust monitoring and analysis
1021 by spark induced breakdown spectroscopy, *Opt. Lasers Eng.*, 50(2), 110–113, 2012.

1022 Kiselev, D., Bonacina, L. and Wolf, J.-P.: Individual bioaerosol particle discrimination by multi-photon excited
1023 fluorescence, *Opt. Express*, 19(24), 24516–24521, 2011.

1024 Kiselev, D., Bonacina, L. and Wolf, J.-P.: A flash-lamp based device for fluorescence detection and identification of
1025 individual pollen grains, *Rev. Sci. Instrum.*, 84(3), 33302, 2013.

1026 Könemann, T., Savage, N. J., Huffman, J. A. and Pöhlker, C.: Characterization of steady-state fluorescence properties
1027 of polystyrene latex spheres using off-and online spectroscopic methods, *Atmos. Meas. Tech.*, 11(7), 3987–
1028 4003, 2018.

1029 Lakowicz, J. R.: *Principles of Fluorescence Spectroscopy*, (1999), 2004.

1030 Li, J. K., Asali, E. C., Humphrey, A. E. and Horvath, J. J.: Monitoring cell concentration and activity by multiple
1031 excitation fluorometry, *Biotechnol. Prog.*, 7(1), 21–27, doi:10.1021/bp00007a004, 1991.

1032 Lorenz, L.: *Lysbevægelsen i og uden for en af plane Lysbølger belyst Kugle*, na., 1890.

1033 Ma, Y., Wang, Z., Yang, D., Diao, Y., Wang, W., Zhang, H., Zhu, W. and Zheng, J.: On-line measurement of fluorescent
1034 aerosols near an industrial zone in the Yangtze River Delta region using a wideband integrated bioaerosol
1035 spectrometer, *Sci. Total Environ.*, 656, 447–457, 2019.

1036 Madelin, T. M.: Fungal aerosols: A review, *J. Aerosol Sci.*, 25, 1405–1412, doi:10.1016/0021-8502(94)90216-X, 1994.

1037 Mie, G.: Considerations on the optics of turbid media, especially metal sols, *Ann. Phys*, 25, 377–442, 1908.

1038 Moran-Zuloaga, D., Ditas, F., Walter, D., Saturno, J., Brito, J., Carbone, S., Chi, X., Hrabě de Angelis, I., Baars, H.,
1039 Godoi, R. H. M., Heese, B., Holanda, B. A., Lavrič, J. V., Martin, S. T., Ming, J., Pöhlker, M. L., Ruckteschler,
1040 N., Su, H., Wang, Y., Wang, Q., Wang, Z., Weber, B., Wolff, S., Artaxo, P., Pöschl, U., Andreae, M. O., and
1041 Pöhlker, C.: Long-term study on coarse mode aerosols in the Amazon rain forest with the frequent intrusion of
1042 Saharan dust plumes, *Atmos. Chem. Phys.*, 18, 10055-10088, <https://doi.org/10.5194/acp-18-10055-2018>,
1043 2018.

1044 Nasir, Z., Rolph, C., Collins, S., Stevenson, D., Gladding, T., Hayes, E., Williams, B., Khera, S., Jackson, S. and Bennett,
1045 A.: A Controlled Study on the Characterisation of Bioaerosols Emissions from Compost, *Atmosphere (Basel)*,
1046 9(10), 379, 2018.

1047 O'Connor, D. J., Healy, D. A. and Sodeau, J. R.: The on-line detection of biological particle emissions from selected
1048 agricultural materials using the WIBS-4 (Waveband Integrated Bioaerosol Sensor) technique, *Atmos. Environ.*,

1049 80, 415–425, 2013.

1050 O'Connor, D. J., Lovera, P., Iacopino, D., O'Riordan, A., Healy, D. A. and Sodeau, J. R.: Using spectral analysis and
1051 fluorescence lifetimes to discriminate between grass and tree pollen for aerobiological applications, *Anal.*
1052 *Methods*, 6(6), 1633–1639, 2014.

1053 Pan, Y.-L.: Detection and characterization of biological and other organic-carbon aerosol particles in atmosphere using
1054 fluorescence, *J. Quant. Spectrosc. Radiat. Transf.*, 150, 12–35, doi:10.1016/j.jqsrt.2014.06.007, 2015.

1055 Pan, Y.-L., Hill, S. C., Pinnick, R. G., Huang, H., Bottiger, J. R. and Chang, R. K.: Fluorescence spectra of atmospheric
1056 aerosol particles measured using one or two excitation wavelengths: Comparison of classification schemes
1057 employing different emission and scattering results, *Opt. Express*, 18(12), 12436–12457,
1058 doi:10.1364/OE.18.012436, 2010.

1059 Pan, Y.-L., Hartings, J., Pinnick, R. G., Hill, S. C., Halverson, J. and Chang, R. K.: Single-particle fluorescence
1060 spectrometer for ambient aerosols, *Aerosol Sci. Technol.*, 37(8), 628–639, 2003.

1061 Pelling, A. E., Sehati, S., Gralla, E. B., Valentine, J. S. and Gimzewski, J. K.: Local nanomechanical motion of the cell
1062 wall of *Saccharomyces cerevisiae*, *Science* (80-.), 305(5687), 1147–1150, 2004.

1063 Perring, A. E., Schwarz, J. P., Baumgardner, D., Hernandez, M. T., Spracklen, D. V., Heald, C. L., Gao, R. S., Kok, G.,
1064 McMeeking, G. R., McQuaid, J. B. and Fahey, D. W.: Airborne observations of regional variation in fluorescent
1065 aerosol across the United States, *J. Geophys. Res. Atmos.*, 120(3), 1153–1170, doi:10.1002/2014JD022495,
1066 2015.

1067 Pinnick, R. G., Hill, S. C., Pan, Y. -L. and Chang, R. K.: Fluorescence spectra of atmospheric aerosol at Adelphi,
1068 Maryland, USA: Measurement and classification of single particles containing organic carbon, *Atmos.*
1069 *Environ.*, 38(11), 1657–1672, doi:10.1016/j.atmosenv.2003.11.017, 2004.

1070 Pöhlker, C., Huffman, J. A. and Pöschl, U.: Autofluorescence of atmospheric bioaerosols – fluorescent biomolecules
1071 and potential interferences, *Atmos. Meas. Tech.*, 5(1), 37–71, doi:10.5194/amt-5-37-2012, 2012.

1072 Pöhlker, C., Huffman, J. A., Förster, J.-D. and Pöschl, U.: Autofluorescence of atmospheric bioaerosols: spectral
1073 fingerprints and taxonomic trends of pollen, *Atmos. Meas. Tech.*, 6(12), 3369–3392, 2013.

1074 Pöschl, U.: Atmospheric Aerosols: Composition, Transformation, Climate and Health Effects, *Angew. Chemie Int. Ed.*,
1075 44(46), 7520–7540, doi:10.1002/anie.200501122, 2005.

1076 Pöschl, U. and Shiraiwa, M.: Multiphase Chemistry at the Atmosphere–Biosphere Interface Influencing Climate and
1077 Public Health in the Anthropocene, *Chem. Rev.*, 115(10), 4440–4475, doi:10.1021/cr500487s, 2015.

1078 Reid, J. S., Jonsson, H. H., Maring, H. B., Smirnov, A., Savoie, D. L., Cliff, S. S., Reid, E. A., Livingston, J. M., Meier,
1079 M. M. and Dubovik, O.: Comparison of size and morphological measurements of coarse mode dust particles
1080 from Africa, *J. Geophys. Res. Atmos.*, 108(D19), 2003.

1081 Reponen, T., Grinshpun, S. A., Conwell, K. L., Wiest, J. and Anderson, M.: Aerodynamic versus physical size of spores:
1082 measurement and implication for respiratory deposition, *Grana*, 40(3), 119–125, 2001.

1083 Richards-Kortum, R. and Sevick-Muraca, E.: Quantitative optical spectroscopy for tissue diagnosis, *Annu. Rev. Phys.*
1084 *Chem.*, 47(1), 555–606, 1996.

1085 Rijgersberg, C. P., Van Grondelle, R. and Ames, J.: Energy transfer and bacteriochlorophyll fluorescence in purple
1086 bacteria at low temperature, *Biochim. Biophys. Acta (BBA)-Bioenergetics*, 592(1), 53–64, 1980.

1087 Robinson, E. S., Gao, R.-S., Schwarz, J. P., Fahey, D. W. and Perring, A. E.: Fluorescence calibration method for single-
1088 particle aerosol fluorescence instruments, *Atmos. Meas. Tech.*, 10(5), 1755–1768, 2017.

1089 Robinson, N. H., Allan, J. D., Huffman, J. A., Kaye, P. H., Foot, V. E. and Gallagher, M. W.: Cluster analysis of WIBS
1090 single-particle bioaerosol data, *Atmos. Meas. Tech.*, 2013.

1091 Ruske, S., Topping, D. O., Foot, V. E., Kaye, P. H., Stanley, W., Crawford, I. P., Morse, A. and Gallagher, M. W.:
1092 Evaluation of machine learning algorithms for classification of primary biological aerosol using a new UV-LIF
1093 spectrometer, *Atmos. Meas. Tech.*, 2017.

1094 Saari, S., Reponen, T. and Keskinen, J.: Performance of Two Fluorescence-Based Real-Time Bioaerosol Detectors:
1095 BioScout vs. UVAPS, *Aerosol Sci. Technol.*, 48(4), 371–378, doi:10.1080/02786826.2013.877579, 2014.

1096 Saari, S. E., Putkiranta, M. J. and Keskinen, J.: Fluorescence spectroscopy of atmospherically relevant bacterial and
1097 fungal spores and potential interferences, *Atmos. Environ.*, 71, 202–209,
1098 doi:http://dx.doi.org/10.1016/j.atmosenv.2013.02.023, 2013.

1099 Savage, N. J. and Huffman, J. A.: Evaluation of a hierarchical agglomerative clustering method applied to WIBS
1100 laboratory data for improved discrimination of biological particles by comparing data preparation techniques,
1101 *Atmos. Meas. Tech.*, 11(8), 4929–4942, 2018.

1102 Savage, N. J., Krentz, C. E., Könemann, T., Han, T. T., Mainelis, G., Pöhlker, C. and Huffman, J. A.: Systematic
1103 characterization and fluorescence threshold strategies for the wideband integrated bioaerosol sensor (WIBS)
1104 using size-resolved biological and interfering particles, *Atmos. Meas. Tech.*, 10(11), 4279–4302,
1105 doi:10.5194/amt-10-4279-2017, 2017.

1106 Schmauss, A. and Wigand, A.: *Die Atmosphäre als Kolloid*, Vieweg+Teubner Verlag, Wiesbaden., 1929.

1107 Schmidt, M. S. and Bauer, A. J. R.: Preliminary correlations of feature strength in spark-induced breakdown
1108 spectroscopy of bioaerosols with concentrations measured in laboratory analyses, *Appl. Opt.*, 49(13), C101–
1109 C109, 2010.

1110 Schumacher, C. J., Pöhlker, C., Aalto, P., Hiltunen, V., Petäjä, T., Kulmala, M., Pöschl, U. and Huffman, J. A.: Seasonal
1111 cycles of fluorescent biological aerosol particles in boreal and semi-arid forests of Finland and Colorado,
1112 *Atmos. Chem. Phys.*, 13(23), 11987–12001, doi:10.5194/acp-13-11987-2013, 2013.

1113 Shaw, S. L., Yeh, E., Bloom, K. and Salmon, E. D.: Imaging green fluorescent protein fusion proteins in *Saccharomyces*
1114 *cerevisiae*, *Curr. Biol.*, 7(9), 701–704, 1997.

1115 Sinski, J. F. and Exner, J.: Concentration dependence in the spectra of polycyclic aromatic hydrocarbon mixtures by
1116 front-surface fluorescence analysis, *Appl. Spectrosc.*, 61(9), 970–977, 2007.

1117 Sivaprakasam, V., Lin, H.-B., Huston, A. L. and Eversole, J. D.: Spectral characterization of biological aerosol particles
1118 using two-wavelength excited laser-induced fluorescence and elastic scattering measurements, *Opt. Express*,
1119 19(7), 6191–6208, doi:10.1364/OE.19.006191, 2011.

1120 Sodeau, J. R. and O'Connor, D. J.: *Bioaerosol Monitoring of the Atmosphere for Occupational and Environmental*
1121 *Purposes*, *Compr. Anal. Chem.*, 2016.

1122 Stanley, W. R., Kaye, P. H., Foot, V. E., Barrington, S. J., Gallagher, M. and Gabey, A.: Continuous bioaerosol
1123 monitoring in a tropical environment using a UV fluorescence particle spectrometer, *Atmos. Sci. Lett.*, 12(2),
1124 195–199, doi:10.1002/asl.310, 2011.

1125 Swanson, B. E. and Huffman, J. A.: Development and characterization of an inexpensive single-particle fluorescence
1126 spectrometer for bioaerosol monitoring, *Opt. Express*, 26(3), 3646–3660, 2018.

1127 Toprak, E. and Schnaiter, M.: Fluorescent biological aerosol particles measured with the Waveband Integrated
1128 Bioaerosol Sensor WIBS-4: laboratory tests combined with a one year field study, *Atmos. Chem. Phys.*, 13(1),
1129 225–243, 2013.

1130 Twohy, C. H., McMeeking, G. R., DeMott, P. J., McCluskey, C. S., Hill, T. C. J., Burrows, S. M., Kulkarni, G. R.,
1131 Tanarhte, M., Kafle, D. N. and Toohey, D. W.: Abundance of fluorescent biological aerosol particles at
1132 temperatures conducive to the formation of mixed-phase and cirrus clouds, *Atmos. Chem. Phys.*, 16(13), 8205–

1133 8225, 2016.

1134 Von der Weiden, S. L., Drewnick, F. and Borrmann, S.: Particle Loss Calculator—a new software tool for the assessment
1135 of the performance of aerosol inlet systems, *Atmos. Meas. Tech.*, 2(2), 479–494, 2009.

1136 Welschmeyer, N. A.: Fluorometric analysis of chlorophyll a in the presence of chlorophyll b and pheopigments, *Limnol.*
1137 *Oceanogr.*, 39(8), 1985–1992, 1994.

1138 Yao, M.: *Bioaerosol: A bridge and opportunity for many scientific research fields*, 2018.

1139 Ziemba, L. D., Beyersdorf, A. J., Chen, G., Corr, C. A., Crumeyrolle, S. N., Diskin, G., Hudgins, C., Martin, R.,
1140 Mikoviny, T. and Moore, R.: Airborne observations of bioaerosol over the Southeast United States using a
1141 wideband integrated bioaerosol sensor, *J. Geophys. Res. Atmos.*, 121(14), 8506–8524, 2016.

1142

1143 **Appendix A:** List of acronyms and symbols.

Acronym/Symbol	Description
AF	Asymmetry factor
APC	Airborne Particle Classifier
CCD	Charge-coupled device
DMT	Droplet Measurement Technologies
EEM	Excitation-emission matrix
EM	Emission
EX	Excitation
IR	Infrared
LIF	Light-induced fluorescence
<i>N</i>	Particle number concentration (cm^{-3})
<i>N_{T,c}</i>	<i>N</i> of total coarse particles (1-20 μm)
<i>N_{F,c(nσ)}</i>	<i>N</i> of fluorescent coarse particles (1-20 μm) at 1, 3, or 6 σ
NAD	Nicotinamide adenine dinucleotide
NAD(P)H	Nicotinamide adenine dinucleotide and nicotinamide adenine dinucleotide phosphate
NIST	National institute of standards and technology
PBAP	Primary biological aerosol particles
PMT	Photomultiplier tube
PAH	Polycyclic aromatic hydrocarbons
PSL	Polystyrene latex sphere
PS-DVB	Polystyrene-divinylbenzene
SD	Standard deviation
SIBS	Spectral intensity bioaerosol sensor
SNR	Signal to noise ratio
TSP	Total suspended particles
UV	Ultraviolet
UV-APS	Ultraviolet aerodynamic particle sizer
Vis	Visible light
WIBS	Wideband integrated bioaerosol sensor

1144

1145 **Table 1.** Lower, mean, and upper wavelength at each PMT detection channel. Nominal data accord-
 1146 ing to manufacturer Hamamatsu.

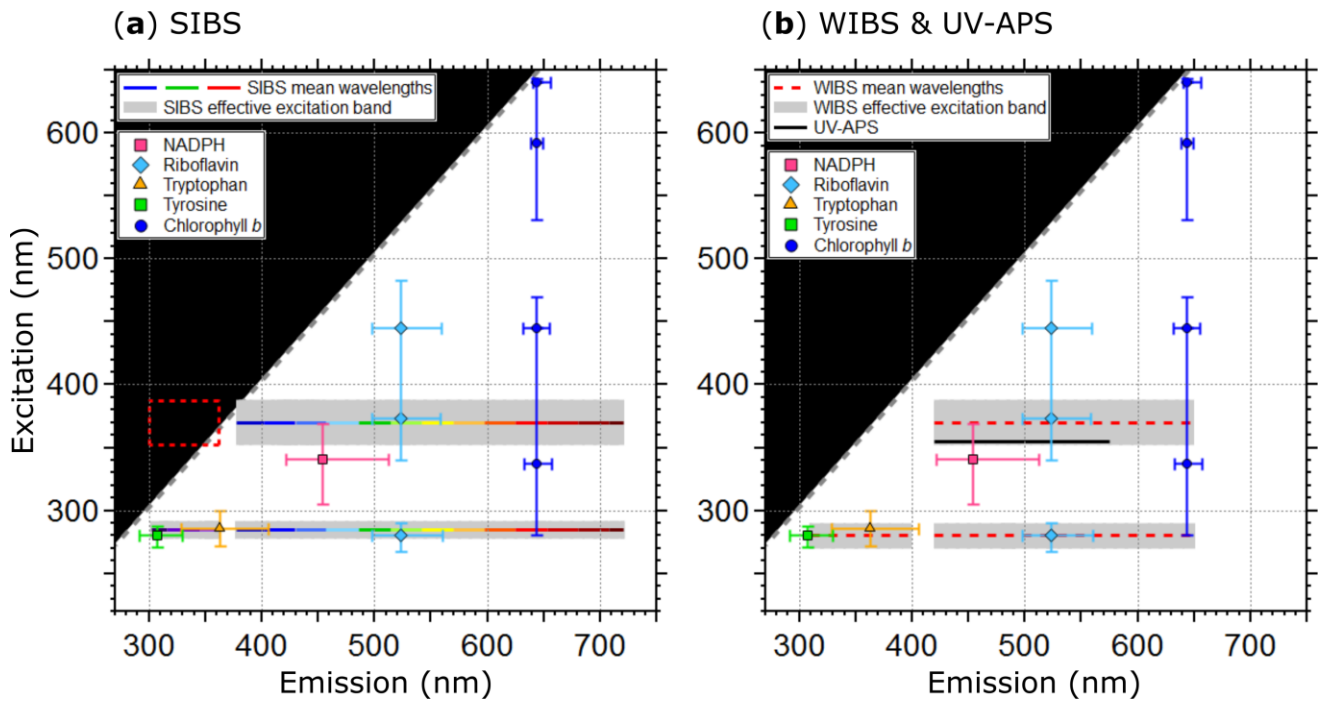
Channel	λ_{lower} (nm)	λ_{mean} (nm)	λ_{upper} (nm)
1	298.2	302.2	316.2
2	316.6	330.6	344.6
3	345.0	359.0	362.5
4	377.5	387.3	401.3
5	401.5	415.6	429.7
6	429.8	443.8	457.8
7	457.9	471.9	485.9
8	486.0	500.0	514.0
9	514.0	528.0	542.0
10	541.9	555.9	569.9
11	569.7	583.7	597.7
12	597.4	611.4	625.4
13	625.0	639.0	653.0
14	652.8	666.5	680.2
15	679.9	693.9	707.9
16	707.1	721.1	735.1

1147 **Table 2.** Parameters and technical components of the SIBS in comparison to the WIBS-NEO and
 1148 WIBS-4A. Data are taken from manufacturer information.

	SIBS	WIBS-NEO	WIBS-4A
<i>First production</i>	<i>2015</i>	<i>2016</i>	<i>2009</i>
Measured parameters	Particle size Asymmetry Factor Fluorescence spectra	Particle size Asymmetry Factor Integrated fluorescence in 3 channels	Particle size Asymmetry Factor Integrated fluorescence in 3 channels
Particle size range	~0.3 – 100 μm	~0.3 0.5 – 100 30 μm	~0.5 – 20 μm
Maximum concentration	$\sim 2 \times 10^4$ particles/L	$\sim 2 \times 10^4$ particles/L	$\sim 2 \times 10^4$ particles/L
Fluorescence excitation	$\lambda_{\text{ex}} = 285$ and $\lambda_{\text{ex}} = 370$ nm	$\lambda_{\text{ex}} = 280$ and $\lambda_{\text{ex}} = 370$ nm	$\lambda_{\text{ex}} = 280$ and $\lambda_{\text{ex}} = 370$ nm
Fluorescence emission	$\lambda_{\text{em}} = 302 - 721$ nm (16-channel PMT)	$\lambda_{\text{em}} = 310-400$ nm and $\lambda_{\text{em}} = 420-650$ nm	$\lambda_{\text{em}} = 310-400$ nm and $\lambda_{\text{em}} = 420-650$ nm
Flow rate	Sample flow: ~0.3 l/min Sheath flow: ~2.2 l/min (re-circulating)	Sample flow: ~0.3 l/min Sheath flow: ~2.2 l/min (re-circulating)	Sample flow: ~0.3 l/min Sheath flow: ~2.2 l/min (re-circulating)
Laser	785 nm diode laser, 55 mW	635 nm diode laser, 15 mW	635 nm diode laser, 12 mW
Pump	Diaphragm pump	Diaphragm pump	Diaphragm pump
Power requirements	200 W, 90 - 230 VAC	150 W, 90 - 230 VAC	150 W, 90 - 230 VAC
Weight (kg)	20.1	12.5	13.6
Dimension W x L x H (cm)	42.5 x 61.5 x 23.5	45.1 x 36.2 x 24.1	30.4 x 38.2 x 17.1

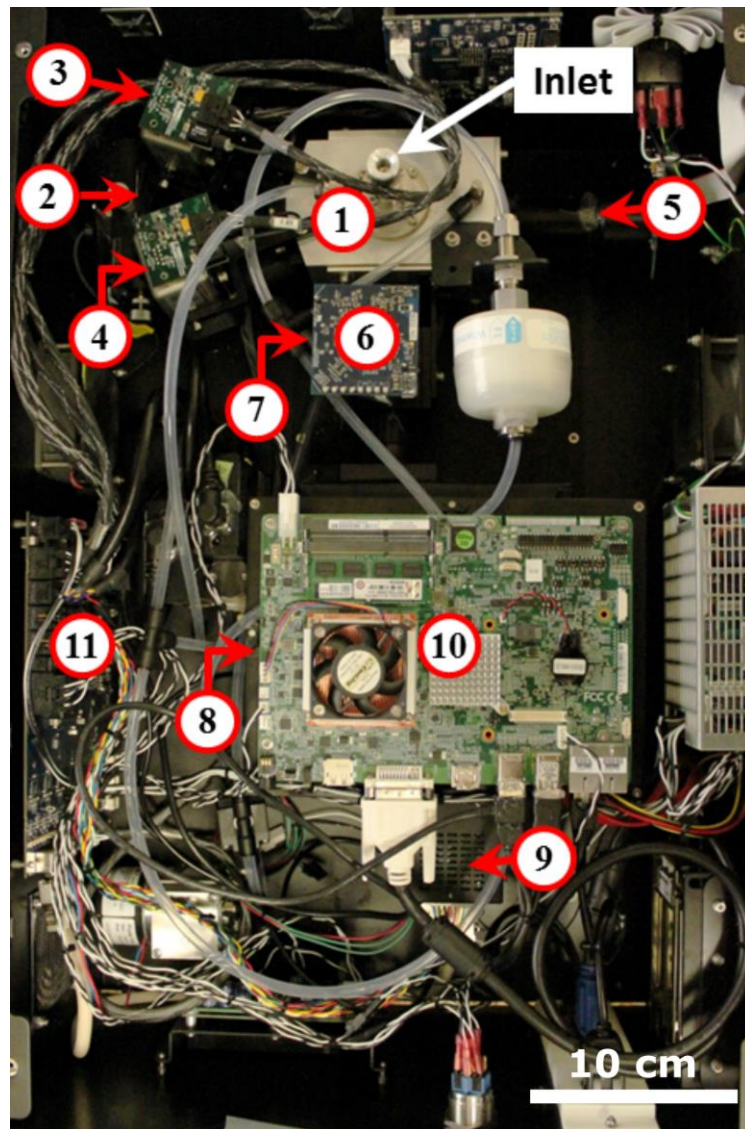
1149 **Table 3.** Asymmetry factor (AF) values for reference particles. Values are based on the mean of a
1150 Gaussian fit applied onto each particle histogram (see also Fig. 10), including 1σ SD.

	AF
2 μm non-fluorescent PSLs	9.9 ± 3.6
Ultrapure water	11.9 ± 2.9
Ammonium sulfate	13.1 ± 8.1
Fe₃O₄	14.4 ± 7.4
Carbon nanotubes	21.6 ± 12.7

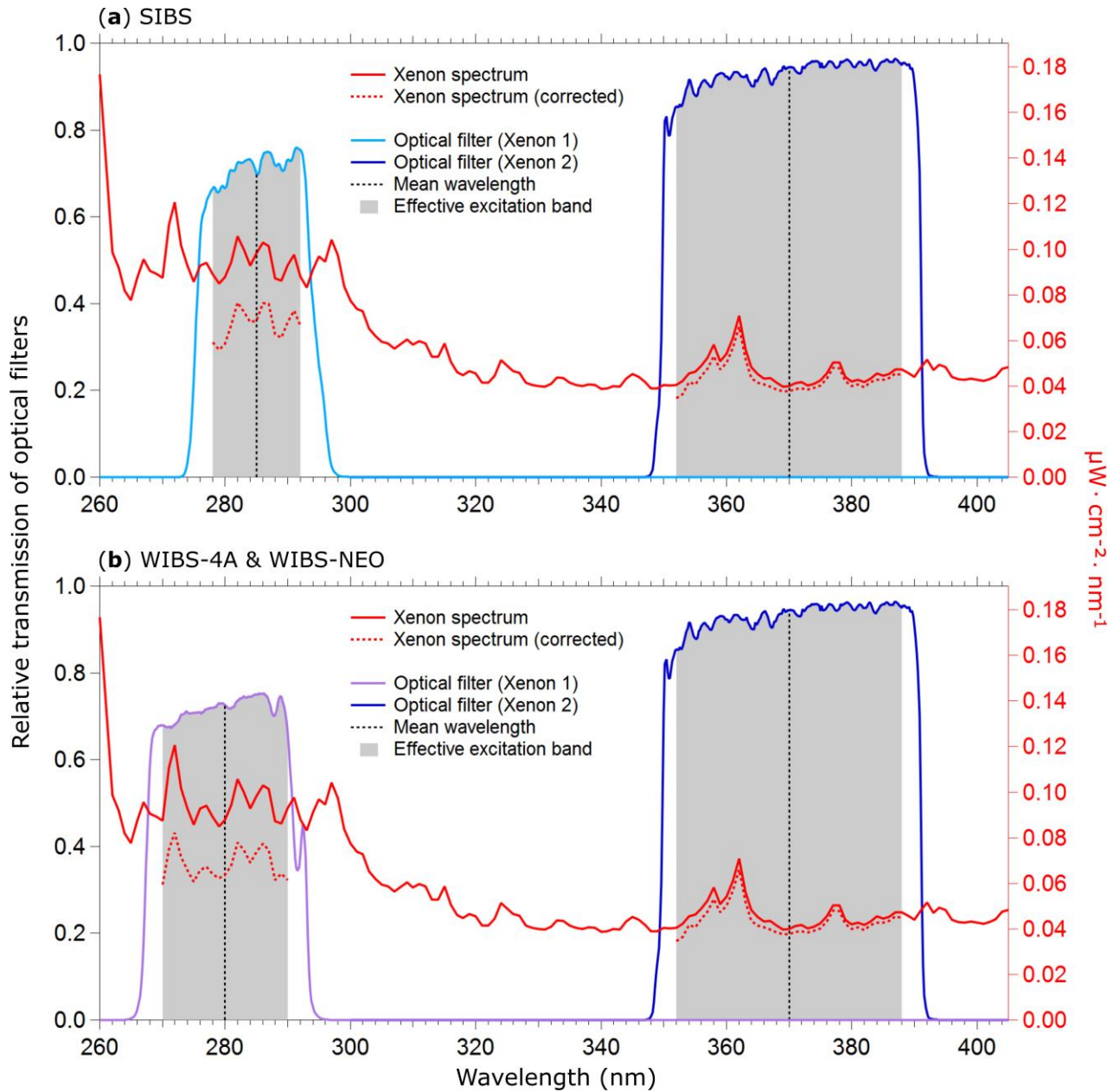


1151 **Figure 1.** Optical design and overview of excitation and emission specifications of the LIF instru-
 1152 ments UV-APS, WIBS, and the SIBS with spectral locations of the autofluorescence modes of the
 1153 biofluorophores tyrosine, tryptophan, NAD(P)H, riboflavin, and chlorophyll *b* (as examples). Here
 1154 the term WIBS includes the WIBS-4A and WIBS-NEO, because both instruments use the same opti-
 1155 cal components. Spectral properties of the emission bands of LIF instruments are illustrated as hori-
 1156 zontal lines. The color-coded bars in (a) illustrate the spectrally resolved fluorescence detection of
 1157 the two excitation wavelengths ($\lambda_{\text{ex}} = 285$ and 370 nm) by the SIBS. The “blind spot” (white notch)
 1158 at $\lambda_{\text{ex}} = 285$ nm between $\lambda_{\text{em}} = 362 - 377$ nm (a) originates from a notch optical filter, used to block
 1159 incident light from the excitation sources. Grey dashed lines show the 1st order elastic scattering. At
 1160 $\lambda_{\text{ex}} = 370$ nm, the detection range of the SIBS includes the spectral range where $\lambda_{\text{em}} < \lambda_{\text{ex}}$, for which
 1161 fluorescence is not defined and so data within the red dashed rectangle is omitted (a). Grey bars
 1162 indicate the effective excitation bands of optical filters used for the WIBS and SIBS (see also Sect.
 1163 3.3 and Fig. 3). The effective excitation bands in the WIBS and SIBS occur in a spectral range span-
 1164 ning several nanometers (up to 36 nm), in contrast to the UV-APS (black line, b), which uses a laser
 1165 source with a defined excitation (Figure adapted from Pöhlker et al., 2012).

1166
1167
1168
1169
1170
1171
1172
1173
1174
1175
1176
1177
1178
1179

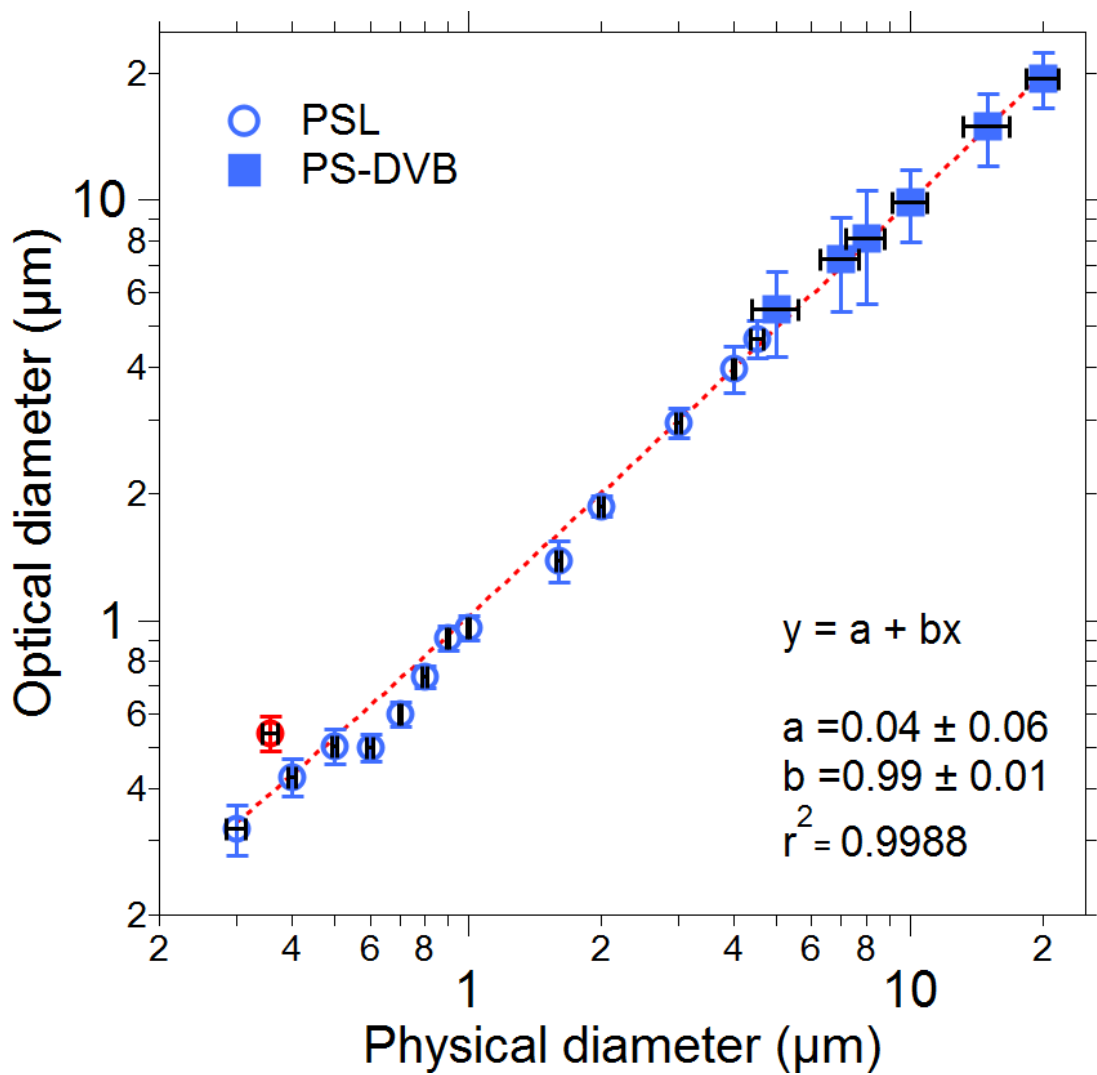


1180 **Figure 2.** Technical components within SIBS body. (1) Optical cavity. (2) Continuous wave diode
1181 laser used for particle detection and sizing. (3) and (4) Xenon light sources. (5) Quadrant PMT used
1182 for the determination of particle asymmetry. (6) PMT used for particle detection and sizing. (7) Di-
1183 chroic beamsplitter separates side-scattered light (particle sizing) and fluorescence emission (not vis-
1184 ible; below component (6)). (8) Grating polychromator (below component (10)). (9) 16-channel PMT
1185 used for detection of fluorescence. (10) Embedded computer unit. (11) Control-board.

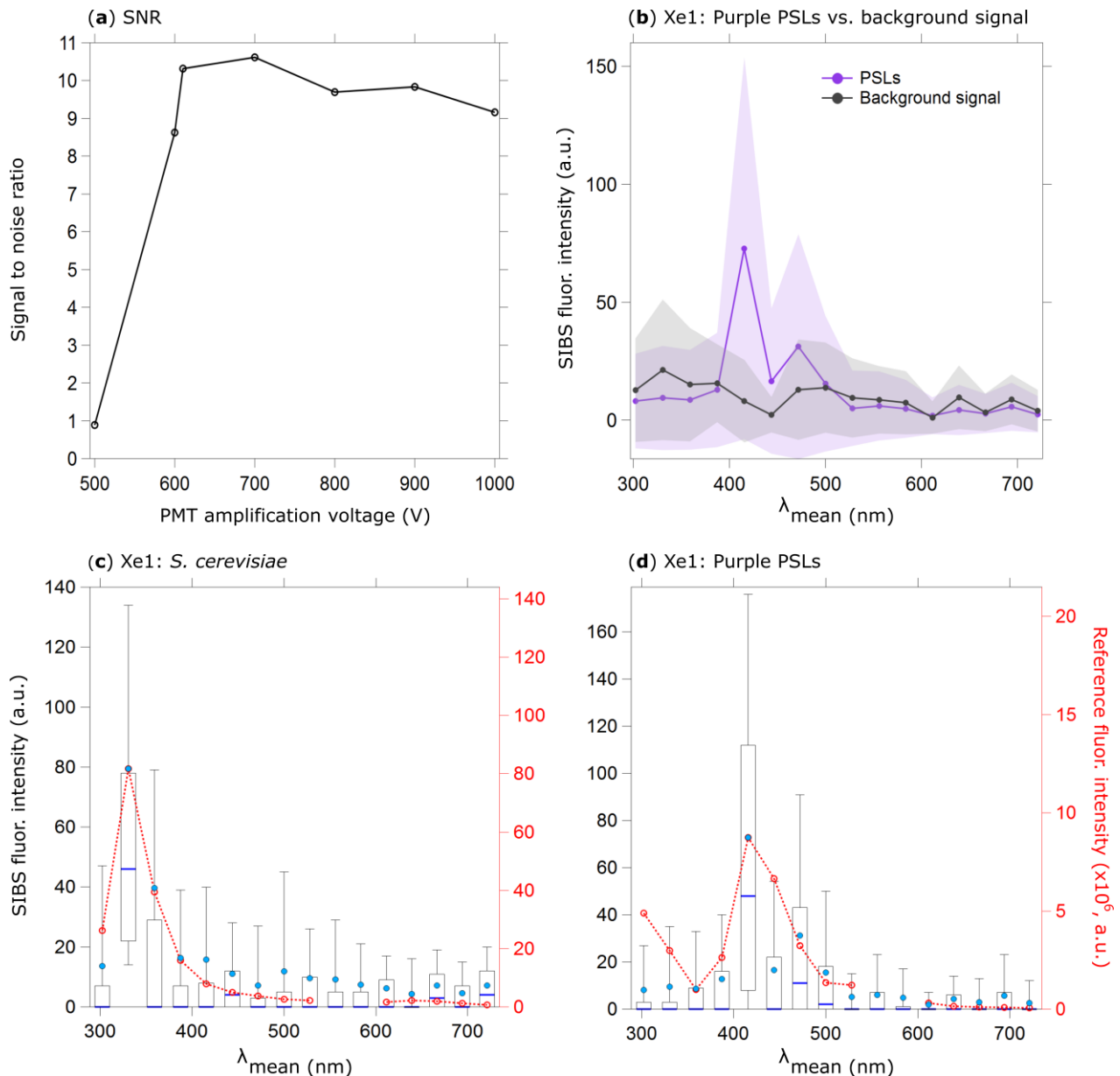


1186 **Figure 3.** Irradiance from xenon flash lamps based on specifications of lamps and optical filters.
 1187 Purple and blue lines show optical transmission of filters (left axes) applied to select excitation wave-
 1188 length. Gray bands indicate where filter transmit light relative from the mean wavelength. Red lines
 1189 show theoretical irradiance values of the xenon flash lamp (right axes): solid line (raw output), dashed
 1190 line (relative output after filtering). Relative output shown as raw output multiplied by effective ex-
 1191 citation band of the bandpass filters used in the: **(a)** SIBS ($\Delta\lambda_{\text{ex}}(\text{Xenon1}) = \sim 14$ nm; $\Delta\lambda_{\text{ex}}(\text{Xenon2}) = \sim 36$
 1192 nm), and **(b)** WIBS-4A and WIBS-NEO ($\Delta\lambda_{\text{ex}}(\text{Xenon1}) = \sim 20$ nm; $\Delta\lambda_{\text{ex}}(\text{Xenon2}) = \sim 36$ nm). Xenon lamp
 1193 operating conditions: 600 V main voltage, 0.22 μF main capacitance, 126 Hz repetition rate, 500 mm
 1194 distance. (Data courtesy: Xenon flash lamps / Hamamatsu; Single-band bandpass filters / Semrock).

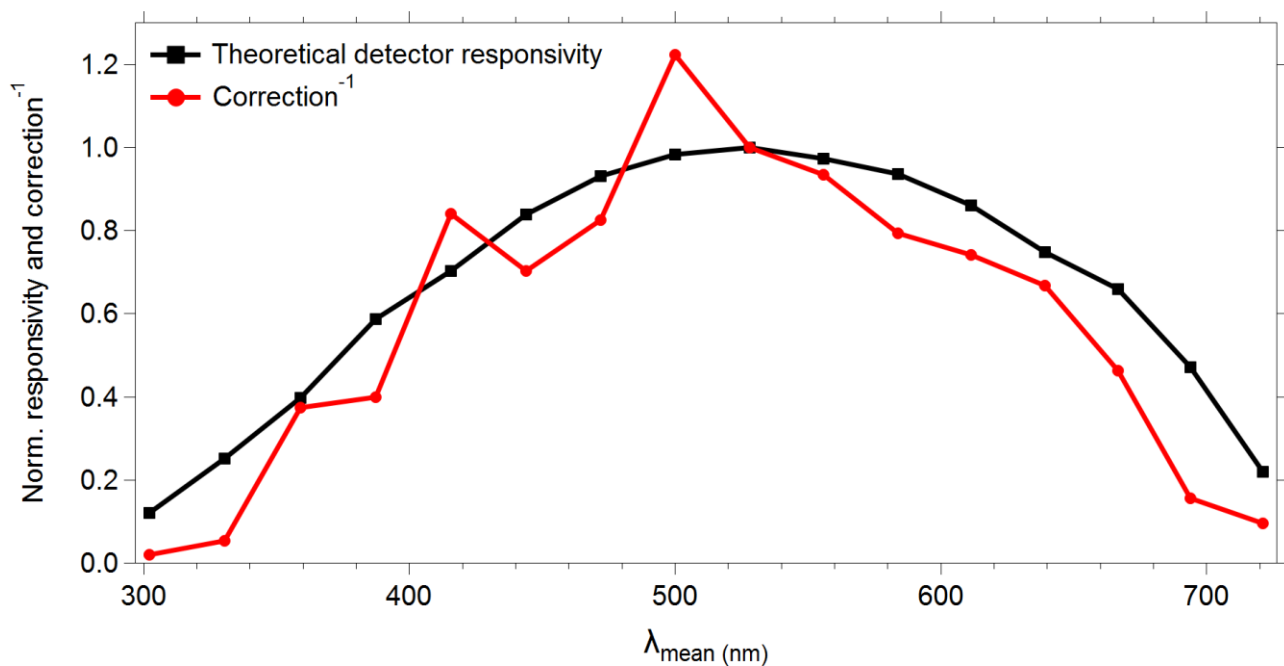
1195
1196
1197
1198
1199
1200
1201
1202
1203
1204
1205
1206
1207



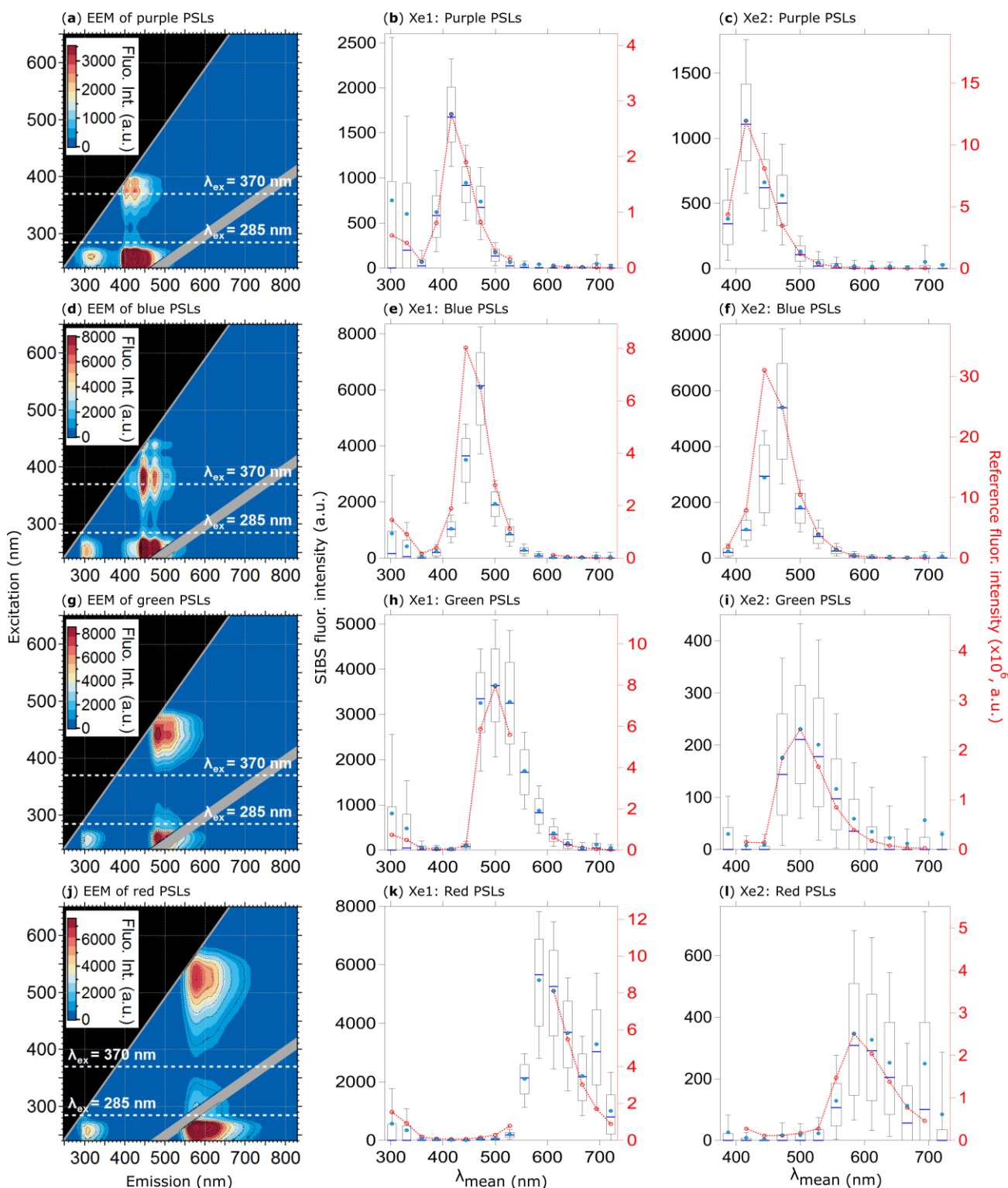
1208 **Figure 4.** Size calibration of SIBS. Black horizontal bars indicate 1σ SD as stated by each manufac-
1209 turer (Table S1). Optical diameter values and related 1σ SD are based on a Gaussian fit, which was
1210 used to average size distributions of several thousand homogeneous particles for each measurement.
1211 The linear fit (red dashed line) excludes the $0.356 \mu\text{m}$ PSL sample (red marker), an outlier potentially
1212 caused by a poor quality PSL batch. Only non-fluorescent particle standards were used for determin-
1213 ing the sizing accuracy.



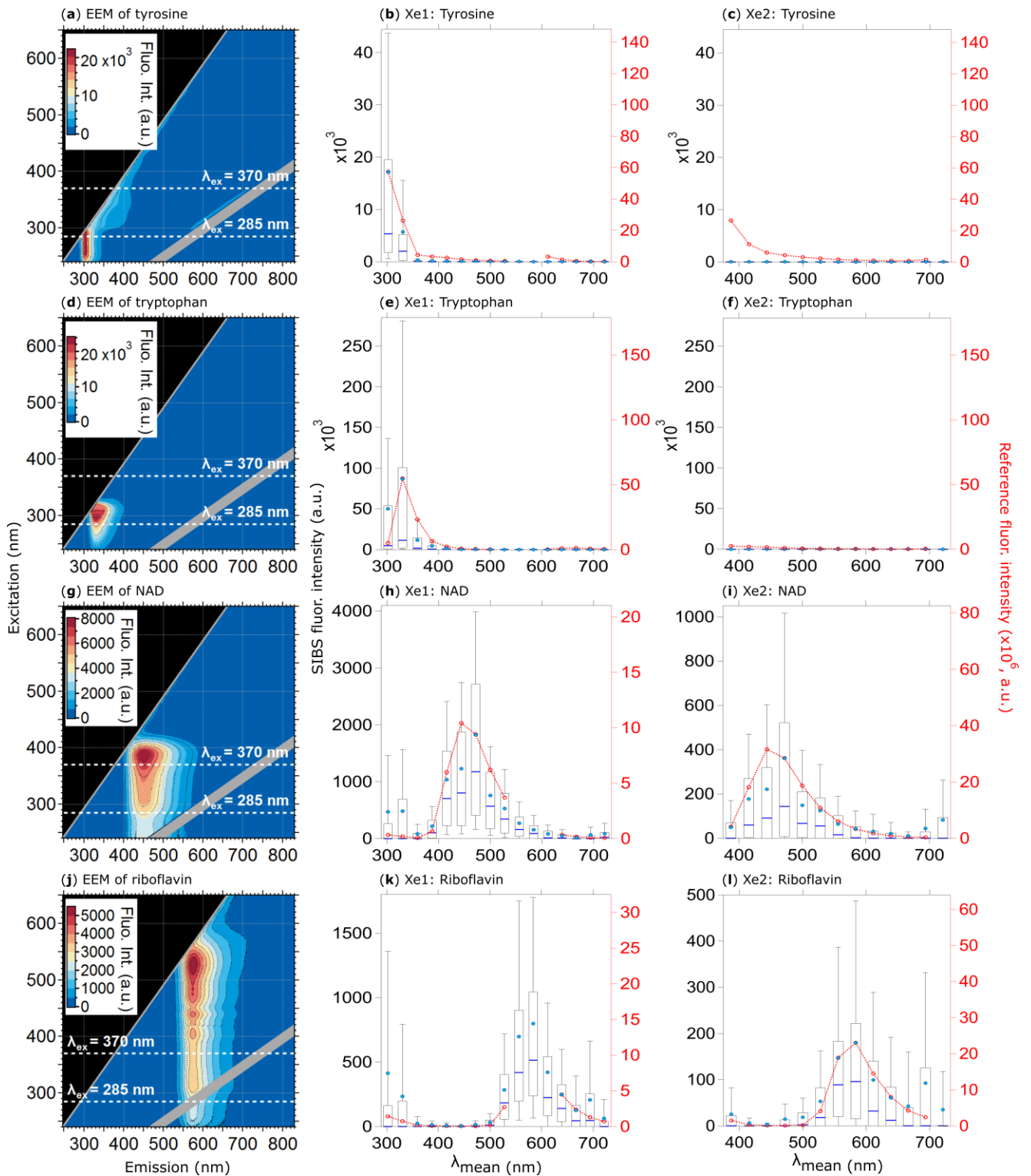
1214 **Figure 5.** SIBS signal to noise ratio (SNR) in (a): emission of $0.53 \mu\text{m}$ purple PSLs (5260 particles,
1215 background signal + 1σ SD subtraction) divided by background signal at different PMT amplification
1216 voltages (both at Xe1, channel 5, averaged, and uncorrected). Background signal measured over 5
1217 min. In (b), fluorescence emission in contrast to background signal at a PMT amplification voltage
1218 of 610 V are shown (same parameters as in (a)). Shaded area: 1σ SD. Fluorescence intensity values
1219 are shown in arbitrary units. Fluorescence emission spectra of (c) *S. cerevisiae* (yeast; 2048 particles,
1220 $0.5 - 1 \mu\text{m}$) and (d) PSLs (as in (b)). Red dashed lines and markers (right axes) show averaged and
1221 re-binned reference spectra. Box and whisker plots (left axes) show SIBS spectra: median (blue line),
1222 mean (circle), boxes 75 and 25 percentile, whiskers 90 and 10 percentile. Data coinciding with 1st or
1223 2nd order elastic scattering were removed from reference spectra.



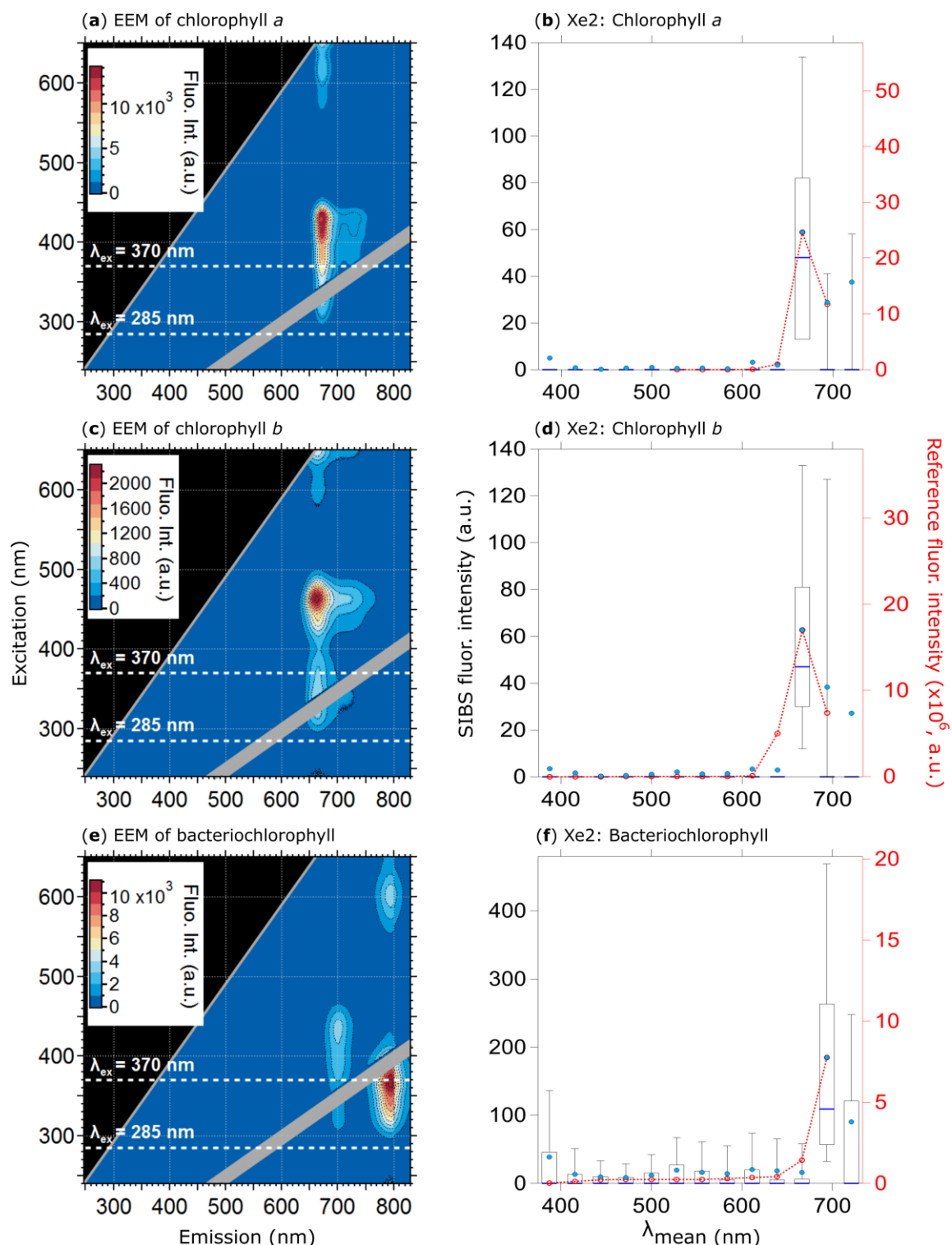
1224 **Figure 6.** Normalized theoretical detector responsivity and spectral correction. Theoretical detector
 1225 responsivity derived from measured cathode radiant sensitivity multiplied by the diffraction effi-
 1226 ciency (as shown in Figure S8). Note that red line shows inverse of spectral correction to match
 1227 detector response.



1228 **Figure 7.** Fluorescence emission spectra of PSLs. Steady-state fluorescence signatures displayed as
 1229 EEMs (left column) and spectra at Xe1 and Xe2 (middle, right columns) for: 2.07 μm purple (**a**, **b**
 1230 and **c**, 1082 particles), 2.1 μm blue (**d**, **e** and **f**, 1557 particles), 2 μm green (**g**, **h**, and **i**, 1174 particles),
 1231 and 2 μm red PSLs (**j**, **k**, and **l**, 1474 particles). Within EEMs: white dashed lines show SIBS excita-
 1232 tion wavelengths ($\lambda_{\text{ex}} = 285$ and 370 nm), grey diagonal lines indicate 1st and 2nd order elastic scat-
 1233 tering bands (both bands were subtracted automatically by the Aqualog V3.6 software). **Red dashed**
 1234 **lines and markers (right axes; middle, right columns): averaged and re-binned reference spectra.**

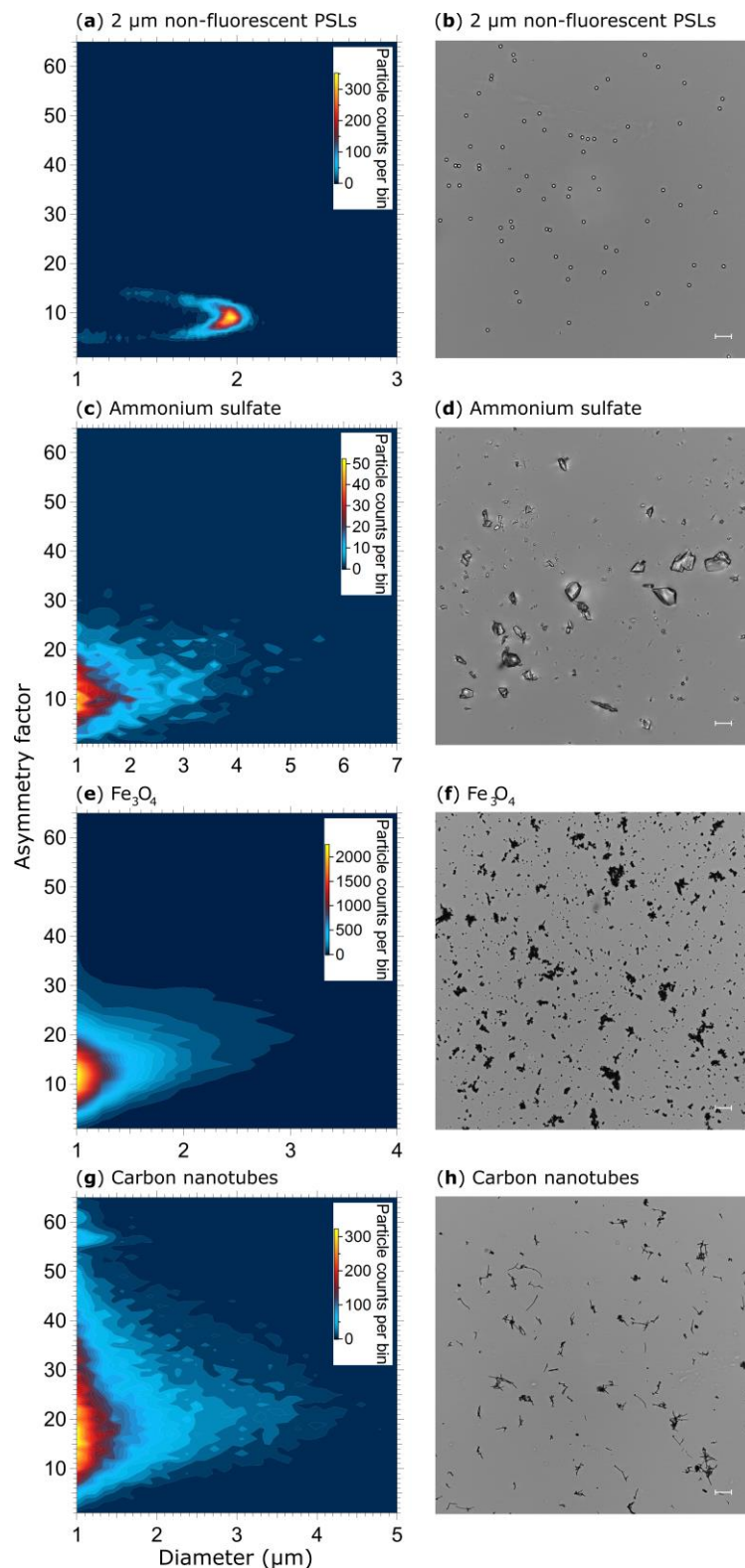


1235 **Figure 8.** Fluorescence emission spectra of biofluorophores. EEMs (left column) and spectra at Xe1
 1236 and Xe2 wavelengths (middle and right columns) shown for: tyrosine (a, b, and c, 209 particles),
 1237 tryptophan (d, e, and f, 193 particles), NAD (g, h, and i, 376 particles), and riboflavin (j, k, and l,
 1238 205 particles). **Red dashed lines and markers (right axes; middle, right columns): averaged and re-**
 1239 **binned reference spectra.** All biofluorophores were size-selected between 1 and 2 μm .

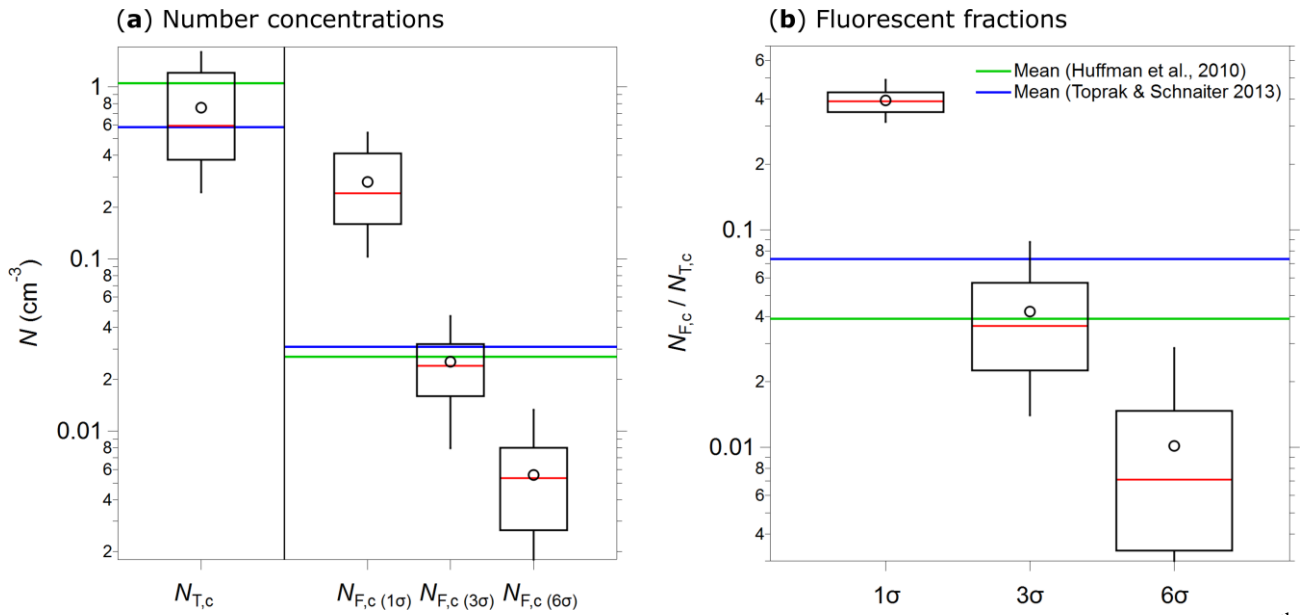


1240 **Figure 9.** Fluorescence emission spectra of three chlorophyll types. Highlighted are EEMs (left col-
 1241 umn) and spectra at Xe2 (right columns) for: chlorophyll *a* (**a** and **b**, 370 particles), chlorophyll *b* (**c**
 1242 and **d**, 585 particles), and bacteriochlorophyll (**e** and **f**, 633 particles). **Red dashed lines and markers**
 1243 **(right axes; right column): averaged and re-binned reference spectra.** Size range chlorophyll *a* and
 1244 *b*: 0.5 - 2 μm , size range bacteriochlorophyll: 0.5 - 1 μm . Emission spectra at Xe1 are excluded due
 1245 to a fluorescence artifact caused by solved components from the polymer of the aerosolization bottles
 1246 (Fig. S12).

1247
1248
1249
1250
1251
1252
1253
1254
1255
1256
1257
1258
1259
1260
1261
1262
1263
1264
1265
1266
1267
1268
1269
1270
1271
1272
1273
1274
1275



1276 **Figure 10.** Particle asymmetry. Shown are particle density histograms (left column) and microscopy
1277 images (right column) for: 2 μm non-fluorescent PSLs (**a** and **b**, 17836 particles), ammonium sulfate
1278 (**c** and **d**, 3496 particles), Fe_3O_4 (**e** and **f**, 65097 particles), and carbon nanotubes (56949 particles, **g**).
1279 Scale bar (right column) indicates a length of 10 μm .



1280 **Figure 11.** Integrated coarse particle (1-20 μm) number concentrations, measured between the 12th
 1281 and 18th of April 2018 (5 min average), for total particles ($N_{T,c}$, fluorescent and non-fluorescent) and
 1282 coarse fluorescent particles ($N_{F,c}$) after 1, 3, and 6 σ SD background signal subtraction (a). The fluo-
 1283 rescent fractions of integrated coarse particle number concentrations ($N_{F,c} / N_{T,c}$) at 1, 3, and 6 σ SD
 1284 are shown in (b). Median (red line), mean (black circles), boxes 75 and 25 percentile, whiskers 95
 1285 and 5 percentile (a and b). Data from Huffman et al. (2010) (green lines) and Toprak & Schnaiter,
 1286 (2013) (blue lines) were taken for comparison (a and b).

1 *Supplement to*

2

3 **Spectral Intensity Bioaerosol Sensor (SIBS):**

4 **An *new* Instrument for Spectrally Resolved Fluorescence Detection of**

5 **Single Particles in Real-Time**

6

7 Tobias Könemann¹, Nicole Savage^{2a}, Thomas Klimach¹, David Walter¹, Janine Fröhlich-
8 Nowoisky¹, Hang Su¹, Ulrich Pöschl¹, J. Alex Huffman², and Christopher Pöhlker¹

9

10 ¹*Max Planck Institute for Chemistry, Multiphase Chemistry Department, P.O. Box 3060,*
11 *D-55020 Mainz, Germany*

12 ²*University of Denver, Department of Chemistry and Biochemistry, 2190 E. Iliff Ave., Denver, Col-*
13 *orado 80208, USA*

14

15 ^a*Now at Aerosol Devices Inc., 430 North College Avenue # 430, Fort Collins, Colorado 80524, USA*

16

17

18 *Correspondence to:*

19 J. A. Huffman (alex.huffman@du.edu) and C. Pöhlker (c.pohlker@mpic.de)

20

21

22 **This file includes:**

23 Supplementary Tables S1 to S2

24 Supplementary Figures S1 to S14

25

26

27

28

29

30

31

32

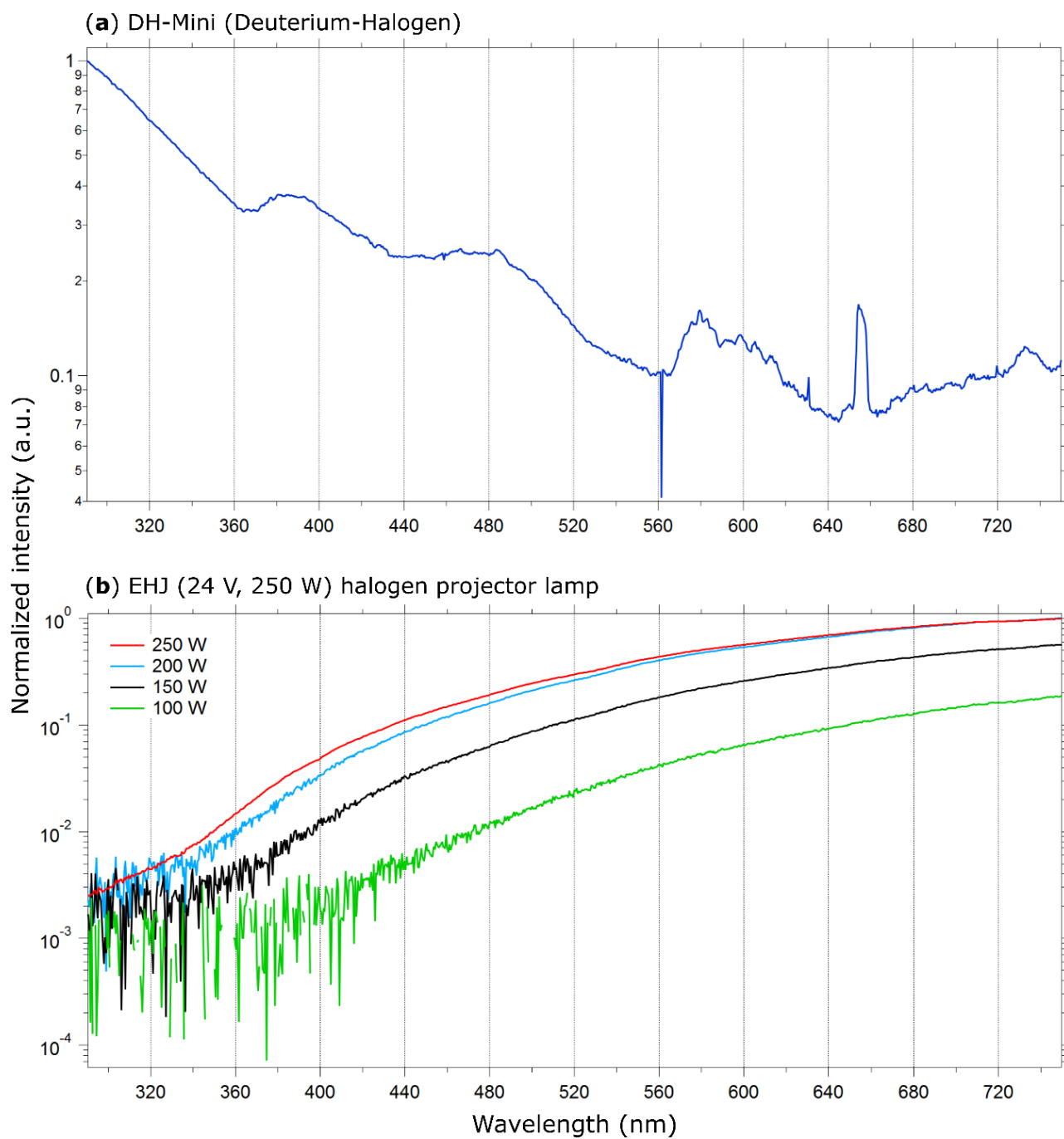
33

34 **Table S1.** Summary of physical properties of Polystyrene latex spheres (PSLs) and polystyrene-
 35 divinylbenzene particles (PS-DVB) used in this study. Stated properties are taken from manufacturer
 36 information. SD: Standard deviation, RI: Refraction index at 589 nm and 25°C.

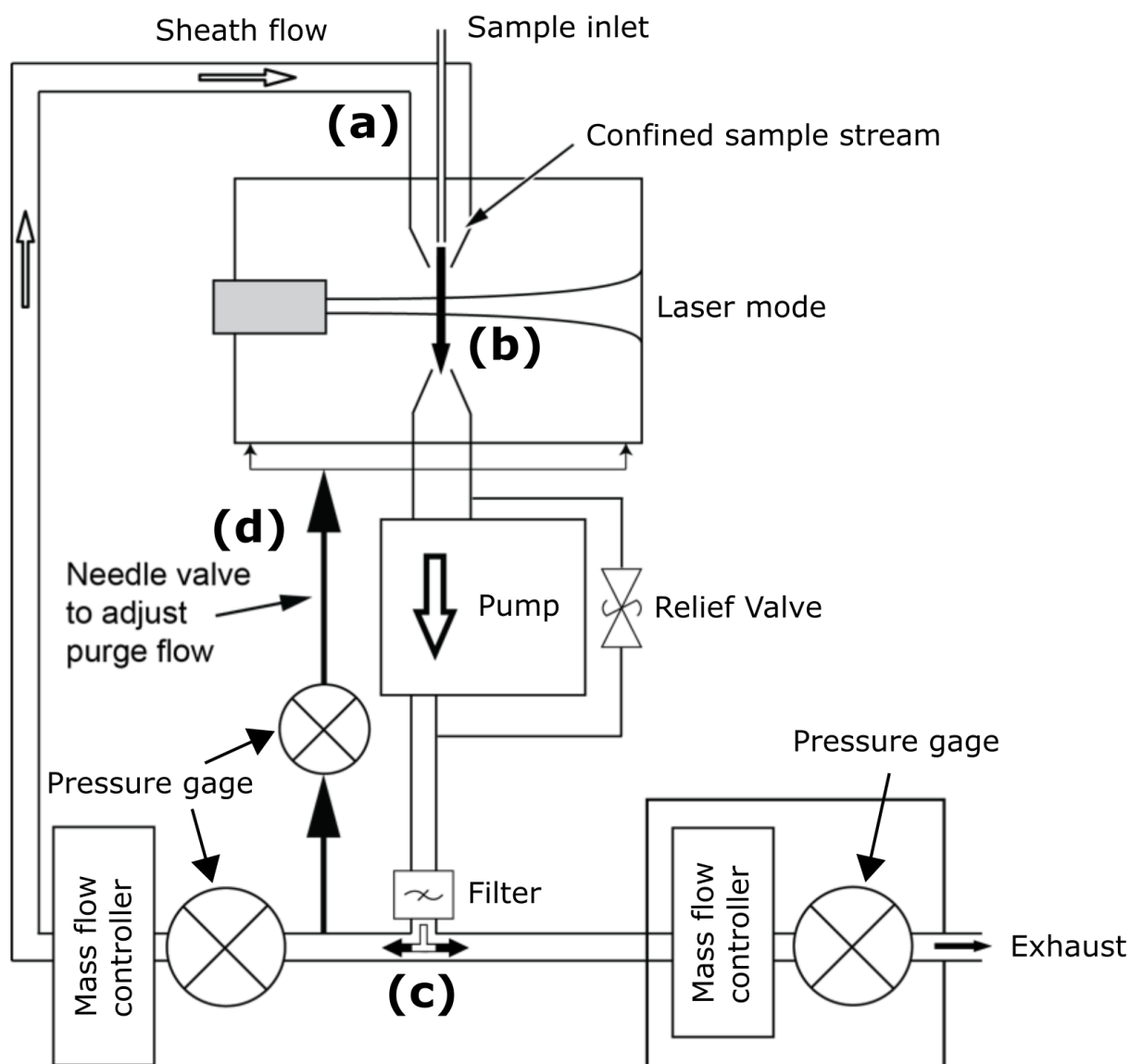
Diameter (μm)	SD (μm)	Confidence	RI	Material	Color / Dye	$\lambda_{ex}/\lambda_{em}$ (nm)	Provider	Catalog code
0.3	0.0148	CV= 5.1%	1.59	PSL	Non-fluorescent	Non-fluorescent	Polysciences Inc.	64015
0.356	0.014	CV= 3.9%	1.59	PSL	Non-fluorescent	Non-fluorescent	Polysciences Inc.	64016
0.4	0.0073	CV= 1.8%	1.59	PSL	Non-fluorescent	Non-fluorescent	Thermo-Fisher	3400A
0.5	0.0079	CV= 1.6%	1.59	PSL	Non-fluorescent	Non-fluorescent	Duke Scientific Corporation	3500A
0.53	N/A	N/A	1.59	PSL	Plum Purple / Proprietary	360 / 420	Bangs Laboratories Inc.	FS03F
0.6	0.010	CV= 1.7%	1.59	PSL	Non-fluorescent	Non-fluorescent	Thermo-Fisher	3600A
0.7	0.0083	CV= 1.2%	1.59	PSL	Non-fluorescent	Non-fluorescent	Thermo-Fisher	3700A
0.8	0.0083	CV= 1%	1.59	PSL	Non-fluorescent	Non-fluorescent	Thermo-Fisher	3800A
0.9	0.0041	CV= 0.5%	1.59	PSL	Non-fluorescent	Non-fluorescent	Thermo-Fisher	3900A
1	0.010	CV = 1.0%	1.59	PSL	Non-fluorescent	Non-fluorescent	Duke Scientific Corporation	4009A
1.6	0.020	CV= 1.3	1.59	PSL	Non-fluorescent	Non-fluorescent	Thermo-Fisher	4016A
2	0.021	CV= 1.0%	1.59	PSL	Non-fluorescent	Non-fluorescent	Thermo-Fisher	4202A
2	N/A	CV= < 5%	1.59	PSL	Red / Firefli™ Fluorescent Red	542 / 612	Thermo-Fisher	R0200
2	N/A	CV= < 5%	1.59	PSL	Green / Firefli™ Fluorescent Green	468 / 508	Thermo-Fisher	G0200
2	N/A	CV= < 5%	1.59	PSL	Blue / Firefli™ Fluorescent Blue	368,388,412 / 445, 445, 473	Thermo-Fisher	B0200B
2.07	0.15	N/A	1.59	PSL	Plum Purple / Proprietary	360 / 420	Bangs Laboratories Inc.	FS05F
3	0.032	CV=1.1%	1.59	PSL	Non-fluorescent	Non-fluorescent	Thermo-Fisher	4203A
4	0.04	CV = 1.0%	1.59	PSL	Non-fluorescent	Non-fluorescent	Thermo-Fisher	4204A
4.52	0.15	CV = 3.0%	1.59	PSL	Non-fluorescent	Non-fluorescent	Polysciences Inc.	17135
5	0.6	CV=11%	1.59	PS-DVB	Non-fluorescent	Non-fluorescent	Thermo-Fisher	DC-05
7	0.7	CV= 10%	1.59	PS-DVB	Non-fluorescent	Non-fluorescent	Thermo-Fisher	DC-07
8	0.8	CV= 10%	1.59	PS-DVB	Non-fluorescent	Non-fluorescent	Thermo-Fisher	DC-08
10	0.9	CV=9.2%	1.59	PS-DVB	Non-fluorescent	Non-fluorescent	Thermo-Fisher	DC-10
15	1.8	CV=11%	1.59	PS-DVB	Non-fluorescent	Non-fluorescent	Thermo-Fisher	DC-15
20	1.7	CV=8.9%	1.59	PS-DVB	Non-fluorescent	Non-fluorescent	Thermo-Fisher	DC-20

37 **Table S2.** Summary of reference particles used within this study. All biofluorophores, iron oxide
38 (Fe_3O_4), and carbon nanotubes were purchased from Sigma-Aldrich, St. Louis, MO, USA. Ammo-
39 nium sulfate was purchased from Fisher Scientific, Hampton, NH, USA.

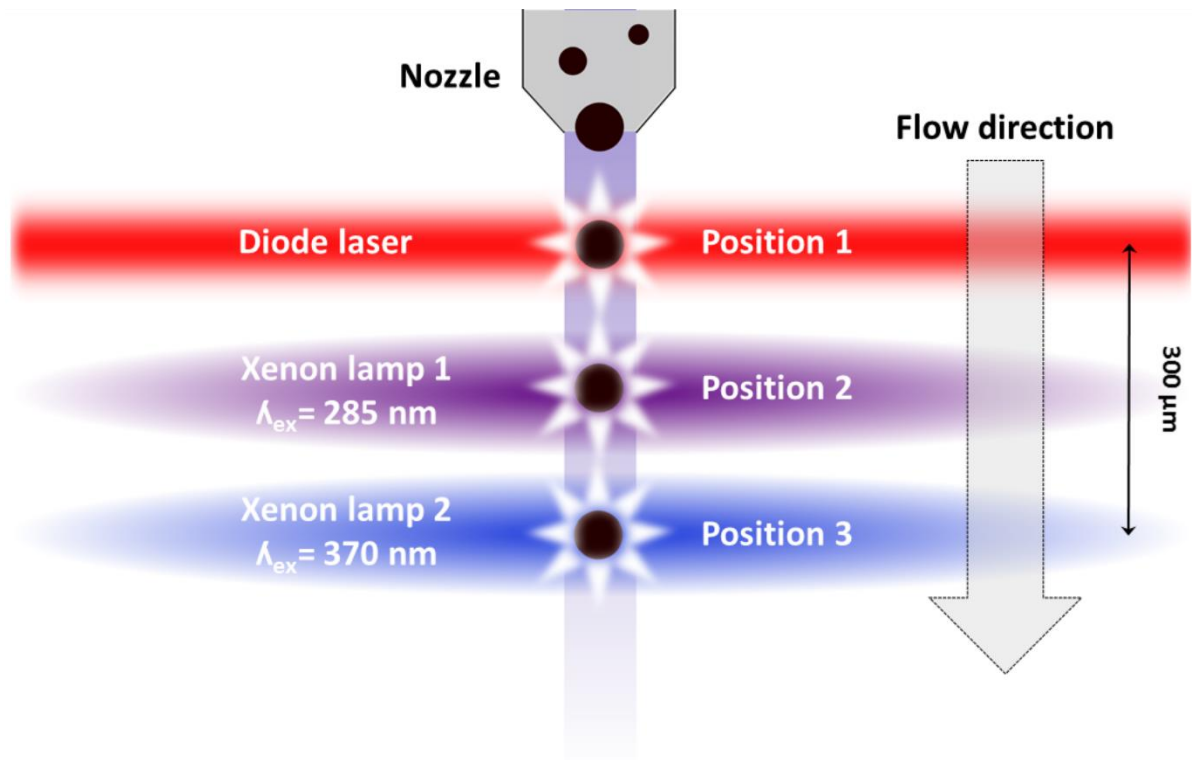
Reference particles	CAS Nr.
Bacteriochlorophyll	17499-98-8
Chlorophyll <i>a</i>	479-61-8
Chlorophyll <i>b</i>	519-62-0
NAD	606-68-8
Riboflavin	83-88-5
Tryptophan	73-22-3
Tyrosine	556-02-5
Fe_3O_4	1317-61-9
Carbon nanotubes	308068-56-6
Ammonium sulfate	7783-20-2



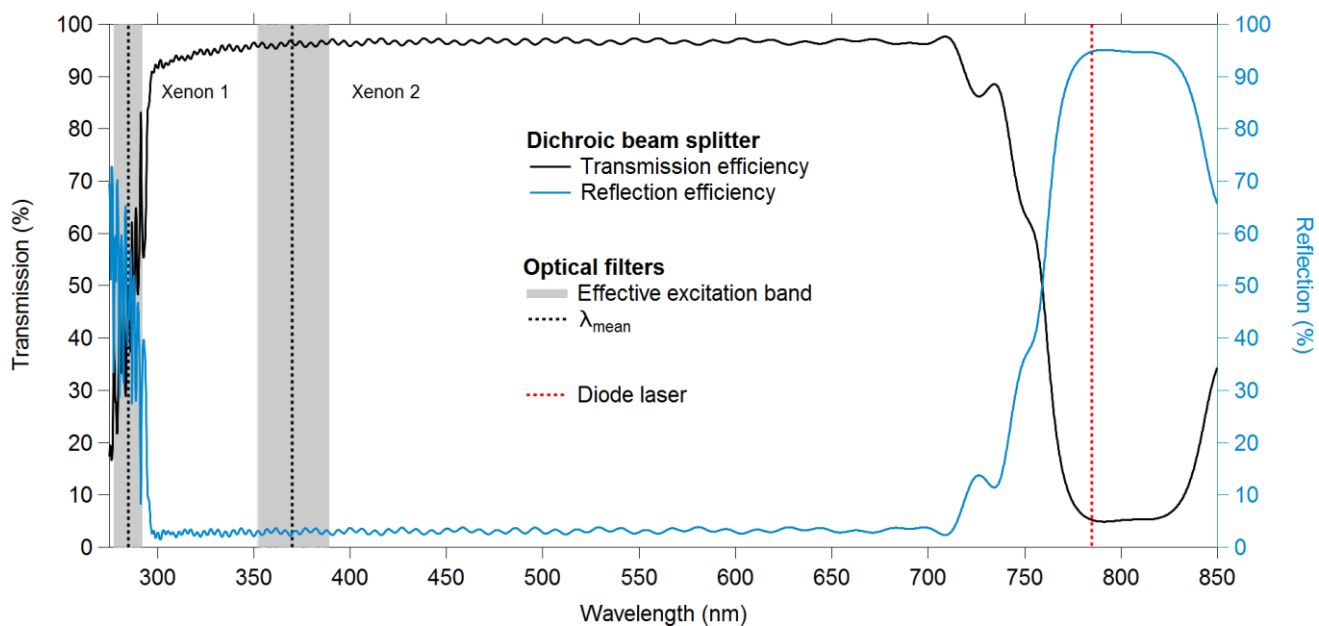
40 **Figure S1.** Normalized and averaged calibration lamp spectra. In (a), the spectrum of a deuterium-
 41 halogen lamp (DH-Mini, Ocean Optics) is shown, in (b) the spectra of a halogen projector lamp (EHJ
 42 24V250W, Ushio), both measured with the Dual-FL spectrometer (Horiba).



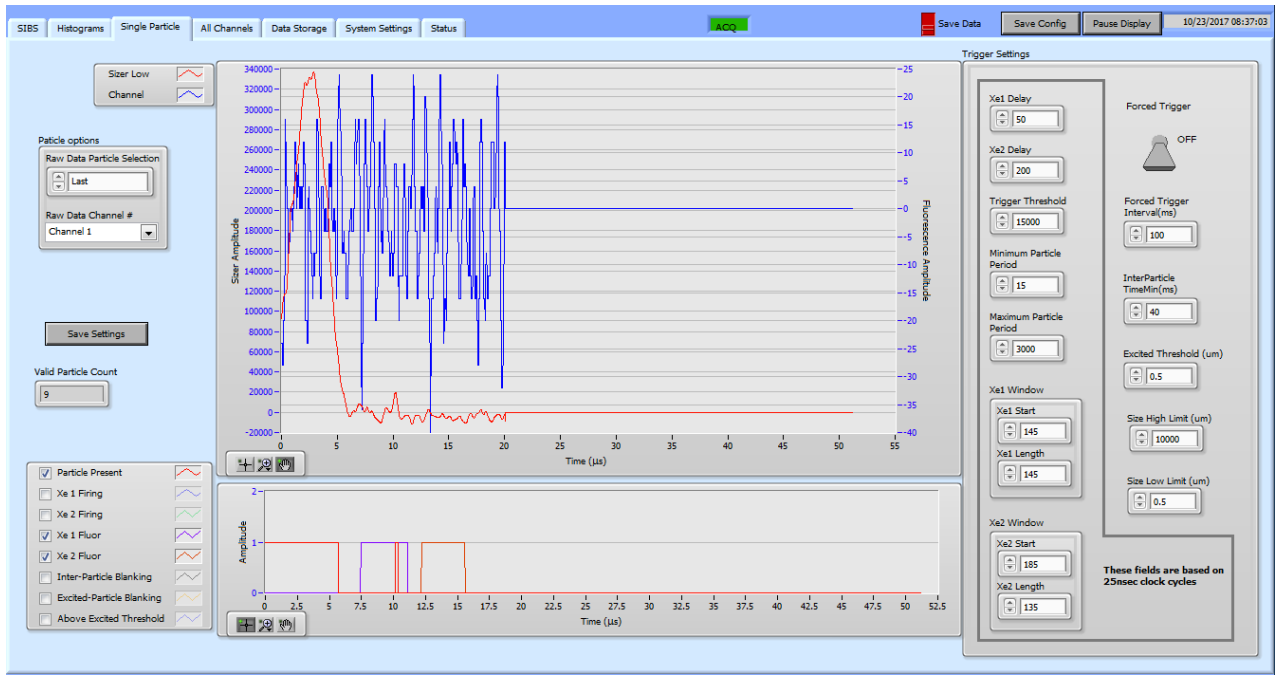
43 **Figure S2.** Flow diagram for the SIBS. Aerosol is drawn via a tapered delivery nozzle (a) into the
 44 optical cavity. The intersection of sample flow and laser beam defines a sampling volume with ap-
 45 proximately 0.7 mm in diameter and 130 μm depth (b). The sheath flow is filtered through a HEPA
 46 filter and recirculates in the system (c). A small purge flow, which is adjusted by a needle valve (d),
 47 constantly purges the optical cavity (Modified, image courtesy: DMT).



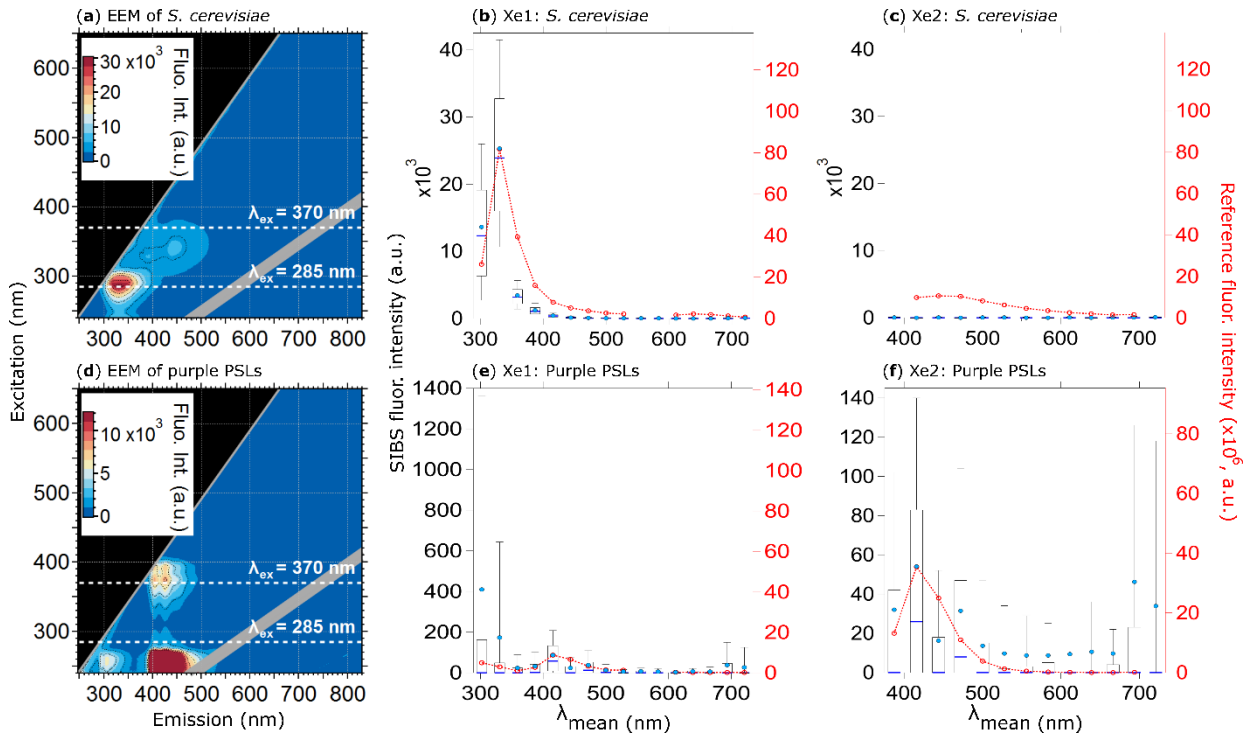
48 **Figure S3.** Schematic diagram of particle size and fluorescence detection. Position 1: Particles scatter
 49 light in all directions after being illuminated by a diode laser ($\lambda = 785 \text{ nm}$). Position 2: Xenon lamp
 50 1 is firing at $\lambda_{\text{ex}} = 285 \text{ nm}$. Position 3: Xenon lamp 2 is firing at $\lambda_{\text{ex}} = 370 \text{ nm}$. The measurement cycle
 51 from position 1 to position 3 takes $\sim 25 \mu\text{s}$ over a distance of $\sim 300 \mu\text{m}$. (Modified, adapted from
 52 WIBS-4A service manual (DOC-0345 Rev A), DMT; 2012).



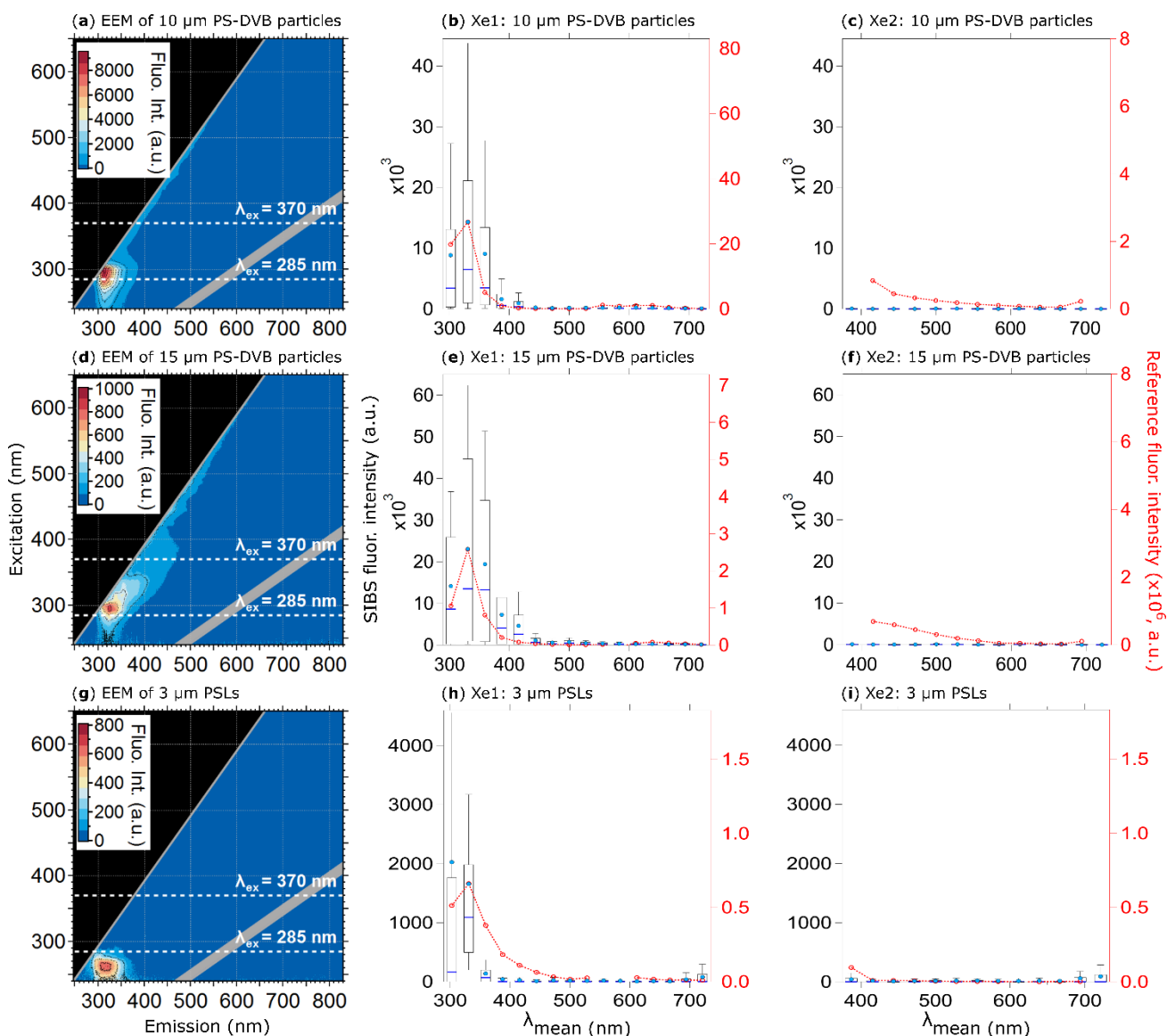
53 **Figure S4.** Transmission and reflection efficiency of the dichroic beam splitter. The beam
 54 splitter transmits fluorescence emission (black line) to the grating polychromator and reflects
 55 scattering light (blue line) to the particle sizing- and detection PMT. (Data courtesy: Semrock).



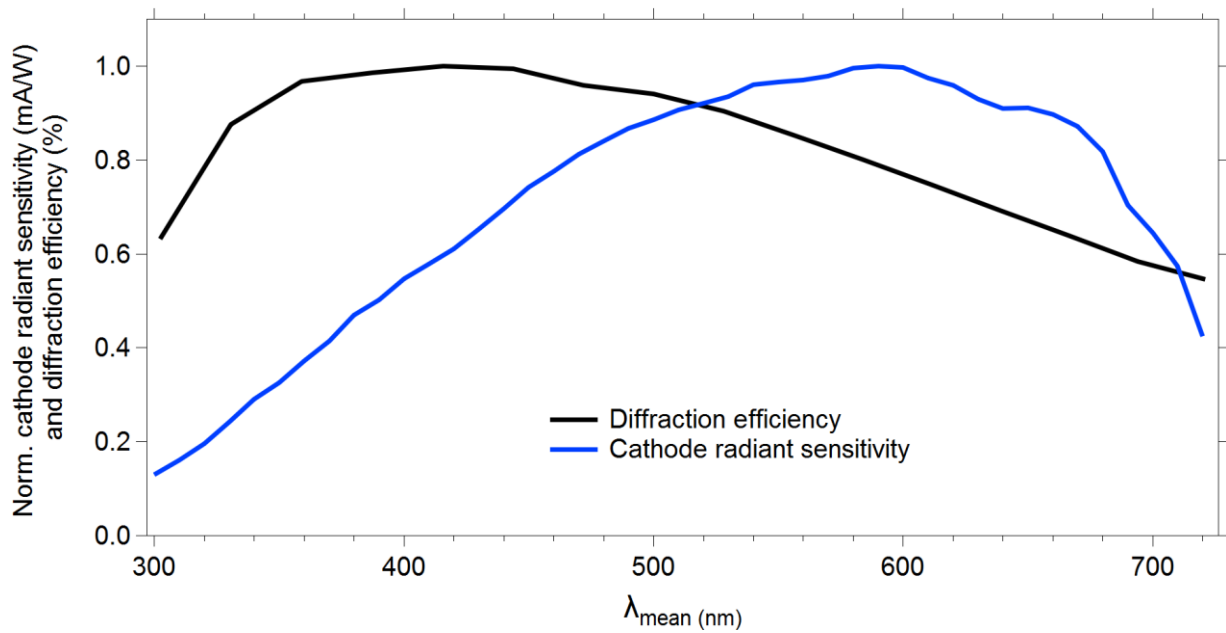
56 **Figure S5.** “Single Particle” tab of the SIBS user interface.



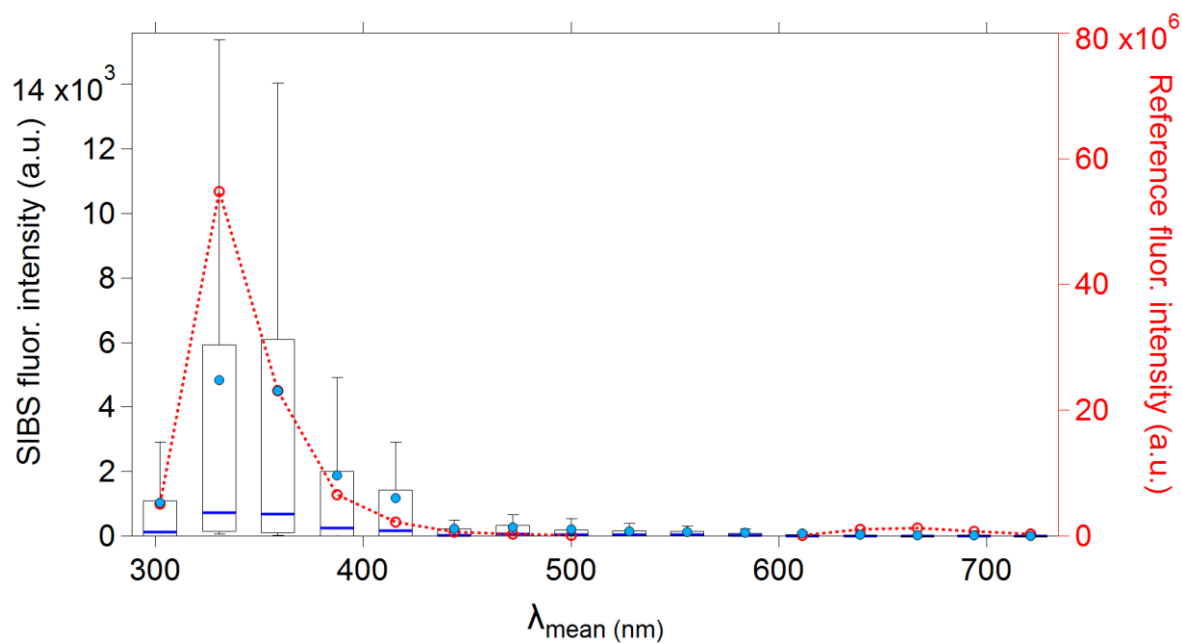
57 **Figure S6.** Corrected fluorescence emission of *S. cerevisiae* and 0.53 μm purple PSLs. Steady-state
58 fluorescence signatures displayed as EEMs (left column) and spectra at Xe1 and Xe2 (middle, right
59 columns) for: *S. cerevisiae* (**a**, **b** and **c**, size range between 4 - 10 μm , 1057 particles), and 0.53 μm
60 purple PSLs (**d**, **e**, and **f**, 5260 particles). Within EEMs: white dashed lines show SIBS excitation
61 wavelengths ($\lambda_{\text{ex}} = 285$ and 370 nm), grey diagonal lines indicate 1st and 2nd order elastic scattering
62 bands (both bands were subtracted automatically by the Aqualog V3.6 software). **Red dashed lines**
63 **and markers (right axes; middle, right columns): averaged and re-binned reference spectra.**



64 **Figure S7.** Fluorescence signatures of non-fluorescent particles. Highlighted are EEMs (left column)
 65 and spectra at Xe1 and Xe2 (middle, right columns) for: 10 μm (a, b, and c, uncorrected, 367 parti-
 66 cles) and 15 μm (d, e, and f, uncorrected, 400 particles) PS-DVB particles, and 3 μm PSLs (g, h, and
 67 i, corrected, 2396 particles). **Red dashed lines and markers (right axes; middle, right columns): av-**
 68 **eraged and re-binned reference spectra.**

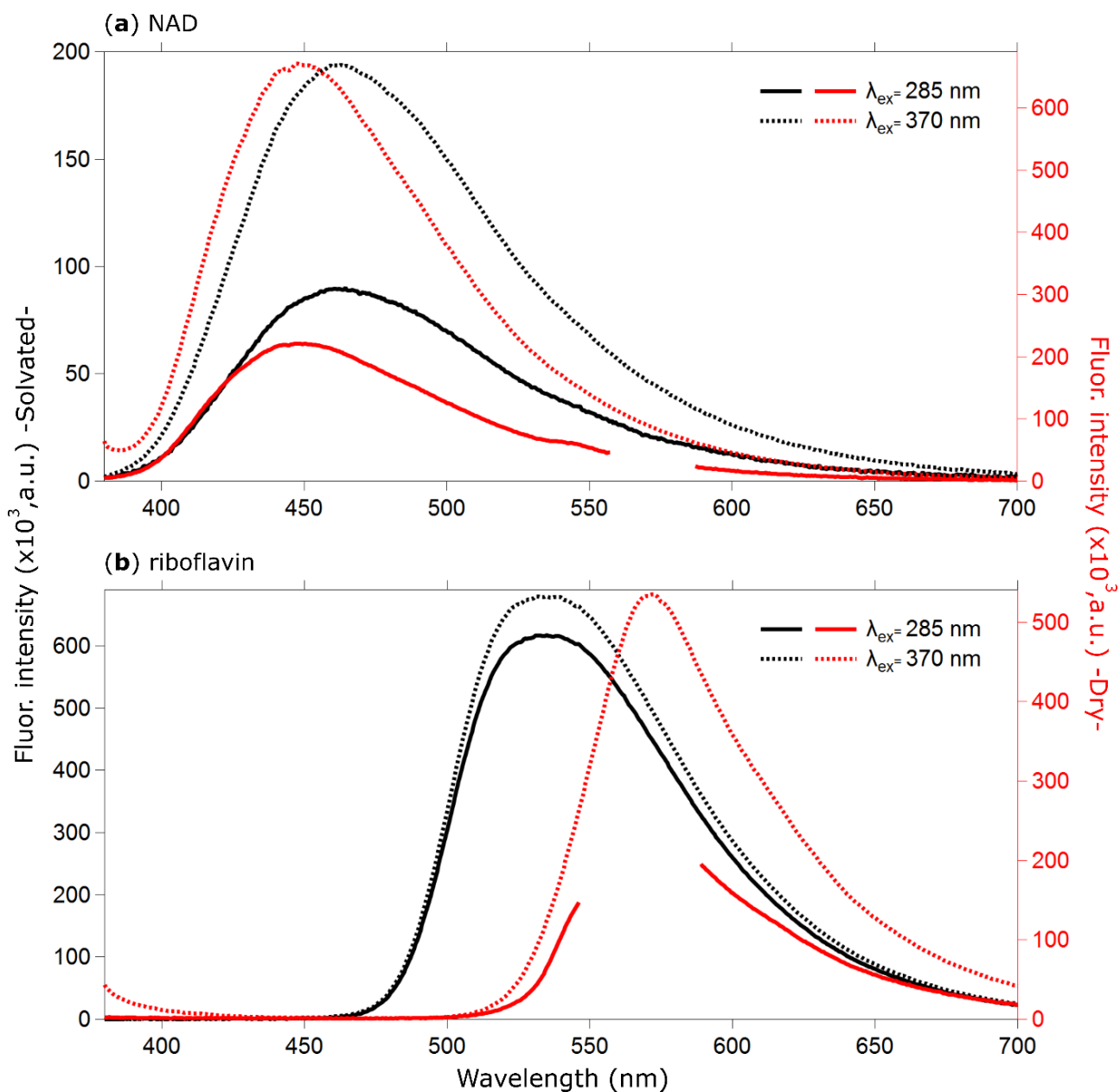


69 **Figure S8.** Normalized cathode radiant sensitivity of the PMT and diffraction efficiency of the grat-
 70 ing. The cathode radiant sensitivity multiplied by the diffraction efficiency results in the theoretical
 71 detector responsivity shown in Figure 6. (Data courtesy: Hamamatsu).

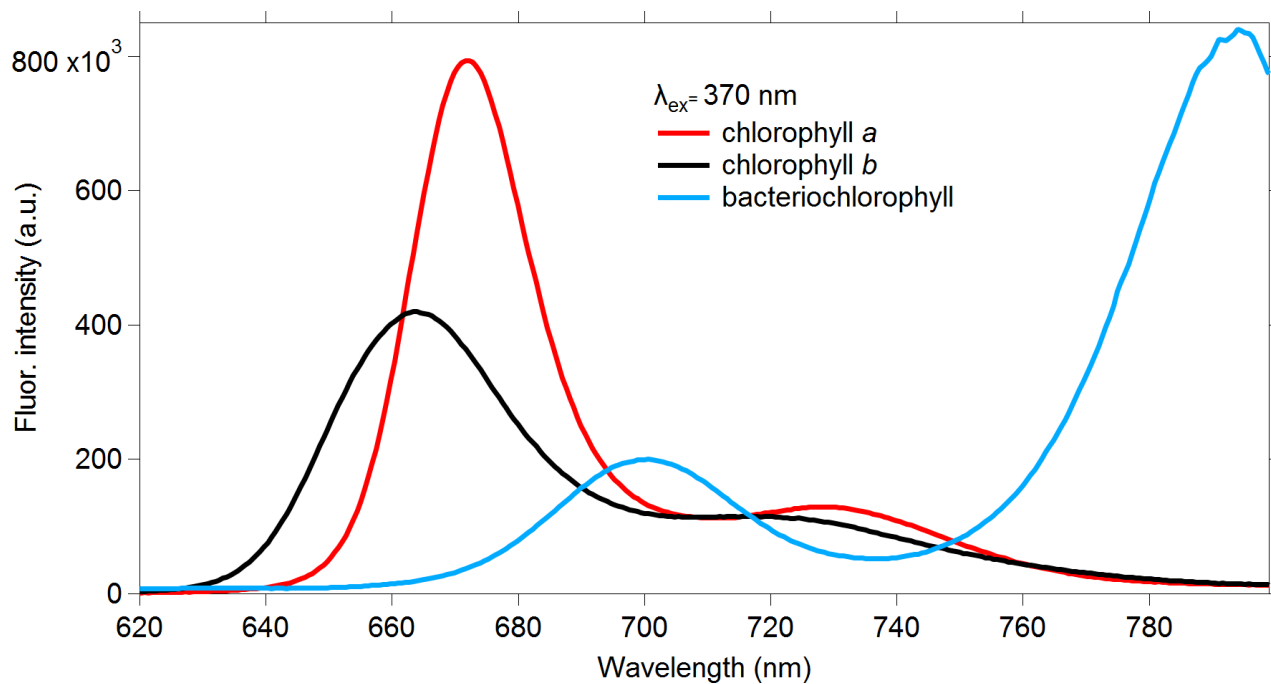


72 **Figure S9.** Uncorrected fluorescence spectra of tryptophan at Xe1 in a size range between 1 – 2 μm .

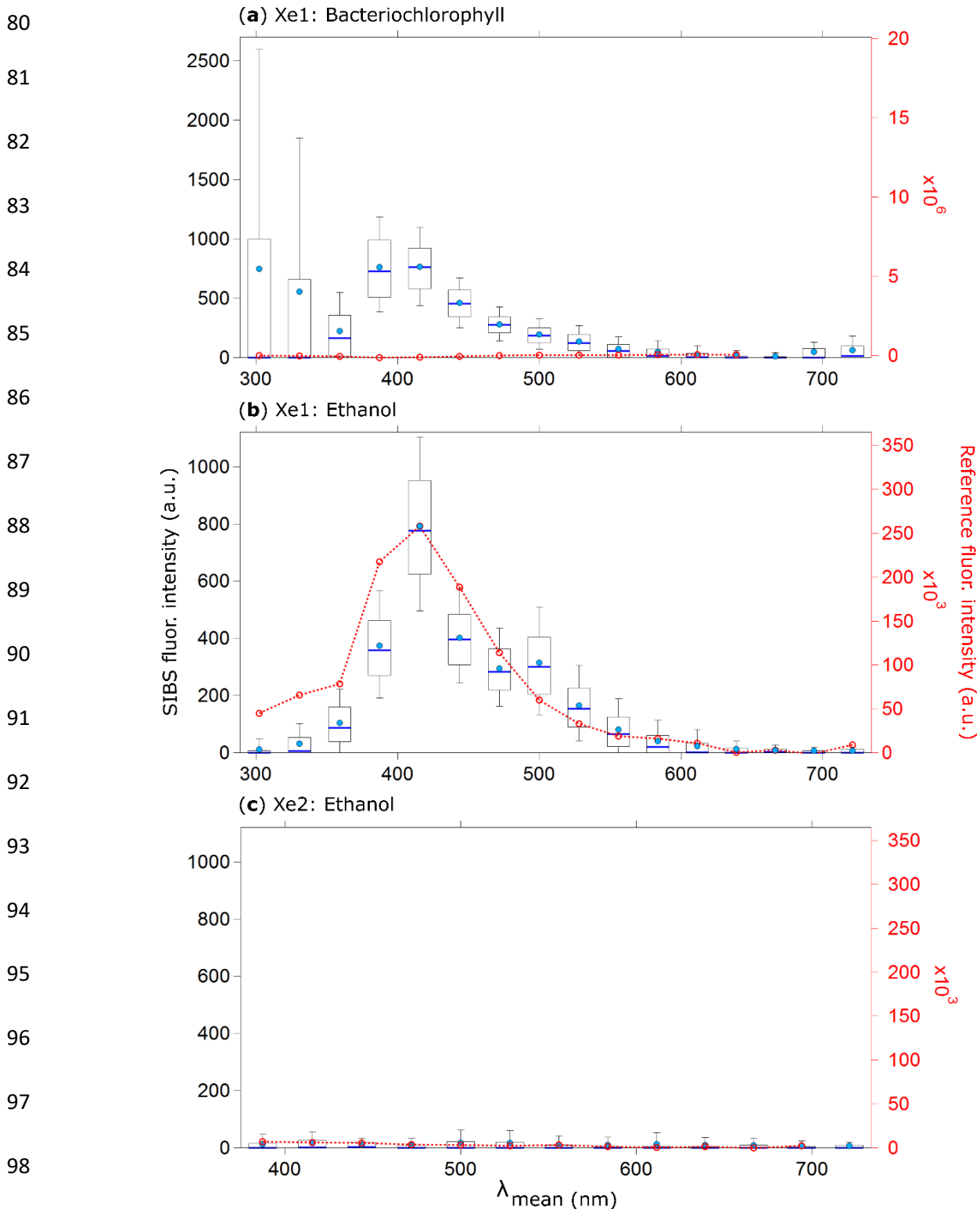
73 ***Red dashed line and markers (right axes): averaged and re-binned reference spectra.***



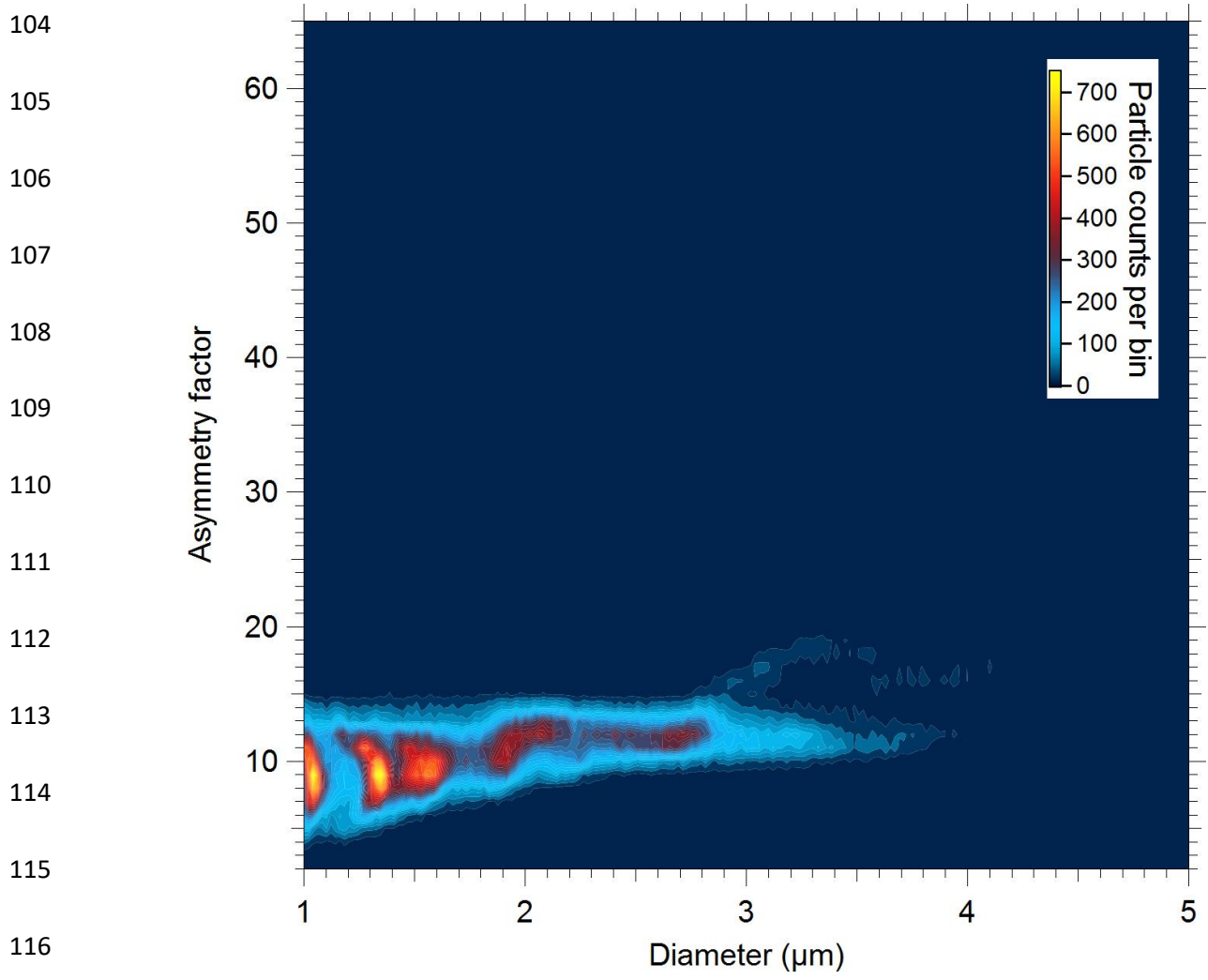
74 **Figure S10.** Dry vs. solv~~ated~~. Shown are reference spectra for NAD (a) and riboflavin (b) in dry
 75 and solv~~ated~~ state. Data coinciding with 2nd order elastic scattering were removed (a and b, red
 76 solid line). Peak maxima: NAD (dry): ~448 nm, NAD (solv~~ated~~): ~463 nm, riboflavin (dry): ~572
 77 nm, riboflavin (solv~~ated~~): ~535 nm.



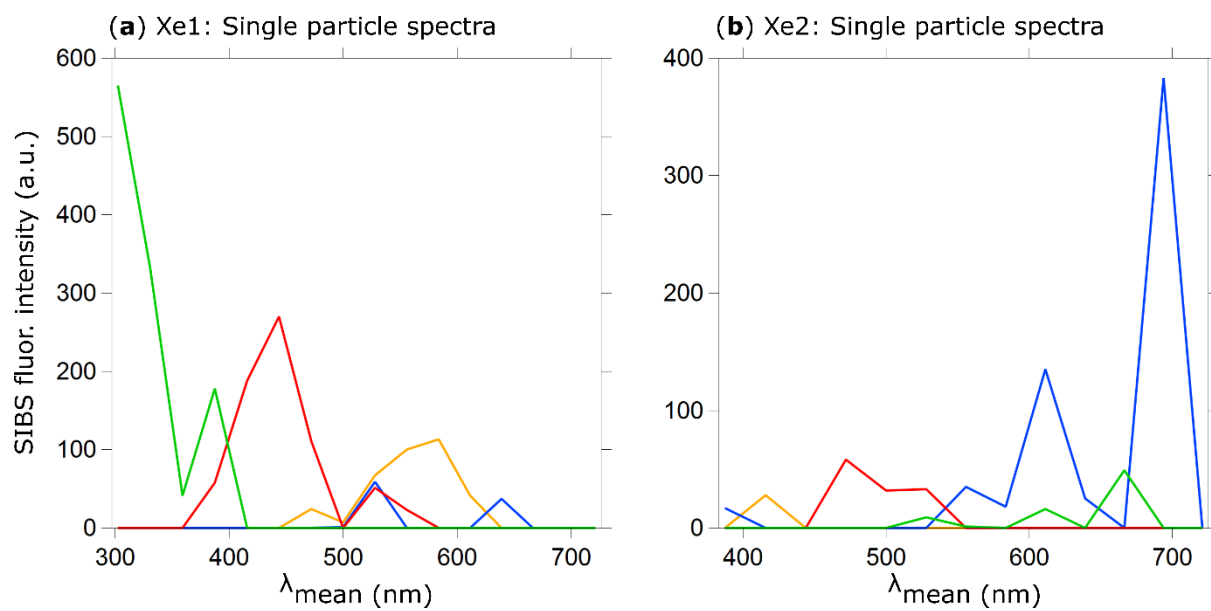
78 **Figure S11.** Fluorescence spectra of different chlorophyll types. Shown are reference spectra for
79 chlorophyll *a*, *b*, and bacteriochlorophyll at $\lambda_{ex} = 370$ nm.



99 **Figure S12.** Fluorescence spectra of ethanol artefact. Highlighted are fluorescence spectra of bacte-
 100 riorchlorophyll at Xe1 (a) and uncorrected spectra of ethanol, after being vortexed for 15 min in neb-
 101 ulizer plastic bottles, at Xe1 (b) and Xe2 (c). **Red dashed lines and markers (right axes;): averaged**
 102 **and re-binned reference spectra.** Since no distinct fluorescence signal is detectable at Xe2 (c), the
 103 fluorescence emission of chlorophyll *a*, *b* and bacteriochlorophyll is considered to be unaffected.



117 **Figure S13.** Particle asymmetry of ultrapure water droplets (163178 particles) displayed as particle
118 density histogram.



119 **Figure S14.** Exemplary fluorescence spectra of single ambient particles at Xe1 (a) and Xe2

120 (b).